THE INFLUENCE OF Ru ADDITIONS ON THE CORROSION PROPERTIES OF WC-Co-Cr HARDMETALS

NDIVHUWO BRAYNER NELWALANI

A dissertation submitted to the faculty of Engineering and the Built Environment, University of the Witwatersrand, Johannesburg, in fulfilment of the requirements for the degree of Master of Science in Engineering.

Johannesburg, May 2019

DECLARATION

I, Ndivhuwo Brayner Nelwalani, declare that this dissertation is my own unaided work. It is being submitted for the degree of Master of Science in Engineering at the University of the Witwatersrand, Johannesburg. It is has not been submitted before for any degree or examination to any other university.

……
Ndivhuwo Brayner Nelwalani

At Johannesburg Date 24 May 2019

ABSTRACT

The aim of this research was to study the effect of adding Ru to WC-10Co-4Cr coating and determining the effect there of on corrosion properties, wear properties and tribo-corrosion properties of the coatings. The Ru powder was added to the 1350 VM/WC-731-1 powder in different concentrations ranging from 0.5wt% to 2wt%. The 1350 VM/WC-731-1 powder, which had a composition of WC-10wt%Co-4wt%Cr was mixed together with Ru powder for several hours before thermally coated on a steel substrate. The powders morphologies were characterized using Field Emission Scanning Electron Microscope (FESEM). The thermal coating method used was the High Velocity Oxygen Fuel (HVOF). After successful coating, the samples were sectioned to smaller pieces and different test were done on the smaller pieces to determine coating properties. FESEM characterization on coating morphologies were done before any test were performed and post-test FESEM characterization were also performed after each test.

On the results obtained, it was evident that the Ru addition had an effect of decreasing the hardness by very low margin. The microstructural analysis showed no to very little effect caused by Ru addition on the powder. The distribution of Ru on the coatings were not constant and it was distributed in small pockets or islands throughout the coatings. Two very corrosive environments, which were composed of synthetic mine water, at pH levels of 3 and 1, were used as corrosion electrolyte and tribo-corrosion electrolyte. The corrosion open circuit potential showed a positive results as the increase in Ru content had an effect of decreasing the corrosion potential. The wear rate of the coating decreased with increasing Ru content and the coefficient of friction also increased with increasing Ru content. Tribo-corrosion rates decreased with increase in Ru content in the coating.

DEDICATIONS

To my late grandmother Munzhedzi Mudanalwo Nelwalani.

To my wife Mulalo Nelwalani and my son Mvuledzo Nelwalani.

To my parents Mr Lawrence Nelwalani and Mrs Annekie Nelwalani.

ACKNOWLEDGMENTS

- Professor. J.W. van der Merwe, heartfelt thank you for your exceptional supervision, patience, tireless sacrifice, guidance and advice during study. I truly appreciate all your help.
- The Department of Science (DST) and National Research Foundation (NRF), South Africa, for supporting the DST/NRF Centre of Excellence in Strong Materials, for granting me the opportunity to do my postgraduate studies in a field I am passionate about and financially supporting my research and up keep. I am truly grateful.
- Mr Donald Mahole, for assistance with tribo-corrosion experiments.
- My sisters (Rendani and Pfano) and brother (Thavhadziawa), for their prayers and support. Thank you very much.
- And lastly but not the least to God almighty, for giving the strength to carry out this work, the courage, the wisdom, for proving for my family, and for the love that you have shown me, thank you for all the blessings in my life.

GLOSSARY

°C	Degree Celsius
µm	micrometre
ASTM	American Society for Testing and Materials
BSD	Backscattered detector
CBN	Cubic Boron Nitride
e^-	Electron symbol
EDS	Energy-dispersive X-ray spectroscopy
FESEM	Field Emission Scanning Electron Microscope
HP	High Pressure
HVOF	High Velocity Oxygen Fuel
Hz	Herts
m/s	Meter per second
mg/l	milligrams per litre
mm	millimetre
MPa	Mega Pascals
N	Newton
OCP	Open Circuit Potential
pH	Scale used to measure acidity of the solution
V	Voltage
VHN	Vickers Hardness Number
Wt%	Weight percentage
XRD	X-ray diffraction

TABLE OF CONTENTS

LIST OF FIGURES

LIST OF TABLES

Chapter 1: Introduction

1.1 Background and motivation

Tungsten carbide hardmetals are widely used in industries because of their high wear resistance due to their high hardness and tough binders. Thermal sprayed coatings are applied to low cost substrates to improve the wear resistance, corrosion resistance, oxidation resistance, hardness, and erosion-corrosion resistance of the substrate [7].

Hardmetals powders can be applied as coatings (thermal coatings or cold spraying) and can also be used for sintering purposes. Comparing thermal spraying and cold spraying, both methods offers different mechanical properties and have different advantages and disadvantages, so to be able to choose which method to use depends on the application of the material. The same applies to sintering, they too are application and cost dependent. In this study, 1350 VM/WC-731-1 powder was mixed with Ru powder in the range from 0.5wt% to 2wt% to determine the effect of Ru addition on corrosion properties, wear properties and tribo-corrosion properties of the coatings. This was done by using high velocity oxygen fuel (HVOF) method to apply the mixed powders on the mild steel substrate.

Tribo-corrosion, corrosion and wear are general causes of material deterioration of flow-handling components such as impellers, turbines, pump casings and piping which are in contact with solid particle-containing corrosive environments at high flow rates. Materials subjected to such slurry environments must not only resist the erosion of solid particles and liquids, but also be resistant to corrosion [5-6]. Transporting minerals such as slurries through pipe lines is an efficient means of transporting and is done during many mineral processing operations, but there is a challenge as the movement of these slurries can cause even more erosion damage and corrosion in places where the slurry flow changes direction [7].

Ruthenium additions to alloys has an effect of decreasing the corrosion rates in previous studies [1-3]. Ru has limited uses in industry and more researches are determined to do more research to determine the performance of Ru infused alloyed at different testing conditions. Ru and other

platinum group metals (PGMs) Pt, Os, Pd, Pd, and Ir and mined in huge quantities in South Africa with very limited industrial uses. Potgieter et al. [1] and Nelwalani [5] showed that Ru additions reduce erosion-corrosion and corrosion rates in synthetic mine solutions at lower pH of 3 (Machio et al. [6])

Significance of this research

This research was aimed at investigating the influence of Ru addition to WC-10Co-4Cr high velocity oxygen fuel (HVOF) hardmetal coatings in terms of corrosion, tribo-corrosion and ball on disc wear properties. Mild steel was selected to be used as a substrate because it is inexpensive but with poor wear and corrosion resistance, so applying the coating to the mild steel substrate will be very beneficial. Hardmetal coatings are costly, but generally have high wear resistance. However, when exposed to corrosive conditions they will deteriorate. From research already done, it is evident that Ru additions to WC-Co and WC-Fe reduces the corrosion rate in different corrosion environments.

Industrial applications

WC-10Co-4Cr hardmetals coatings are used in industry where a hardmetal coating with better corrosion resistance and high wear resistance are desired. WC-Co-Cr hardmetal coating have better corrosion properties than WC-Co hardmetal coatings, because of Cr present in WC-Co-Cr coatings. WC-Co hardmetals are used in applications like spray nozzles, seals in slurry pumps, drill bits, cutting tools, impellers, pump casings, valves, forming dies, projectiles, and rolls [9-11]. Since WC-Cr-Co hardmetals are used in applications where corrosion and tribo-corrosion are important factors, manufacturing coatings with even better corrosion and wear properties will be of benefit to the industry as it will save down time and costs due to maintenance and replacement.

Research questions

1. What is the effect of Ru additions of up to 2wt% to WC-Co-Cr HVOF coating on corrosion properties, tribo-corrosion properties and friction wear properties?
2. How does Ru additions to WC-Co-Cr affect the microstructure and hardness of the coatings?

1.2 Research aim and objectives

The main aim of the research was to investigate the effect of Ru additions to WC-10Co-4Cr hardmetals coatings on corrosion properties, tribo-corrosion properties and friction wear properties. The main objectives of the research were:

- To determine the effects of Ru additions on WC-10Co-4Cr HVOF hardmetal coatings in terms of corrosion behavior in synthetic mine water at pH of 3.
- To determine the effects of Ru additions on WC-10Co-4Cr HVOF hardmetal coatings and in terms of tribo-corrosion properties in synthetic mine water at the pH of 3.
- To determine the effects of Ru additions on WC-10Cr-4Co HVOF hardmetal coatings in terms of friction wear properties.
- To determine the effect of Ru additions on WC-10Co-4Cr HVOF hardmetal coatings in terms of microstructure and hardness.

1.3 Structure of the thesis

This research consists of 7 chapters which are;

- Chapter 1 Introduction

  The research motivation, research aims and objectives for the research are outlined in this chapter.
- Chapter 2 Literature review

  The literature review covered the background of the Tungsten carbides, Ruthenium addition to hardmetals, High velocity oxygen fuel process, Corrosion of metals, wear of meatal and tribo-corrosion of metals.
- Chapter 3 Experimental

  Procedure-Experimental procedure covered the powder preparations, material characterization, electrochemical corrosion testing, wear testing, tribo-corrosion testing, and scanning electron microscope.
- Chapter 4 Microstructure and mechanical properties results

Powder morphology results, as received sample cross section, phase composition results, grain size and contiguity results and hardness results are shown in this chapter.

- Chapter 5 Sliding wear, electrochemical corrosion, and tribo-corrosion results

  Sliding wear results, electrochemical corrosion results, and tribo-corrosion results are shown in this chapter.

- Chapter 6 Discussion of results

  Discussion of characterization of samples results, grain size and contiguity, hardness and thickness, sliding wear, electrochemical corrosion, tribo-corrosion results were discussed in this chapter.

- Chapter 7 Conclusions and recommendations

  Conclusion remarks of the work and future work recommendation are shown in this chapter.

Chapter 2: Literature review

2.1 Tungsten Carbide

Tungsten carbide is an iron-grey powder of micron-sized cubical crystals with a Mohs hardness above 9.5 and a melting point of about 2982°C. It is produced by the reaction of a hydrocarbon vapor with tungsten at high temperature. The composition is WC, but at high temperature, it may decompose into W_2C, W_3C, W_3C_4 and C, and the carbide may be a mixture of the two forms. WC is used mainly for cutting tool bits and for heat and erosion-resistant parts and coatings. Briquetting of tungsten carbide into a usable form was first patented in Germany and produced by Krupp Works under the name of Widia metal [19].

Tungsten carbide hardmetals are materials that are widely used in applications where abrasion resistance is required. Materials which incorporate tungsten carbide as the hard phase are often chosen due to their proven longevity, wear resistance, stiffness and high temperature resistance. Hardmetals are powder metallurgical products consisting of refractory metal carbides and a binder metal. The most common refractory carbide used is WC, together with cobalt as the binder, though other binder systems are also well established for more specialized applications [13]. Small amounts of vanadium carbide (about 0.5wt%) are usually added in the WC–Co industry to produce a fine gained WC–Co material. The hardness of WC–Co improves with fine WC grain sizes [16]. They initially consisted of 6wt% Co bonded WC, and due to their good hardness and wear resistance, cemented carbides were further developed into cutting tools, wear parts and machine components by Krupp in Germany [54].

Cobalt is the most widely used binder in WC-base hardmetals. Cobalt is the preferred binder due to its outstanding wetting and adhesion characteristics. Cobalt has a low-temperature hexagonal phase and as high temperature cubic phase, with a phase transition at about 415°C. Cobalt is manufactured through reduction of cobalt oxides or derived from organic salts, particularly cobalt oxalate [50].

2.1.1 Microstructures and phases of WC-Co-Cr coatings

Microstructure of WC-10Co-4Cr contains splat-like structure where WC grains are embedded in Co and Cr binder phases. Phase analysis of the coatings has WC as main phase and low amounts of W_2C phases, and W_2C is present as results of WC decarburizing because of high heat from the spraying process. During the coating process, WC dissolves into the binder and C oxidized to CO or CO_2 and during cooling process, W precipitate to W_2C. Furthermore, rapid solidification of the supersaturated Co (W, C) matrix can cause the formation of an amorphous or monocrystalline phase [37-38]. Figure 2.1 shows a typical scanning micrograph of WC-Co HVOF coating.

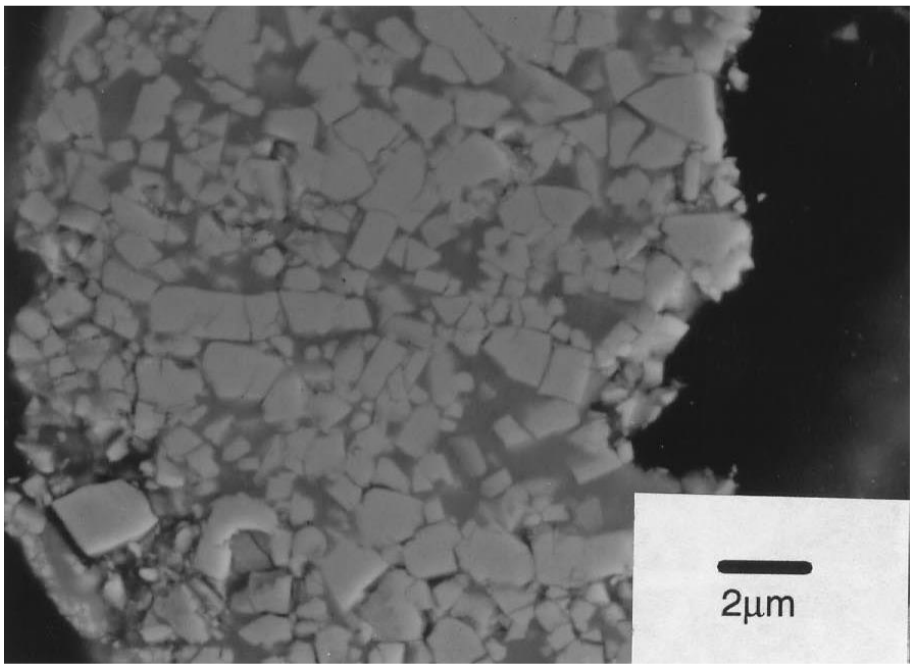

Figure 2.1. Typical SEM micrograph of WC-Co HVOF coating microstructure [34].

Coatings formed from porous powders manufactured by agglomeration and sintering tend to form a coating that is less porous and dense, whereas coatings produced from dense sintered and crushed powders tend to have more voids on the coatings and thus increased wear [42]. Carbon evaporate by oxidation as indicated by the lower carbon content of the coating compared to the powder. At the same time, part of WC dissolves in the cobalt matrix and can either form an amorphous or

nanocrystalline supersaturated solid cobalt (tungsten, carbide) solution or an η-phase upon solidification. Tungsten and WC can precipitate from the supersaturated solid solution [32].

2.2 Ruthenium addition to hardmetals

Ruthenium is a hard silvery-white metal having a specific gravity of 12.4, a melting point of about 2310°C, and a Brinell hardness of 220 in the annealed state. The metal is obtained from the residue of platinum ores by heat reduction of ruthenium oxide (RuO_2) in hydrogen [19]. Ruthenium is the most chemically resistant of the platinum group metals and does not dissolved by aqua regia. Ruthenium has a close-packed hexagonal crystal structure. Ruthenium-platinum alloys are used for electric contacts, electronic wires, chemical equipment, and jewelry in manufacturing. Several ruthenium intermetallic compounds hold promise for potential high-temperature, aircraft-turbine parts because of their high melting temperature and evidence of room-temperature ductility [19].

Research by Shing at al [36] showed that Ru additions on WC-10Co hardmetals has an effect of increasing the hardness of hardmetals and decrease in toughness on sintered samples due to the fact that Ru inhibits the growth of WC grains. Ru addition to sintered hardmetals can decrease the toughness of the WC-Co due to the hardening effect of the binder, which results from Ru remaining in the solution in the cobalt matrix.

Bonjour et al. and Masuku et al. [41, 42] has shown that the addition of Ru into a cobalt binder had stabilizing properties in the WC-Co composite. Ruthenium could inhibit the formation of eta phase in sub stoichiometric WC-Co and normally only a minimum amount of Ru is required. Research done by Van der Merwe and Tharandt [55] showed that Ru additions to stainless steel has an effect of decreasing corrosion rates but is very important to have an even distribution for better corrosion resistance.

The corrosion rate of the alloys in sulphuric acid slightly decreased as the ruthenium content increased. Alloys containing 1wt% and 1.5wt% Ru showed almost similar corrosion rate as shown in Figure 2.2 [40].

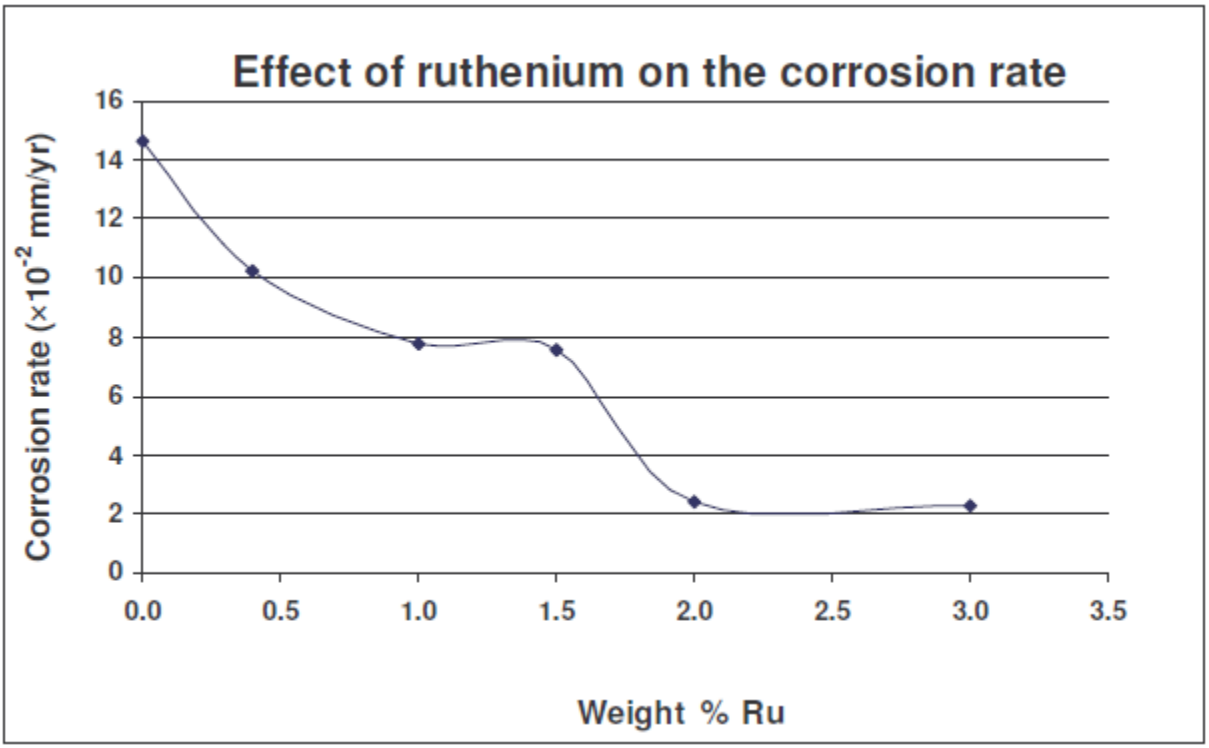

Figure 2.2. The effect of ruthenium additions on corrosion rate of sintered WC-Co alloys in 1M H_2SO_4 [40].

The addition of ruthenium changes both anodic and cathodic Tafel constants. The additions of ruthenium in sulphuric acid solution influence both anodic and cathodic sites at the surface of the WC-Co-Ru, and more specifically the cathodic sites [40]. For OCP the polarization currents decreased with the increasing exposure time and increasing ruthenium content.

2.3 High Velocity Oxygen Fuel (HVOF) WC-Co coatings

The High Velocity Oxygen Fuel (HVOF) coating method is widely used in engineering applications to extend component life by retarding wear degradation and erosion-corrosion damage. Since their inception, thermal spray technologies have been the subject of studies aimed at optimizing the process parameters to consistently yield coatings with good bond strength, minimum residual stresses and low porosity. The use of WC-Co coatings in wear applications is mainly due to their high hardness and the good bond strength between the different phases. Control

of the coating properties is complex because the properties are derived from the interaction of various factors such as the properties of the feedstock powders, type of spraying technique employed and the spraying process parameters [11]. The thermal spray process is one of the most versatile methods for surface treatment in terms of economy, range of materials applied and protected, and the scope of application [12]. Figure 2.3 show the HVOF process overview.

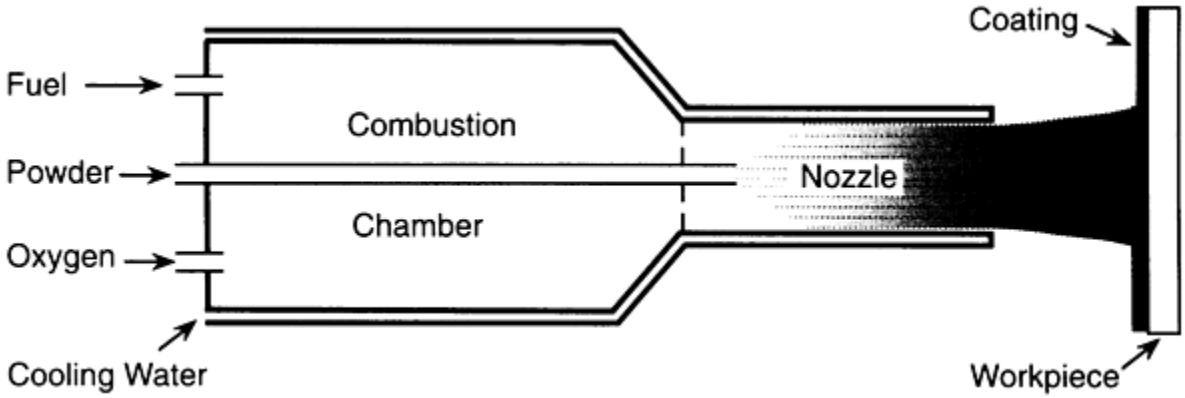

Figure 2.3. HVOF process overview [47].

The HVOF, shown in Figure 2.3 combines a fuel like kerosene, propylene, which burns with a large amount of oxygen to produce a flame with a relatively low temperature (around 3000°C) and an extremely high gas molecule velocity. The velocity may reach values near 2000 m/s (or HVOF in contrast to about 100 m/s flame spraying or 1000 m/s plasma spraying) [14]. It can result in very dense and tightly adherent coatings, having low residual stresses with little or no oxidation [12]. Powders sprayed using HVOF can have different coating properties according to their manufacturing, initial characteristics (composition, shape, morphology, etc.) and spray parameters. The cermet powders, consisting of carbides and metallic binder, are highly suitable for HVOF spraying because the high velocities and low temperatures involved cause no melting of carbides, diminishing their thermal degradation [11].

The HVOF process uses extremely high kinetic energy and controlled thermal energy output to produce very-low-porosity coatings that exhibit high bond strength, fine as-sprayed surface finish,

and low residual stresses. Bonding of thermal spray coatings relies primarily on mechanical interlocking with the substrate material. Good surface preparation cannot be overemphasized. The coating deposition rate is limited by the method used and the melting point of the coating material [50]. Powders having a narrow powder grain size distribution results in coatings of higher quality than powders with wider grain size distributions. Small grains are more easily overheated than larger grains. Overheating may produce coating phases with poor quality [8].

High deposition rates are possible with little significant change in composition occurring from the powder feedstock through to the coating, even when the elements in the coating have widely differing vapour pressures. The most obvious limitations of this process are that the coating process is 'line of sight', requiring complexed robotic manipulation for complete coverage, and that the more reactive elements may well oxidise during the spraying process if conducted in air. Porosity problems previously reported for plasma spray coatings can largely be overcome using post coating thermomechanical treatments [52].

The various HVOF systems differ in the type of powder injection, design of the combustion chamber, and nozzle geometry. The powder feedstock is usually axially injected into the hot exhaust gases, or into the combustion chamber, depending on the type of HVOF-system and nozzle system. Heating and acceleration of the particles takes place within the barrel of the torch as well as in the free jet outside the barrel. The flame temperature is about 3000°C and the velocity of the exiting and further expanding gases may be as high as 1200 m/s. The powder particles can reach velocities of up to 600 m/s depending on the density, shape, and size of the feedstock material [47].

Due to the high particle velocities and the rather moderate temperatures, these processes are preferably used for coating materials that tend to decompose at higher temperatures. This is the reason for their main field of application, the deposition of hard metals/ cemented carbides such as WC-Co and Cr_3C_2/NiCr, since the density and the wear resistance of these coatings is extremely high. The main field for HVOF is applications for abrasion and sliding wear. Components like nozzles of water jet cutting tools, rolls for paper and foil producing industries, sliding areas of pressing irons, valves and pumps in petrochemical applications, and mechanical seals [21].

Variations in fuel type, gas flow and powder type have all been shown to affect the wear resistance through their influence on the microstructure. The microstructure is not the only spray related feature to have an effect on the wear resistance. Because of the nature of the spray process, significant residual stresses, which are often tensile in nature, exist within the coatings [34].

The stresses develop because the splats are physically unable to deform enough to accommodate the strain arising from the solidification and cooling. Mismatch between the thermal expansion coefficients of coating and substrate can generate stresses. The residual stress state following spraying also depends on the ability of the system to deform and thus allow relaxation of the stresses, which in turn depends on the system geometry. A thin planar substrate will allow considerable bending and will thus result in reduced stresses but a high stress gradient in the coating; a thicker substrate will result in a larger overall coating residual stress but a smaller stress gradient. Similarly, geometries other than planar will impose different constrains on coating stress relief [34].

Thermally sprayed cermet coatings have emerged as a viable solution for a wide range of wear resistance applications to improve the service life of machine components [15]. Thermal coatings using tungsten carbides powders on steel pipelines have been used for years in mining industries for applications where materials with high erosion-corrosion properties are required. Transporting minerals as slurry is an efficient means of moving it and is done during many mineral processing operations, but there is a challenge as the movement of these slurries can cause significant erosion and corrosion in places where the slurry flow changes direction. Pumps, elbows, tee junctions, valves, flotation cells, and hydrocyclones are parts of mineral beneficiation systems that are subject to wear and corrosion [17].

WC-Co-Cr coatings derive its wear resistant properties from the presence of high volume fraction of hard, wear resistant WC grains in a Co based metallic binder phase. The presence of the metallic binder provides some toughness in the coating compared to pure ceramic coatings; however, the binder can exhibit some brittleness if high W and C are dissolved in the binder during spraying [33]. Compared to other thermal spraying methods, HVOF spraying is capable of producing dense WC-Co system cermet coatings with low porosity, limited oxide content, less decarburization,

high hardness and superior bond strength [38]. Thermal spraying can cause some decarburization of WC to ditungsten carbide (W_2C) in some coatings, formation of eta phase and can also cause the Co binder phase to acquire an amorphous structure the coatings [6].

2.3.1 Mechanical properties of WC-Co coatings

Hardness of WC-Co depends not only on grain size of WC but also on the volume fraction of WC, the mean free path of the binder and the contiguity of WC particles [35]. Results from O'Quigley at al [37] on sintered samples showed that the mean free path increase with increase in Co content, hardness decrease with increase in Co content, and hardness increase with increase in mean free path. The mechanical properties of hardmetals can be improved if there are fewer fracture pathways within its matrix. In order to reduce fracture pathways, a major requirement is that the binder should possess very good wettability so that the fracture path could pass through the binder phase rather WC-binder phase interface [45].

WC-Co also exhibited a constant profile when compared to other coatings, which is indicative of its low porosity and increased splat cohesion of the coating obtained by the HVOF spraying process. The cobalt as the binder phase could have melted and the unmelted carbide particles passed along with the flame depositing them during the HVOF process, thus resulting in high strength and good adhesion between the matrix and the particles [48]. Thermal spray coatings consist of many layers of thin, overlapping, essentially lamellar particles, frequently called splats. Oxidation may occur because of the oxidizing potential of the fuel-gas mixture in flame spraying. Generally, the wear resistance of the coatings increases with their density and cohesive strength, so the higher-velocity coatings such as HVOF and particularly detonation gun coatings provide the greatest wear resistance for a given composition. In HVOF coating application, an explosive gas mixture ignites in the barrel of the spray gun, which melts a powdered coating material and propels it (with a carrier gas) at supersonic speeds toward the substrate [47].

Fracture toughness (K_{Ic}) values indicate the resistance of a material to fracture from intrinsic flaws. A variety of test methods and specimen geometries are used, so caution must be exercised when comparing reported values from different manufacturers. Fracture toughness increases with both increased cobalt content or WC grain size [50]. Vickers hardness number (VHN) values range

from 800 to 2000 VHN. The precision and accuracy of hardness testing is influenced significantly by the surface finish of the test piece, parallelism between top and bottom surfaces, and the quality of hardness standards and diamond penetrators. Density varies inversely with cobalt content, as shown in Figure 2.4. Porosity levels also influence density [50].

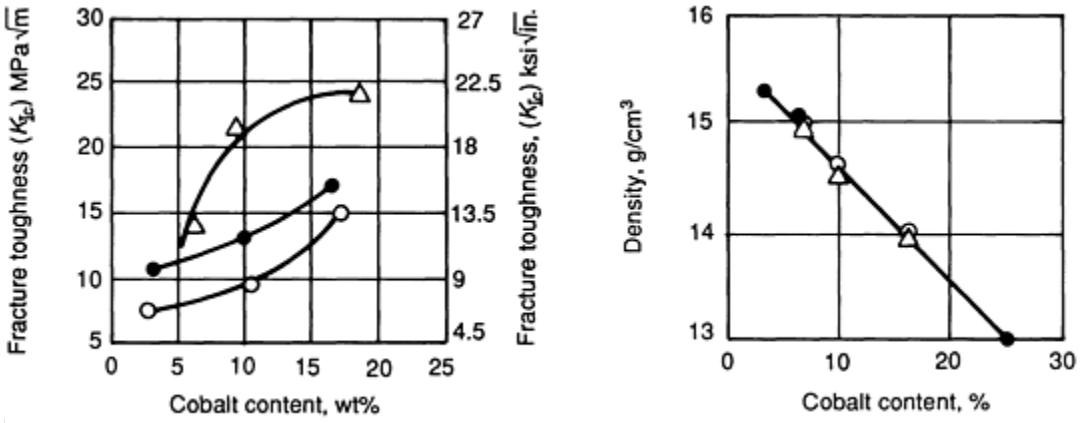

Figure 2.4. Effect of Co content on fracture toughness and effect of Co content on density [50].

Hardness increased by a combination of grain size decrease, and to a greater extent, solid solution strengthening. Ruthenium additions are more effective in improving hardness when substituting Co than when replacing WC [49]. The mean free path decreased with increased Ru additions for sample WC-10Co-10VC and for sample WC-10Co-0.8VC the mean free path increases with increase in Ru additions [51]. Another very important parameter to assess corrosion protection of the HVOF coatings is the porosity level in the deposited layer [12].

2.4 Corrosion

Corrosion is an important surface degradation process in some applications of carbide WC-Co based hardmetals [7]. The corrosion resistance of WC-Co can be improved by some transition carbides, which are added in small amounts. Chromium carbide (Cr_3C_2), for example, added to WC-Co in amounts of about 0.5wt% markedly improves corrosion resistance [18]. Deterioration as a result of corrosion is often accepted as unavoidable, which has led to widespread lack of awareness of the importance of cost of corrosion [20].

The widespread use of WC-Co hardmetals, in which hard WC particles are bonded with metallic Co-based alloys for advanced tribological applications under harsh environmental conditions calls for a fundamental understanding of its corrosion behavior [25]. The exposed surface area of the binder (Co) phase corrodes preferentially rather than the carbide phase. Corrosion of the binder phase occurs by a pitting mechanism, and attack at the carbide/binder interfaces is exaggerated [4]. Therefore, the corrosion resistance of WC–Co hardmetals in acidic and neutral electrolytes is controlled by the corrosion resistance of the binder (Co). This is because the oxidation potential of WC is nobler than that of Co [23], and it is expected that as the binder corrosion resistance is increased, the effect of the galvanic coupling between WC and Co is reduced and corrosion of both WC and Co can take place [24]. The corrosion potential of the WC-Co hardmetal shifts to more negative values in synthetic mine water compared to sulphuric acid. The current density increases with increased polarization and pseudo passivity is not as pronounced as it is in the case of sulphuric acid [4]. Potentiodynamic measurements on WC–Co have shown that Co dissolves in acidic and neutral solutions, while it passivates in alkaline solutions and WC dissolves in alkaline solutions but not in acidic or lower pH solutions [23].

The need to withstand wear and corrosion is an old and well-recognized problem that limits the useful life of engineered components. There are several tactics to combat wear and corrosion. One direct approach is to construct components entirely from specialty wear and corrosion resistant materials, but this can be very expensive and impractical. Since wear and corrosion are surface phenomena, a coating approach can be effective for minimizing costs and maximizing the performance life of components. With the performance needs and operating conditions of today's engineered components, especially those conditions associated with high temperatures, hard coating materials with inert and refractory properties are required [21].

Thermally sprayed WC coatings exhibit poor corrosion resistance in aqueous solutions as a result of delamination of the coated layer from the substrate, mainly due to internal stresses of coated layers and interconnected pores [26]. The rate of corrosion depends upon the environment and the type of material, and it can be rapid in highly corrosive environments [27]. The corrosion resistance of WC-VC-Co grades increases with increasing Co content when polarized in H_2SO_4.

This corrosion behavior is in agreement with the straight WC-Co grades, since there is an increase in corrosion resistance with an increase in Co [30].

HVOF WC–Co coatings have been widely applied to engineering components. They have been successfully used as internal sealing faces of gate valves to overcome tribological and tribo-corrosion issues associated with leakage and jamming [22].

Cemented carbides are often confronted with deterioration problems in corrosive solutions via dissolution of the binder. Their poor corrosion resistance in aqueous solutions reduces the spectrum of their applications. The presence of aggressive chloride ions in electrolyte solution could cause increasing corrosion rates. At room temperature, cemented carbides show an excellent resistance in basic and neutral aqueous solutions. However, strong acid solutions such as hydrochloric and sulphuric acid can cause severe corrosion and material degradation. The corrosion of cemented carbides could be determined by studying the dissolution of the binder in acid and neutral solution. In alkaline solution, WC might dissolve at higher rates. Increasing the pH value can also shift corrosion potential to the more negative direction. In acidic and neutral solutions, pure WC-Co alloys could show pseudo passivity [40].

Cobalt is a member of the transition metals with main oxidation states Co^{2+} and Co^{3+} as shown in equation (1) and (2).

$$Co \longrightarrow Co^{2+} + 2e^{-} \quad \text{..... Equation 2.1}$$

$$Co^{2+} \longrightarrow Co^{3+} + e^{-} \quad \text{..... Equation 2.2}$$

The Co^{3+} ion is unstable and can be reduced to a more stable Co^{2+}, and Co^{3+} can be disregarded for the consideration of the corrosion behaviour in acid solutions. Cobalt corrodes actively in acidic media and oxide formation occurs at pH levels around 7 in oxygenated environments.

Passivity is defined as the loss of chemical reactivity experienced by certain metals and alloys under certain environmental conditions. Passivity is caused by the formation of a thin protective hydrated oxide. The corrosion product surface film act as a barrier to the anodic dissolution reaction. Figure 2.5 illustrates the typical behaviour of a metal that demonstrates passivity effects.

The behaviour of this metal can be conveniently divided into three regions: active, passive and transpassive. In the active region the behaviour region the behaviour of this metal is identical to that of the normal metal. If more oxidising agent is added, the corrosion rate will decrease and it will be the beginning of passive region. At very high concentrations of oxidisers the corrosion rate again increases, and it will proceed to trans-passive region [28].

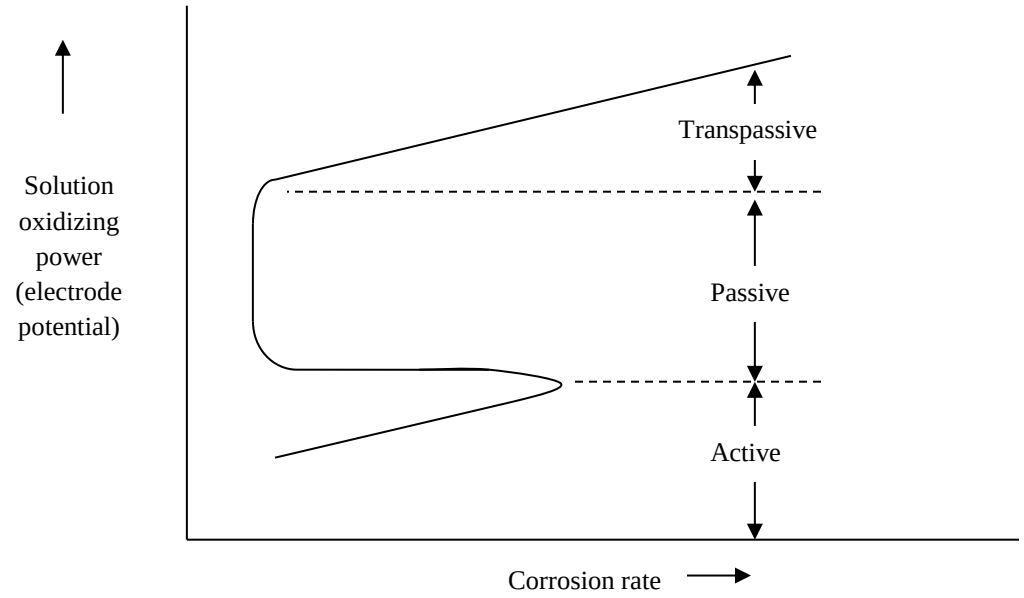

Figure 2.5. Corrosion characteristics of an active metal as a function of solution oxidising power [28].

2.4.1 Corrosion of WC-Co hardmetals

Electrochemical reactions are usually discussed in terms of the change in valence that occurs between the reacting elements, that is, oxidation and reduction. Oxidation and reduction are commonly defined as follows. Oxidation is the removal of electrons from atoms or groups of atoms, resulting in an increase in valence, and reduction is the addition of electrons to an atom or group of atoms, resulting in the decrease in valence.

Electrochemical reactions or oxidation-reduction reactions can be represented in terms of an electrochemical cell with oxidation reactions occurring at one electrode and reduction occurring at the other electrode, electrochemical reactions are often further defined as cathodic reactions and

anodic reactions. By definition, cathodic reactions are those types of reactions that result in reduction, such as:

$M^{2+} + 2e^- \longrightarrow M(s)$ ..... **Equation 2.3**

Anodic reactions are those types of reactions that result in oxidation, such as:

$M(s) \longrightarrow M^{2+} + 2e^-$ ..... **Equation 2.4**

This metal/aqueous interface is complex, as is the mechanism by which the reactions take place across the interface. Because the reduction-oxidation reactions involve species in the electrolyte reacting at or near the metal interface, the electrode surface is charged relative to the solution, and the reactions are associated with specific electrode potentials.

Thermodynamic studies and calculations can be used to predict the direction of a reaction and to predict whether corrosion is possible or not under given conditions. Thermodynamics and electrochemistry are very important in understanding and controlling corrosion, since nearly all metallic corrosion processes involve transfer of electric charge in aqueous solutions [32 and 33].

Alternative to electrochemical methods are non-electrochemical methods, such as immersion corrosion tests and solution analysis. These are valuable where corrosion products are non-adherent and when knowledge of the corroding system at equilibrium is of importance. They require relatively long exposure periods for the results to be meaningful. Quantitative analysis of potentiodynamic polarisation is can be done by using either the Tafel method or linear polarisation resistance, appropriately known as the Stern-Geary method [48].

Corrosion resistance is not usually considered a prime requirement of hardmetals, but it is important in the use of hardmetals in mechanical seals and valves in industrial pumps and in seawater [39]. Remarkable corrosion resistance of alloys containing small amounts of noble metals relies on the principle that the high exchange-current density for the reduction of hydrogen can shift the corrosion potential of the alloy to a value in the passive region, causing it to passivate spontaneously [2].

Corrosion resistance depends on many factors. It is a complete and comprehensive study and requires knowledge of several fields of scientific knowledge as indicated in Figure 2.6.

Thermodynamics and electrochemistry are very important in understanding and controlling corrosion. Thermodynamics which is a study and calculations indicates the spontaneous direction of a reaction and thermodynamics calculations can determine whether corrosion is possible or not possible under given conditions. Nearly all metallic corrosion processes involve transfer of electric charge in aqueous solutions that is the reason why electrochemistry study is important for understanding corrosion mechanism [28 and 58].

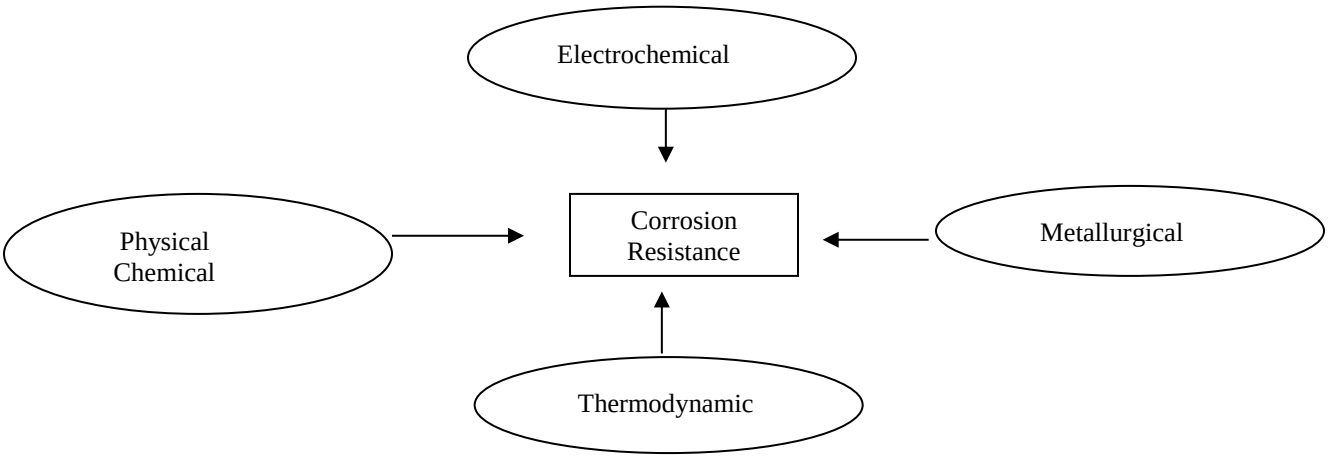

Figure 2.6. Factors affecting corrosion resistance of a metal [58].

The corrosion resistance of carbides is limited by the susceptibility of the cobalt binder to chemical attack, although there are some corrosive media that attack WC. The corrosive media typically dissolve the cobalt binder from the matrix, leaving behind a weak, unsupported skeleton of tungsten carbide grains, which are easily abraded away. The corrosion resistance of straight WC-Co alloys is, in general, inversely related to that of the binder content as shown in Figure 2.7 [50].

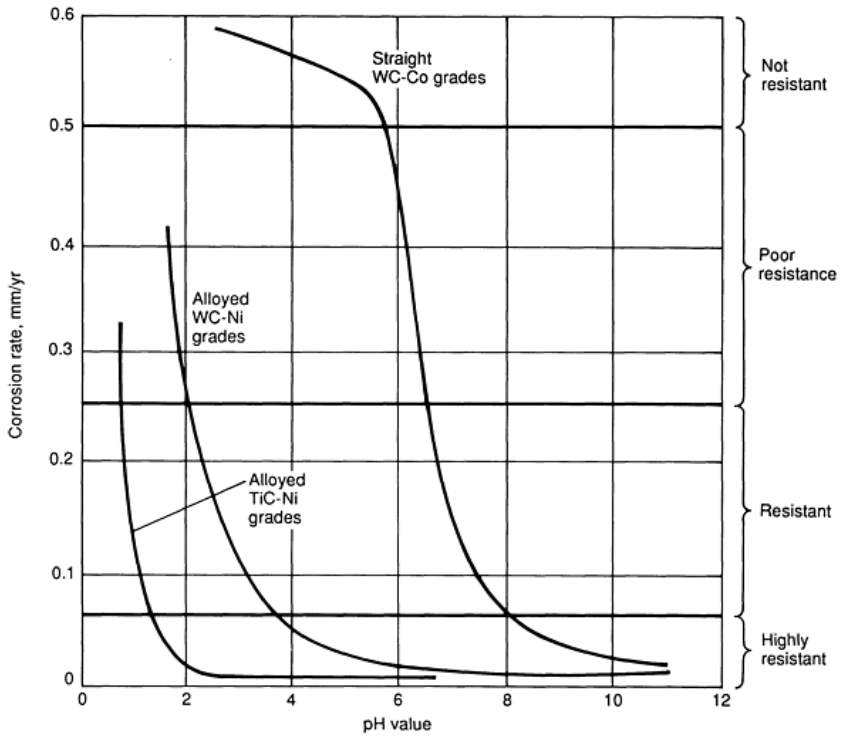

Figure 2.7. Corrosion resistance of cemented carbides [50].

2.4.2 Effect of Ru additions on corrosion

Addition of Ru on duplex stainless steel has an effect on the open-circuit corrosion potential in a positive way. The OCP was displaced towards more noble values by the small ruthenium additions in both the sulphuric and hydrochloric acid solutions. The alloys containing ruthenium passivated spontaneously in 1M H_2SO_4 at room temperature, while they all corroded actively in the 1M HC1 solution at the same temperature. Ruthenium inhibit the anodic dissolution cathodically modified alloys, this was observed by the decreases in the corrosion current densities and critical current densities in the two reducing acid media [3]. Corrosion electrochemical tests of sintered WC-Co-Ru alloys in sulphuric acid showed that the OCP values of the samples increased with an increase of ruthenium. This positive shift of potentials could be due to the spontaneous formation of a passive film that would decrease the dissolution of the samples as the ruthenium content is increased. This implies that dissolution of the samples decreases with time and this is probably due to spontaneous passivation [1].

Research done by Nelwalani [5] on the effect of Ru additions on WC-Fe plasma transferred arc hardfacing coating in synthetic mine water showed that at lower pH of 3 the erosion-corrosion results of the Ru alloyed coatings are much better than the sample with no Ru. However, the alloyed coatings did not show much of an increase at the lower pH level but remained at a very similar average penetration rate indicating that the more corrosive medium did not have an effect on the erosion-corrosion. At the lower pH the addition of Ru actually caused a decrease in the corrosion rate of the hardmetal over time for Ru content above 0.7wt%, whereas the unalloyed coating showed a significant increase in corrosion rate after a 12 hours exposure.

2.5 Wear of hardmetals

Wear is generally quantified by wear rate. Wear rate is defined as the volume or mass of material removed per unit time or per unit sliding distance. Figure 2.8 shows different stages of wear. Wear rate may start low and increase or start high and then decrease [46].

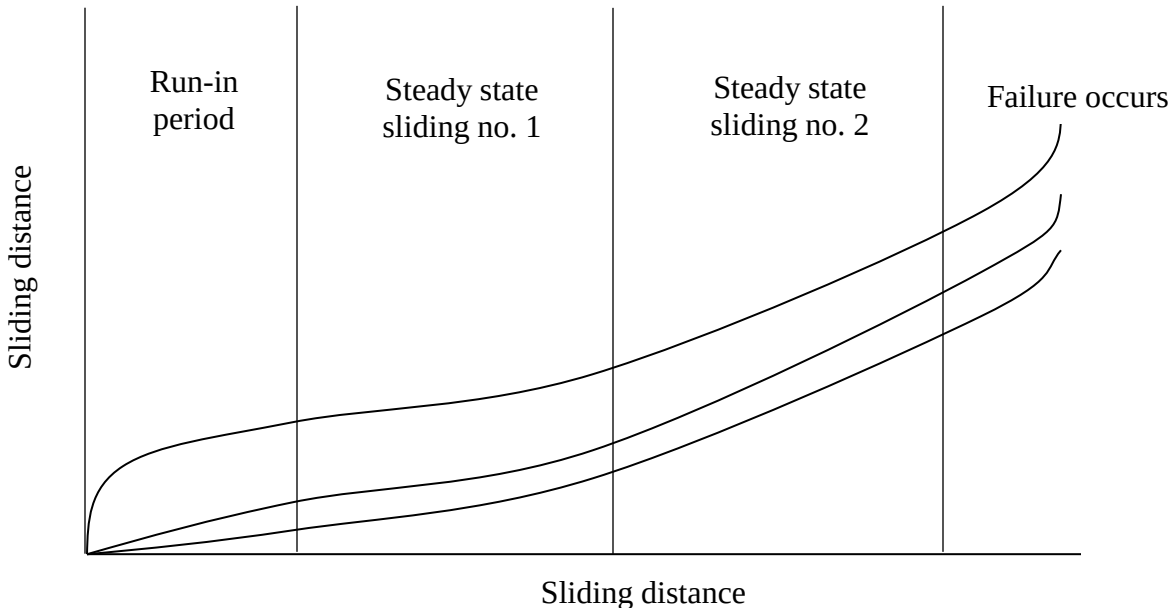

Figure 2.8. Hypothetical case of wear volume as a function of sliding distance showing run-in stage, steady-state and failure regions [46].

The initial period during which wear rate changes is known as the run-in or break-in period. Wear during run-in depends on the initial material structure and properties and on surface conditions

such as surface finish and nature of any film present. In this region the surface roughness is modified to a steady-state condition by plastic deformation. The wear rate is dependent upon the counterface or matting material, surface preparation, and operating conditions [46].

Friction and wear between two moving surfaces depend on mechanical properties of the mating materials such as: hardness, elastic modulus, fracture toughness; other physical and chemical properties such as: thermal conductivity, surface energy, adsorption characteristics, chemical reactivity; surface conditions such as: roughness and apparent area of contact; and operating conditions such as: load, speed, interface temperature, and environment. Various friction mechanisms such as adhesion and ploughing which contribute to friction and wear are strongly affected by the properties of mating surfaces and operating conditions. Surface roughness of mating surfaces and area of contact between these surfaces play a key role in deciding friction [21].

Thermally sprayed WC–Co coatings of thickness of 200–400 μm are widely used to protect the components from sliding, abrasion, fretting and erosive wear as they offer an effective and economic method of conferring wear resistance without compromising other attributes of the component [28]. The sliding wear mechanism for the HVOF sprayed WC–Co coatings shows the continuous wear of binder and WC grains, removal of entire WC grains and removal of splats. These mechanisms operated in all coatings to different degrees, depending on the coating properties that resulted from the processing parameters [31].

Binder dissolution appeared to be the rate-governing step in determining volume loss in acidic environments. Under mildly acidic conditions evidence of WC grain fracture and correspondingly less of binder dissolution. Exposure to the alkali solution has the least wear rate. Volume loss increased with decreasing pH of the medium employed [13].

2.5.1 Sliding wear

Sliding wear is when two solid surfaces slide over each other. In most applications sliding surfaces are lubricated in some way, and the wear that occurs is then termed lubricated sliding wear. In other applications surfaces slide in air without any lubricant and the resulting wear is called dry

sliding wear [45]. Generally, wear mechanisms for the coatings against the balls are very similar. Smearing of worn particles**,** ploughing of wear particles, which had contributed to groove formation. Preferential binder removal, carbide grain cracking and fragmentations, grain pull-out, adhesion and formation of thin tribo-layer oxides during wear. The binder removal occurs first, followed by subsequent carbide grain cracking and carbide grain pull-out. The grooves formed are normally parallel with the sliding direction [11]. The ball wear rates increase with increase in sample hardness, since the higher hardness samples act as the abrasive body on the balls [53].

2.6 Tribo-corrosion

Tribo-corrosion occur when there is friction between two or more bodies in a corrosive environment. Tribo-corrosion is a combined action of wear and corrosion. Tribo-corrosion is an irreversible transformation of a material resulting from simultaneous physical-chemical and mechanical surface interactions in a tribological contact [63]. Pumping corrosive liquids, tribochemical wear is another problem arising especially for Co-bonded carbide material [9]. Coating composition, microstructure, defect level, adhesion, cohesion and substrate properties are seen as some of the critical elements in coating performance when subjected to tribo-corrosion contacts [43]. The material loss is frequently found to be greater than would be expected, due to the corrosive nature of the carrier medium. The conjoint action of abrasion and a corrosive medium can be encountered in industries such as power generation, construction, mineral extraction and processing; and wood processing. Reducing binder volume fraction reduces the wear rate, but in turn also reduces fracture toughness and impact resistance [13].

Understanding how coatings perform under these tribo-corrosion conditions is essential if the service life of equipment is to be predicted and to allow service life to be extended. There is demand for a much better understanding of surface degradation processes particularly when tribological components are operating in corrosive environments [43]. Equation 2.5 shows how wear-corrosion relates to mechanical wear and electrochemical corrosion.

Wear-corrosion = mechanical wear processes + electrochemical (and/or chemical) response…… **Equation 2.5**

Tribo-corrosion degradation affects components in numerous industries such as mining, automotive, food, nuclear, offshore, marine and biomedical just to name a few. Tribo-corrosion is a complex discipline involving interactions between wear and corrosion. Simple mechanistic models based on electrochemical theory of corrosion provide a yet rudimentary but nevertheless useful tool for understanding tribo-corrosion as shown in Figure 2.9 [43].

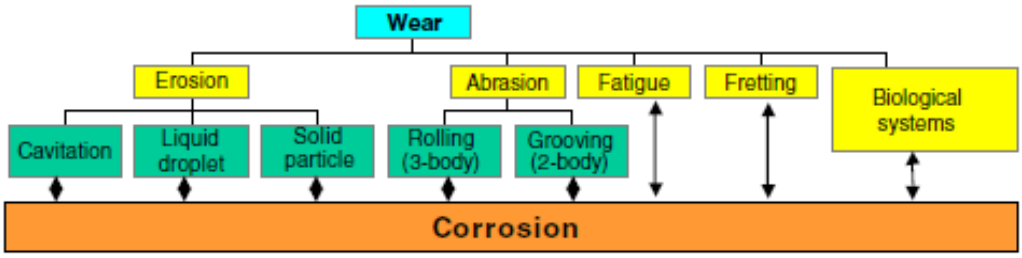

Figure 2.9. Possible interactions between corrosion and the various wear mechanisms [43].

Typical arrangements involving an antagonist rubbing against a flat plate are shown schematically in Figure 2.10. The antagonist may be a cylindrical pin (I), a truncated cone (II), or a sphere (III). A flat pin surface has the advantage that the nominal contact area is well defined. However, the alignment of the contacting surfaces is extremely critical for the reproducibility of results. Spherical contacts are free of alignment problems, but the nominal contact area is less well defined and it may vary during the experiment due to formation of a wear scar. To allow for potential control, the sliding contact must be contained in an electrolyte solution [56].

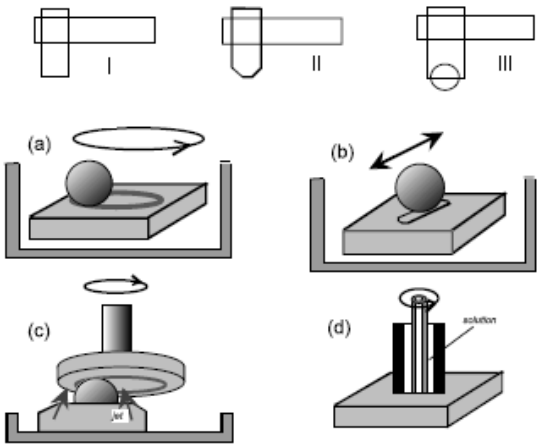

Figure 2.10. Experimental arrangements used in tribo-corrosion studies [56].

In tribological contacts one often observes material transfer from the softer to the harder body, leading to an alteration of the friction and wear conditions in the contact. The extent of material transfer depends on the prevailing electrochemical conditions among others. Therefore, electrochemical conditions can affect mechanical wear rate [56].

2.7.1 Tribo-corrosion of hardmetals

Surface roughness plays an important role in tribo-corrosion of passive metals because it affects the rate of depassivation and of mechanical wear. When a hard body rubs against a softer body the surface roughness of the softer body will adapt rapidly to the rubbing conditions but not that of the hard body [56]. Figure 2.11 shows the tribo-corrosion is inter-connected to material being tested, electrochemical of the system, mechanical interactions, and solution being used.

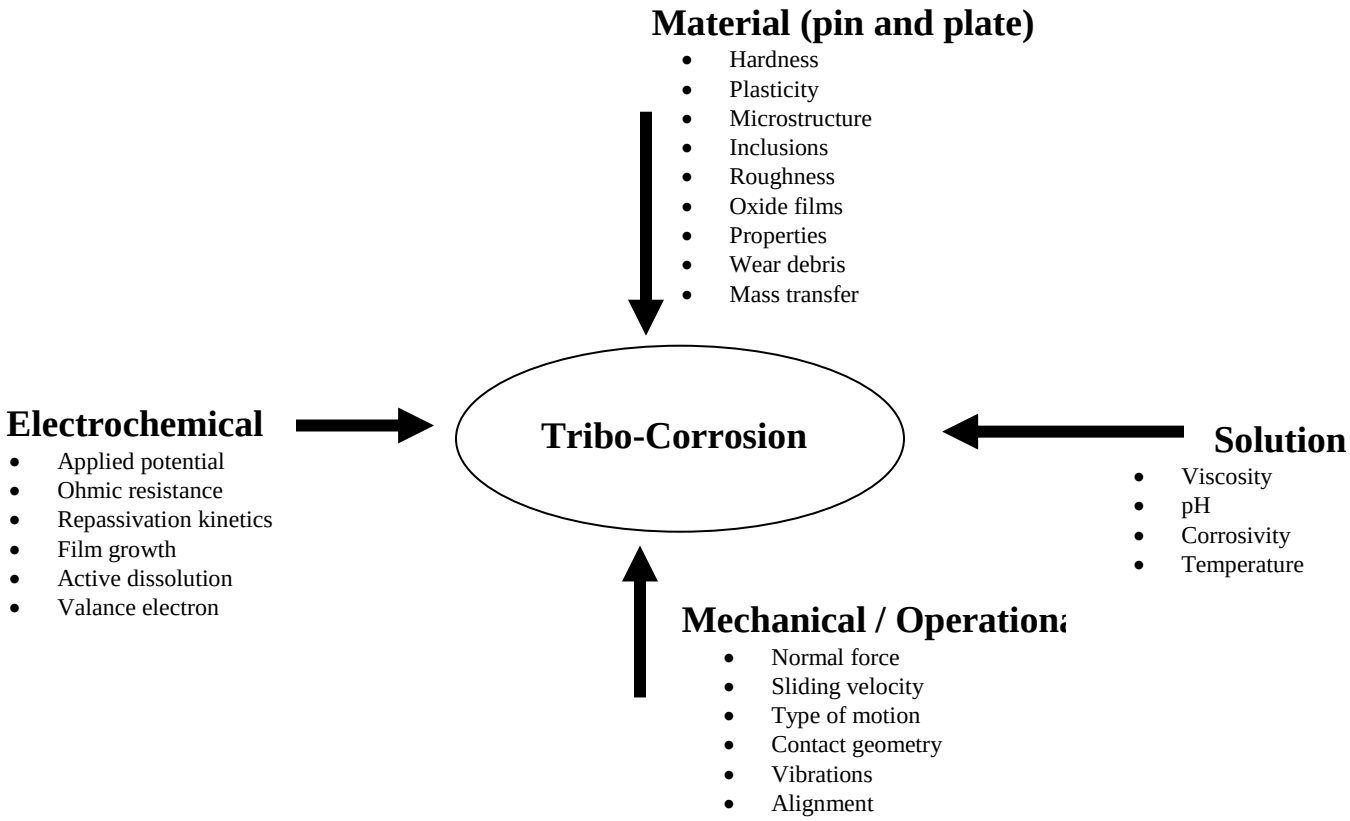

Figure 2.11. Schematic showing four types of parameters, which affect the tribo-corrosion behaviour of a sliding contact (tribo-corrosion system) under electrochemical control [56].

Wear–corrosion resistance in coatings can be improved by increasing corrosion resistance and wear resistance of the coatings and those can be enhanced by; improving the binder integrity, improving the hard phase stability, and improving the integrity of the hard phase/binder interface [11]. Electrochemical processes in coatings are directly affected by the substrate reactivity, and degradation mechanism. In tribo-corrosion of coatings, the wear mechanism is not only governed by surface tribo-corrosion phenomena, but by the corrosion properties of the coating as well. When chromium is alloyed in the metal matrix, tribo-corrosion behaviour of WC-Co based systems is enhanced, and tribo-corrosion rates decreases [57].

Chapter 3 : Experimental procedure

3.1 Introduction

The research was done by first mixing the Ru powder with WC-10Co-4Cr powder which is called 1350VM/WC-731-1 commercially and then manufacturing HVOF coatings from the mixed powders. Electrochemical corrosion tests, tribo-corrosion and sliding wear tests were done on the coatings to compare the coating performance in synthetic mine water at pH of 3 and 1. Tribo-corrosion tests were carried out using a machine self-developed in our laboratories and it was connected to the potentiostat. Electrochemical corrosion tests were done on a potentiostat instrument. A ball-on-disc friction wear test was also done on coatings to determine the wear rates and wear coefficient of friction for different coatings. FESEM instrument was used to determine powder morphology and to analyse the coating surface before and after corrosion, tribo-corrosion and sliding wear tests. Chemical characterisation of the samples was done using a FESEM coupled with an energy dispersive x-ray spectroscopy EDS unit to determine the elemental composition of the samples. The techniques used are described briefly in the next sections. Figure 3.1 shows the experimental flow-sheet.

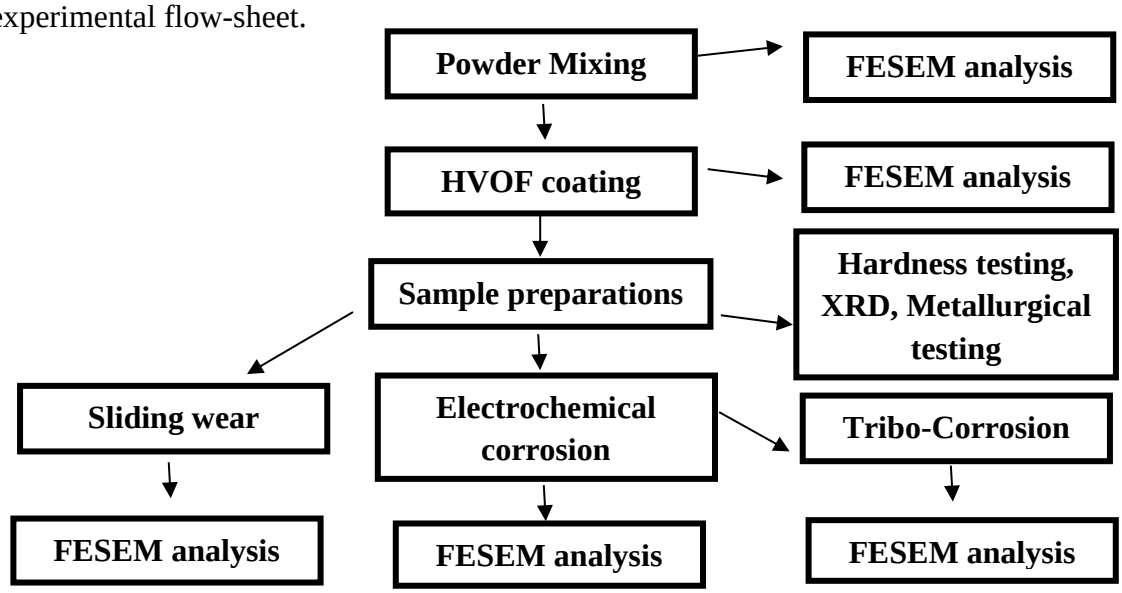

Figure 3.1. Experimental setup flow-sheet.

3.2 Powder preparation

Hardmetal powder 1350VM/WC-731-1 which was supplied by WearTech (pty)LTD was mixed using turbulence mixed with different wt% of Ru to produce sets of WC-10Co-4C-(x) Ru powders with compositions as shown in Table 3.1. The as received 1350VM/WC-731-1 powder was agglomerated and sintered and had average grain size bigger than 16µm and smaller than 45µm and ruthenium powder used had average grain size of 50 µm. The powders were analyzed using SEM to determine the morphology of the powders.

Table 3.1. Powder compositions.

Sample	%WC	%Co	%Cr	%Ru
WC-10Co-4Cr	Bal	10	4	0
WC-10Co-4Cr-0.5Ru	Bal	10	4	0.5
WC-10Co-4Cr-1Ru	Bal	10	4	1
WC-10Co-4Cr-2Ru	Bal	10	4	2

3.3 HVOF coating process

The supplied mild steel was sand blasted prior to applying the coat on it. This was done to clean the substrates. The mild steel substrates used had dimensions of 100mm X 100mm X 20mm. The coating was done using HP/HVOF JP 5000 thermal spray system at Thermaspray (Pty). Figure 3.2 shows the mild steel substrate used.

Figure 3.2. Mild steel sample used as substrate.

3.4 Material characterization

Coatings were sectioned using a CBN (Cubic Boron Nitride) cutting disc because of their high hardness. The cutting machine used was an ATA Brillant 200. Samples for metallography and hardness testing were mounted using an ATA Opal 410 hot mounting press with polyfast resin. ASTM standard E3-95(1995) was used as a guide for metallographic sample preparations. A Carl Zeiss Sigma Field Emission Scanning Electron Microscope (FESEM) equipped with Oxford x-act EDS detector was for sample micrographs.

Samples for metallography and hardness testing were ground and polished using ATA Saphir 520 automatic grinding and polishing machine. Samples were ground from 220 grit followed by 600 grit and then finally by 1200 grit using diamond grinding discs. Samples for hardness and cross-section FESEM evaluations were polished to 1µm mirror finished. After polishing some samples were etched using Murakami reagent at room temperature for 30 seconds followed by a rinse with ethanol and drying with a drier.

3.4.1 Coating porosity, contiguity, binder mean free path and hardness

Coating porosity levels were measured from FESEM micrographs at low magnifications from coating cross-sections using ImageJ software. The hardness was obtained using a Future-Tech FM 800 micro Vickers hardness tester with a load of 500 g and dwell time of 15 seconds. Indents were made on coating cross-sections with ten measurements made for each coating and the average hardness value determined from there. FESEM micrographs at high magnifications were used to determine the WC grain size of the coatings. Grain size measurements were done according to Intercept Method ASTM E 112. The contiguity, C, was determined according to Equation 3.1:

$$C = \frac{2N_{WC/WC}}{\left(2N_{WC/WC} + N_{WC/Co}\right)} \quad \text{..... Equation 3.1}$$

where $N_{WC/WC}$ and $N_{WC/Co}$ are the number of WC grains touching and the number of non-touching WC grain boundaries, respectively. The binder mean free path, λ, was calculated according to Equation 3.2:

$$\lambda = \bar{d}\left[\frac{V_b}{(1-V_b)(1-C)}\right] \quad \text{.....Equation 3.2}$$

Where $\bar{d}$ is the mean grain size and V_b the volume fraction of the binder.

3.5 Electrochemical characterization

Electrochemical corrosion tests were done in a three electrode cell. The cell consists of a graphite counter electrode and a Ag/AgCl, 3M KCl, reference electrode and the working electrode as the coating surface. Corrosion behavior of the samples were investigated in synthetic mine water solutions at the pH of 3. Synthetic mine water solution was prepared according to the work of Allen [29] and for Machio [52], the concentration is shown in Table 3.2. Electrochemical measurements were carried out at room temperature (25 ± 1°C) with a Metrohm Autolab potentiostatic PGSTAT302 computer controlled using the Autolab Nova version 1.11 software. All electrochemical corrosion tests were done on as coated samples. Figure 3.3 shows the potentiostat used for the experiment and Figure 3.4 shows the electrochemical setup that was used for the tests.

Open circuit potential (OCP) measurements were done to assess the thermodynamic stability of the coated samples. OCP were done at zero applied current and they were done for period of 12 hours per sample. Polarisation was done at a scan rate of 0.005 mV/s from -0.5 V to 1.2V potentials for all the samples and corrosion rates were calculated from polarisation curves obtained potentiodynamic curves. Post corrosion examination of the corroded surfaces were done using FESEM.

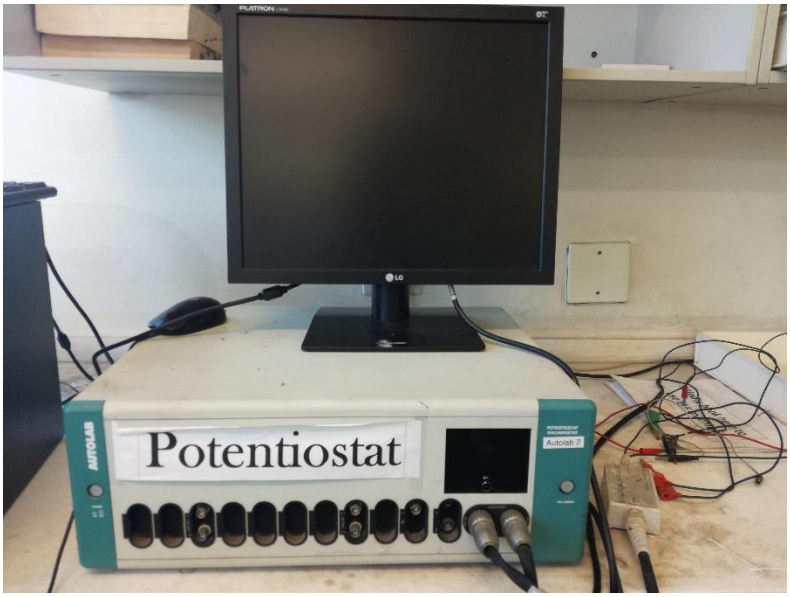

Figure 3.3. Metrohm Autolab potentiostat used for the corrosion and tribo-corrosion experiment.

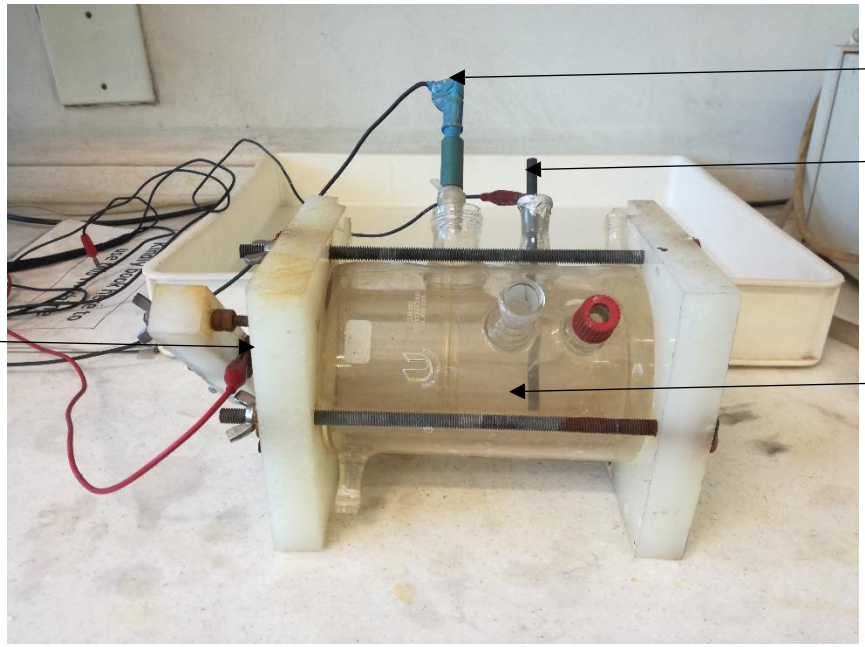

Figure 3.4. Electrochemical corrosion cell used for the test.

Table 3.2 The chemical composition of synthetic mine water [29] and [52].

Salt	Salt Concentration (mg/l)
Na_2SO_4	1237
$MgSO_4$	199
$CaCl_2$	1038
NaCl	1380

3.6 Tribo-corrosion characterization

Tribo-corrosion tests were carried out using a machine self-developed in our laboratories. The design of self-developed tribo-corrosion machine is shown in Figure 3.5 and the design setup is shown in Figure 3.6. The setup used is a pin-on-disk configuration, where the specimen rotate around the transmission shaft that is in contact with a counter-face material with the tribo-corrosion equipment connected to the potentiostatic machine. Alumina ball with a diameter of 6mm was used as a pin. Synthetic mine water at pH of 1 was used as an electrolyte at room temperature and the corrosion current density and corrosion potential was measured to determine the effect of sliding the samples with different compositions. The samples were tested as coated without any grinding or polishing. Tribo-corrosion equipment was connected to the potentiostat to be able to determine the tribo-corrosion characteristics from the electrochemical data.

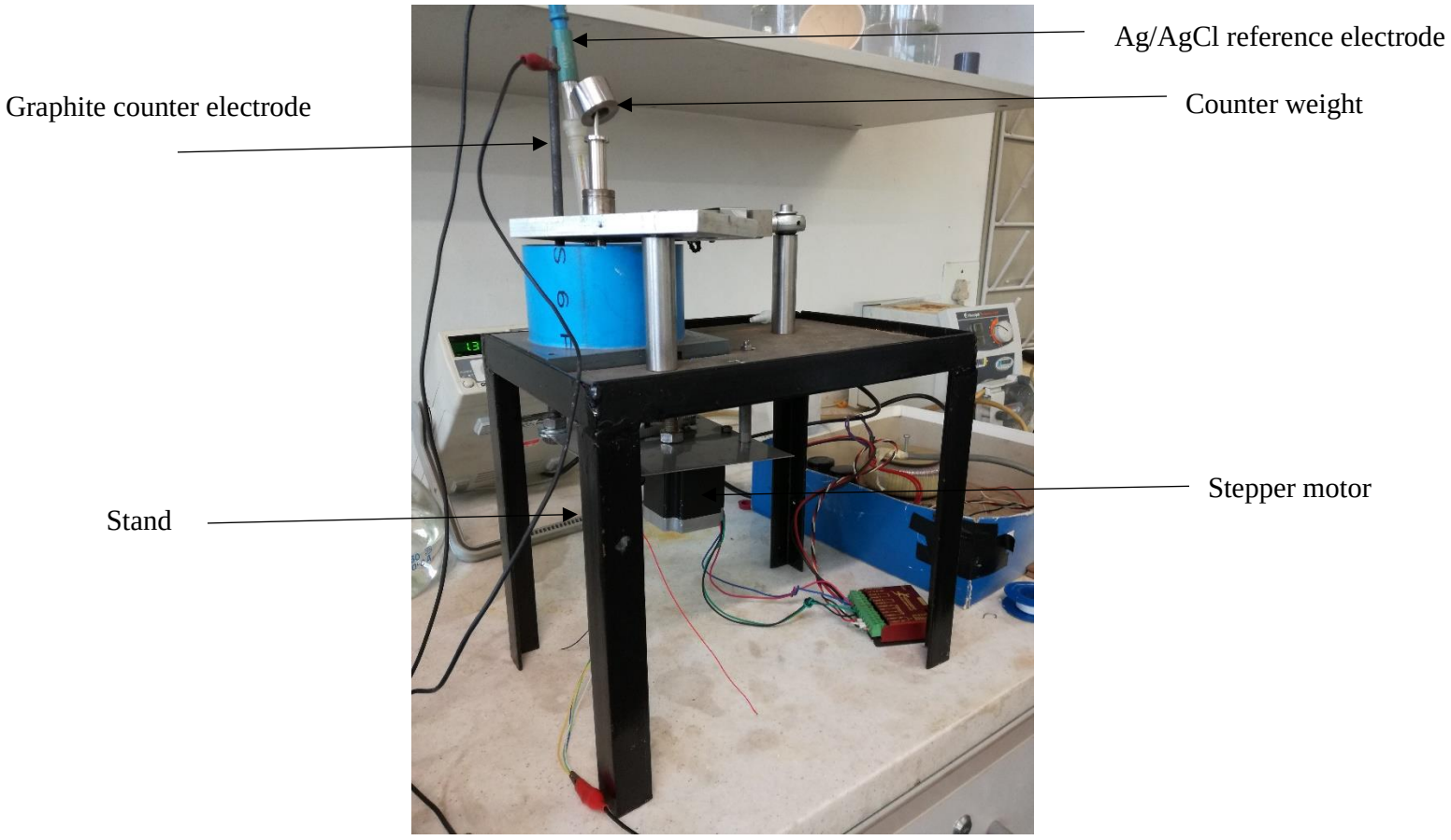

Figure 3.5. Self-developed tribo-corrosion equipment used for the test.

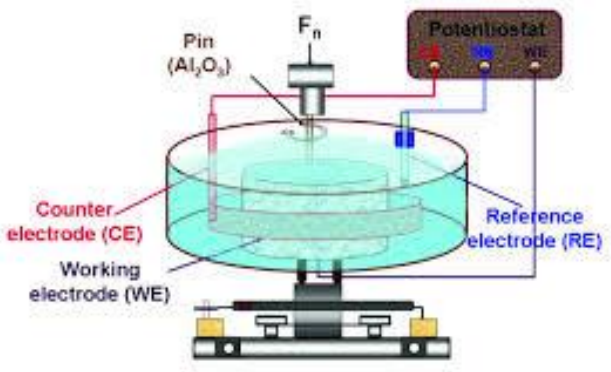

Figure 3.6. Tribo-corrosion setup [60].

3.7 Friction and sliding wear

A CSM Tribometer ball-on-disc instrument was used to perform friction and sliding wear for all coatings. A 6 mm diameter Cr steel ball was used and the load of 10 Newtons was used. The test parameters are listed in Table 3.3. The coatings were tested as coated without any grinding or polishing as the sample coatings was too thin to be grinded and polished and polishing will remove the whole coating. Figure 3.7 shows the Tribometer used for the experiment.

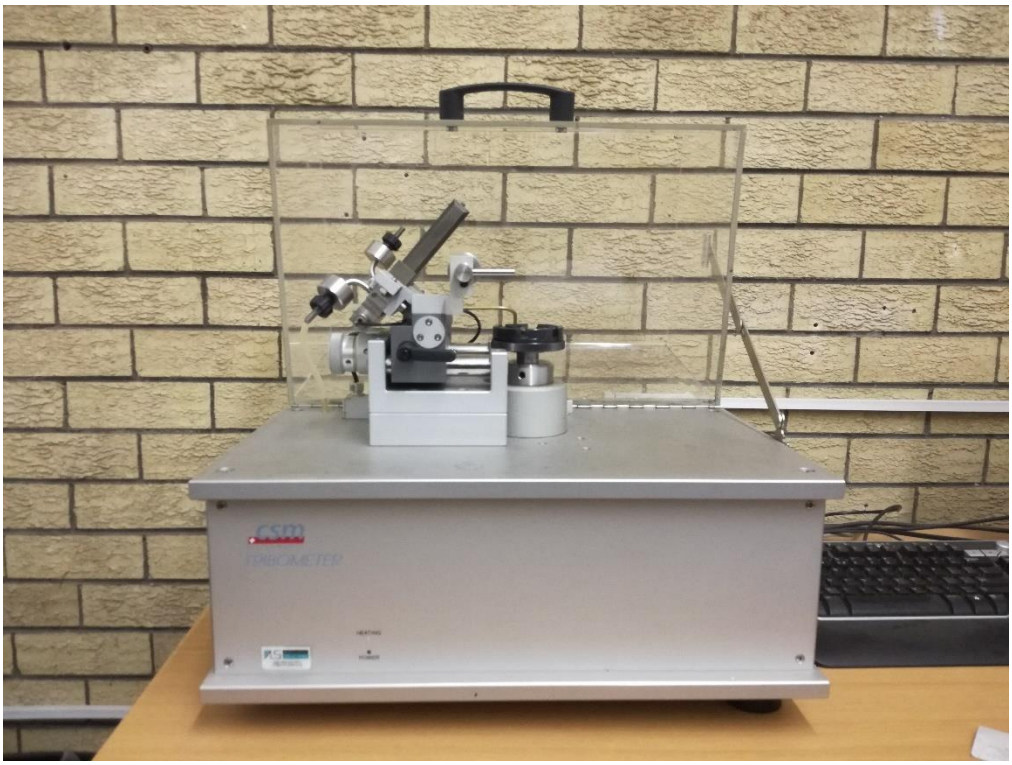

Figure 3.7. CSM Tribometer used for sliding wear testing.

Table 3.3. Friction and sliding wear test parameters.

Test conditions	**Value**
Acquisition radius	2.0 mm
Linear speed	0.12 m/s
Normal Load	10 N
Sliding distance	300 m
Acquisition rate	30 Hz
Temperature	Room temperature

3.8 Scanning electron microscopy (SEM)

Morphological and qualitative analyses of the powders and coatings were performed using a Carl Zeiss Sigma FESEM equipped with an Oxford x-act detector for Energy Dispersive X-ray Spectroscopy (EDS) analysis. Figure 3.8 shows the FESEM used in this research.

Figure 3.8. Carl Zeiss Sigma Field Emission Scanning Electron Microscope.

3.9 X-ray diffraction (XRD)

XRD analysis were done on HVOF coatings to determine the phases formed during the HVOF coating process. The XRD was done on a Bruker D2 phaser with LynxEye detector and the XRD matching was done using EVA software.

Chapter 4: Microstructure and mechanical properties results

4.1 Introduction

This chapter presents the results obtained from characterization and testing of HVOF coated samples. The as received powder's morphology were analyzed using FESEM. HVOF process was used to apply WC-Cr-Co-Ru mixed powders to steel substrates. Thereafter the coated steel substrates were sectioned to workable size sections for different test. Surface microstructures and cross-sectional microstructures of the coatings were obtained using FESEM. XRD equipment was used to determine phase compositions.

4.2 Powder morphology

The micrographs of the starting WC-10Co-4Cr powders are shown in Figures 4.1–4.2. The as-received WC-10Co-4Cr powder had a spherical shape were mainly agglomerates of WC-10Co-4Cr powders. The micrographs showed that the as received powders were very porous and had a wide size distribution as in Figure 4.1. As received powder elemental maps shown in Appendix A2.

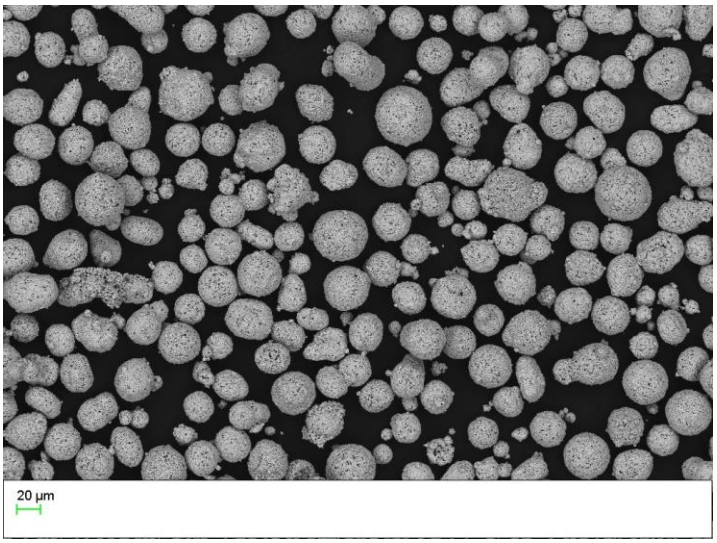

Figure 4.1. FESEM micrograph of as-received WC-10Co-4Cr powder, showing spheroidal agglomerated particles with diameter range from -10 ~60µm at low magnification.

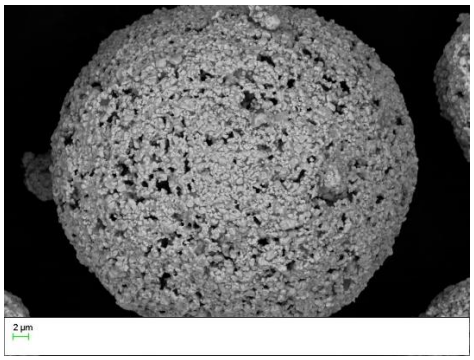

Figure 4.2. FESEM micrograph of as-received WC-10Co-4Cr powder, showing smooth surface with high percentages of porosity at higher magnification.

The as-received Ru powder a sponge-like structure, irregular shaped particles and had wide size distribution (Figure 4.3 and Figure 4.4).

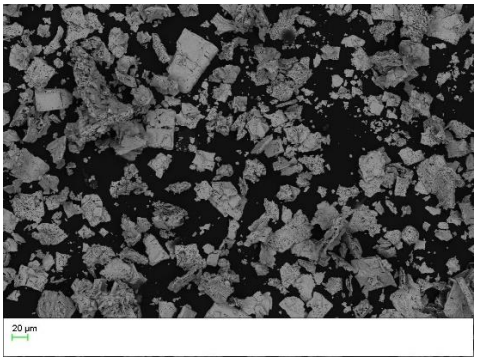

Figure 4.3. FESEM micrograph of as-received Ru powder, showing irregular shaped particles with a wide range in size at low magnification.

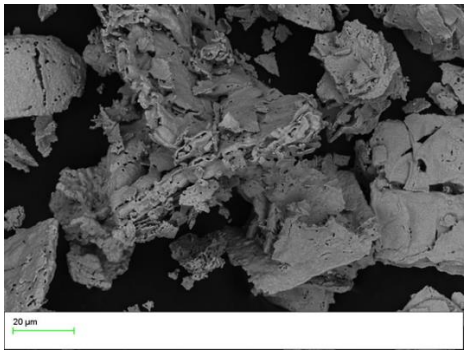

Figure 4.4. FESEM micrograph of as-received Ru powder, showing a sponge like structure with some pores.

Figure 4.5 shows the powders after mixing for 2 hours in a turbulence mixer. The distribution of Ru powder was poor and the size of Ru particle attributed to the poor distribution. It can be seen in the Figure 4.5 that a particle of Ru is surrounded by several particles of WC-Co-Cr particles. Many particles of WC-Co-Cr were not close to Ru particles. Appendix A5 shows the EDS composition of the powder.

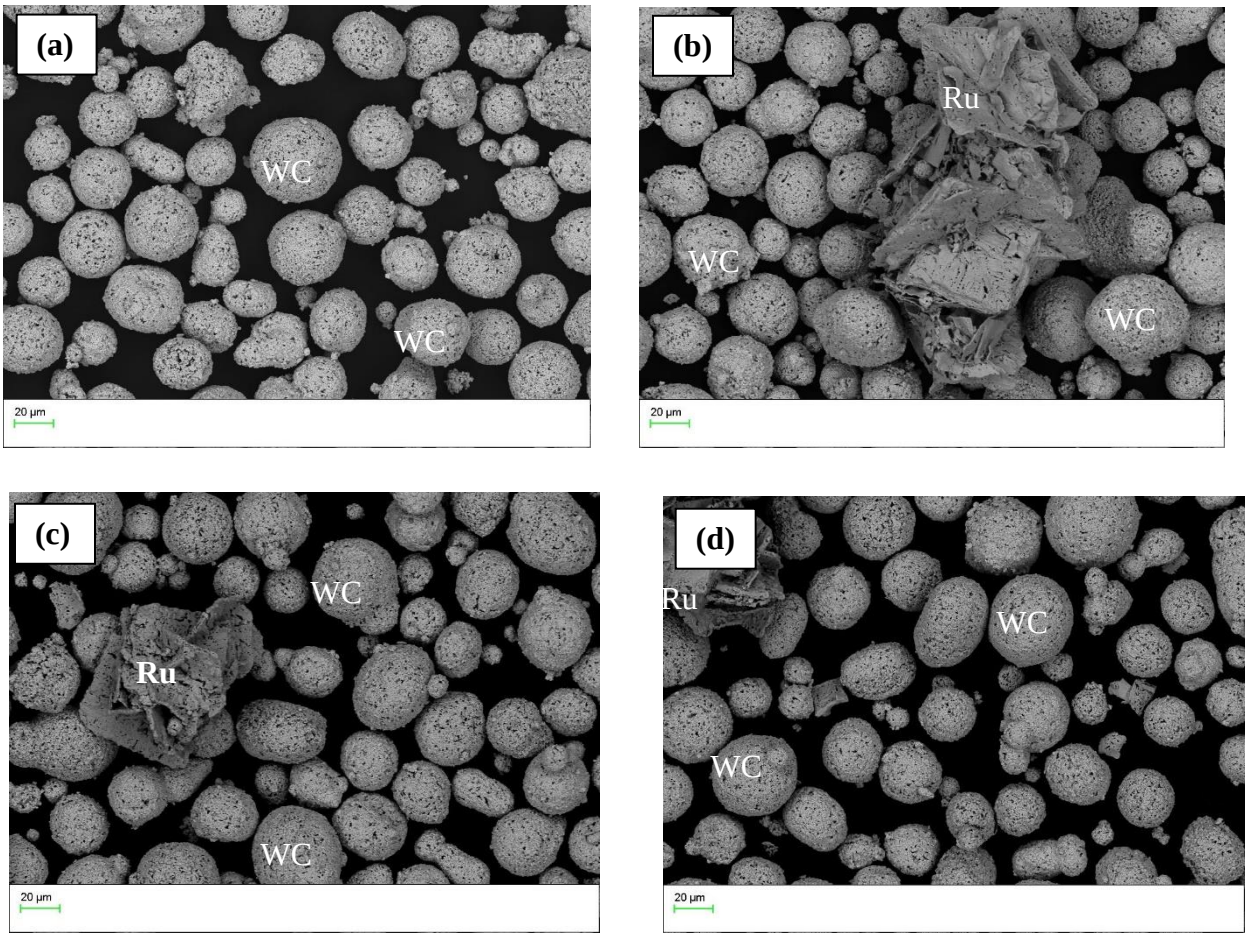

Figure 4.5. FESEM micrograph showing mixed powders ready for HVOF coating at low magnifications. (a) WC-10wt%Co-4wt%Cr powder (b) WC-10wt%Co-4wt%Cr-0.5wt%Ru (c) WC-10wt%Co-4wt%Cr-1wt%Ru (d) WC-10wt%Co-4wt%Cr-2wt%Ru.

4.3 High Velocity Oxygen Fuel (HVOF) Coating results

4.3.1 As received coating surfaces

Figure 4.6 shows the as received coating surface FESEM micrographs for all the coatings. The coating surfaces for all the samples were very porous, inhomogeneous and rough. Aggregates of particles and solidified liquid phase as a results of heating in the spray gun were evident in all the micrographs.

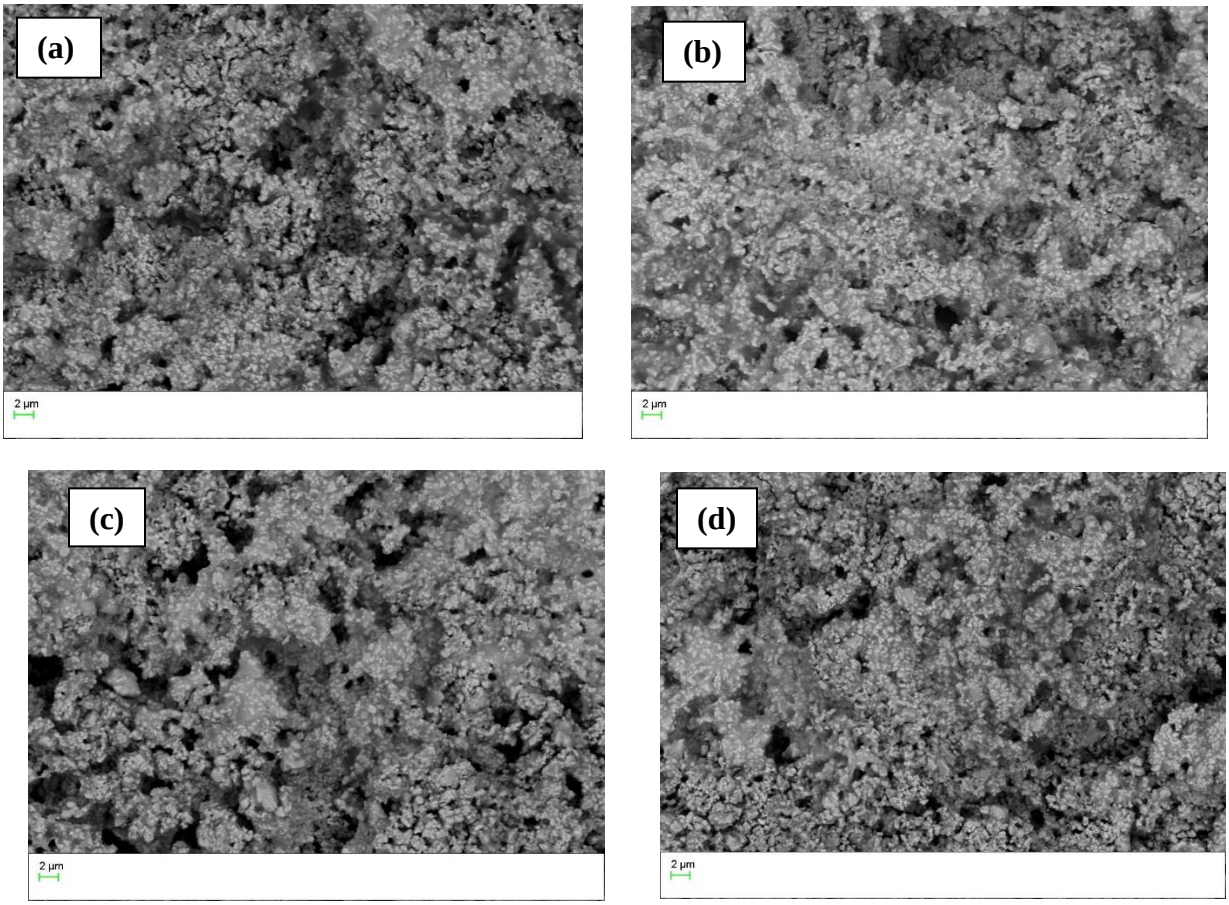

Figure 4.6. FESEM micrograph showing as received coating surfaces. (a) WC-10wt%Co-4wt%Cr (b) WC-10wt%Co-4wt%Cr-0.5wt%Ru (c) WC-10wt%Co-4wt%Cr-1wt%Ru (d) WC-10wt%Co-4wt%Cr-2wt%Ru.

Figure 4.7 shows the FESEM elementals maps taken on the surface of a coating with no Ru. The distribution of W, Co, and Cr was very good as seen on the maps. It can also be seen that the sample was very porous.

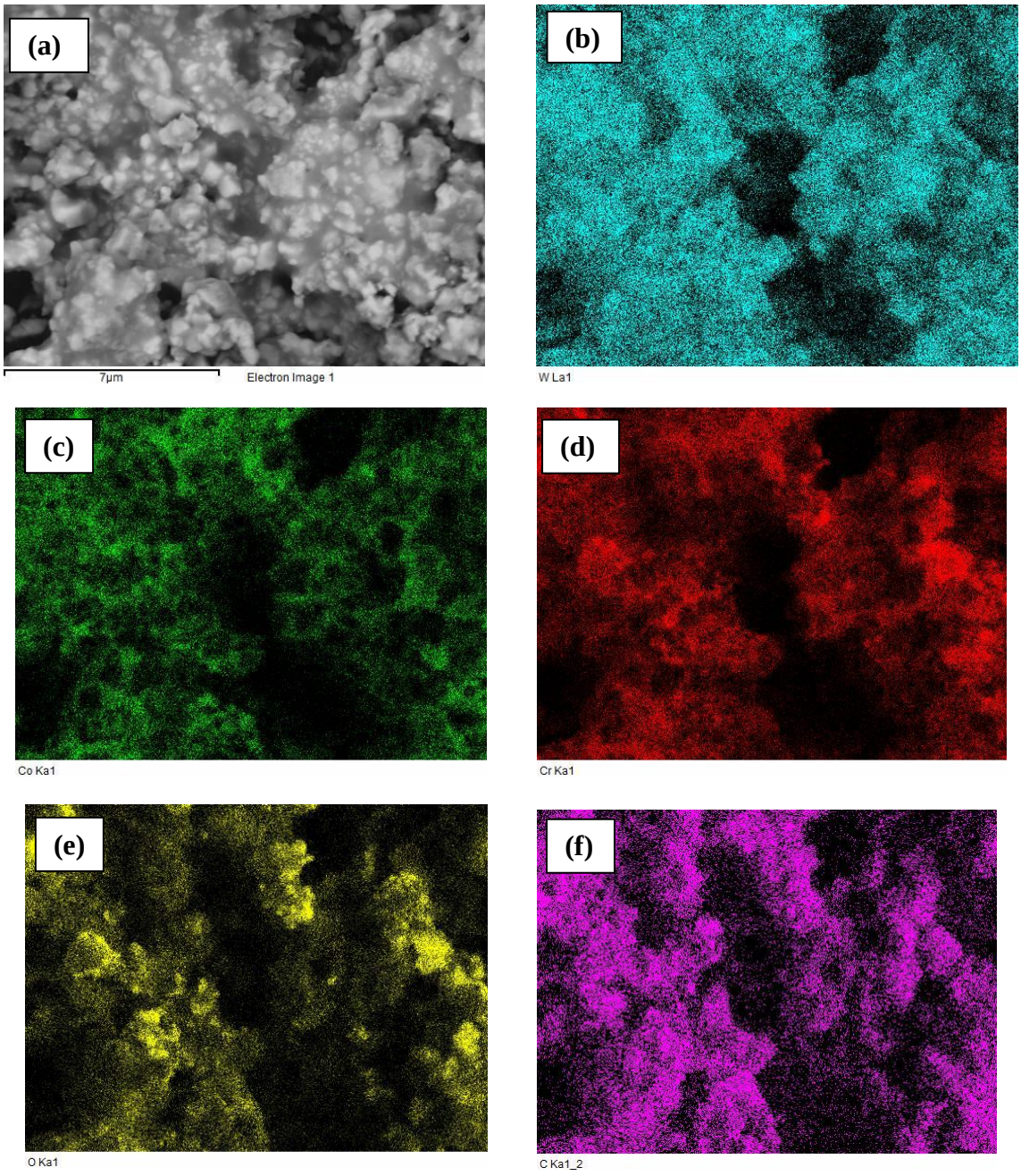

Figure 4.7. FESEM micrograph showing coating cross-section elemental maps for sample WC-10wt%Co-4wt%Cr (a) BSD electron image (b) W elemental map (c) Co elemental map (d) Cr elemental map (e) O elemental map (f) C elemental map.

4.3.2 HVOF Coatings microstructures

Table 4.1 shows and compare the porosity of coatings and coating thickness and Figure 4.8 shows SEM micrographs of all cross-sections of coatings. The interface between the coating and steel substrates were clean and had less interference of any obstacles and were free of cracks. The bonding between the coating and the substrate was adequate. The graph to compare the percentage of porosity of the coating is shown in Appendix A1.

Table 4.1. Coating porosity and coating thickness.

HVOF Coatings	Porosity (%)	Thickness (µm)
WC-10wt%Co-4wt%Cr	3.23 ± 0.4	243 ± 3.9
WC-10wt%Co-4wt%Cr-0.5wt%Ru	3.04 ± 0.2	251 ± 12.9
WC-10wt%Co-4wt%Cr-1.0wt%Ru	3.20 ± 0.2	250 ± 6.6
WC-10wt%Co-4wt%Cr-2.0wt%Ru	3.84 ± 0.3	265 ± 13.1

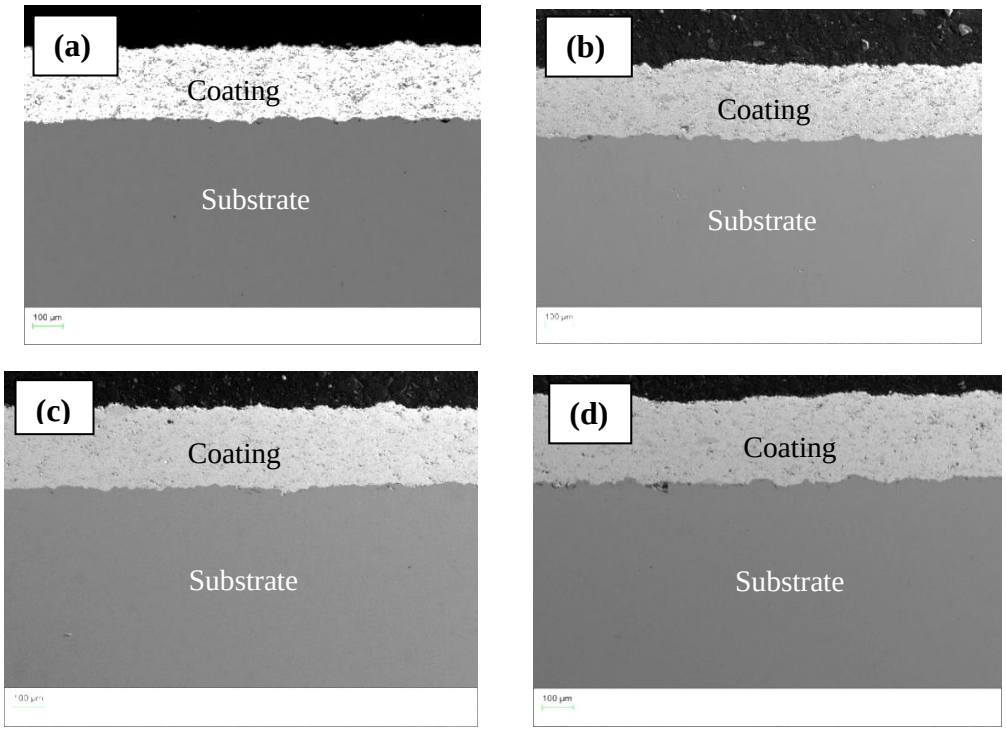

Figure 4.8. FESEM micrograph showing coating cross-sections. (a) WC-10wt%Co-4wt%Cr (b) WC-10wt%Co-4wt%Cr-0.5wt%Ru (c) WC-10wt%Co-4wt%Cr-1wt%Ru (d) WC-10wt%Co-4wt%Cr-2wt%Ru.

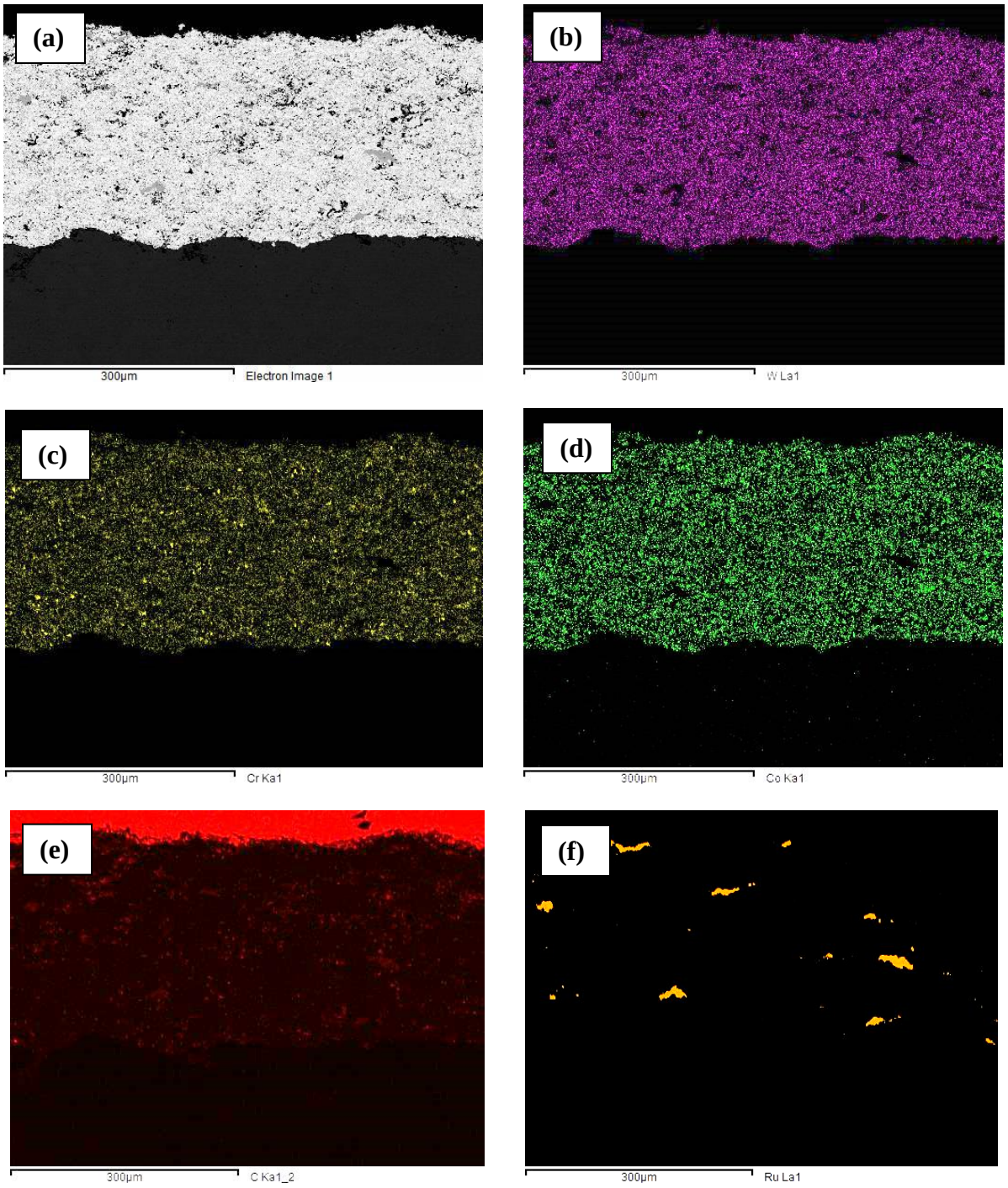

Figure 4.9. FESEM micrograph showing coating cross-section elemental maps for sample WC-10wt%Co-4wt%Cr-2wt%Ru. (a) BSD electron image (b) W elemental map (c) Cr elemental map (d) Co elemental map (e) C elemental map (f) Ru elemental map.

Figure 4.9 shows the FESEM EDS elemental maps of different elements for sample WC-10wt%Co-4wt%Cr-2wt%Ru. The distribution of Ru particles in the coating was very poor and for other elements such as W, Co and Cr the distribution was very good. Table 4.2 shows the EDS results of coatings. Appendix A3 shows the EDS elemental composition of the coating and Appendix A4 shows the EDS composition of the substrate used.

Table 4.2. EDS results of coatings.

Sample	Designation	wt%W	wt%Co	wt%Cr	wt%Ru
WC-10Co-4Cr	0wt%Ru	75.85±1.01	10.0±0.14	3.85±0.07	0
WC-10Co-4Cr-0.5Ru	0.5wt%Ru	74.05±0.21	9.85±0.07	3.80±0.14	0.65±0.07
WC-10Co-4Cr-1Ru	1wt%Ru	74.75±0.07	9.65±0.07	3.75±0.07	1.5±0.14
WC-10Co-4Cr-2Ru	2wt%Ru	74.55±1.34	9.40±0.14	3.75±0.07	2.20±0.42

All the coatings had a splat-like structure (Figure 4.10). All the coating FESEM micrograph showed that the coatings had pores. WC particles appeared as grey rounded particles on the micrographs and Co as dark irregular shaped particles. The Cr dissolved in the Co binder and it was not easy to be picked up by BSD detector, but the EDS elemental mapping as shown is Figure 4.11 only picked showed traces of the element.

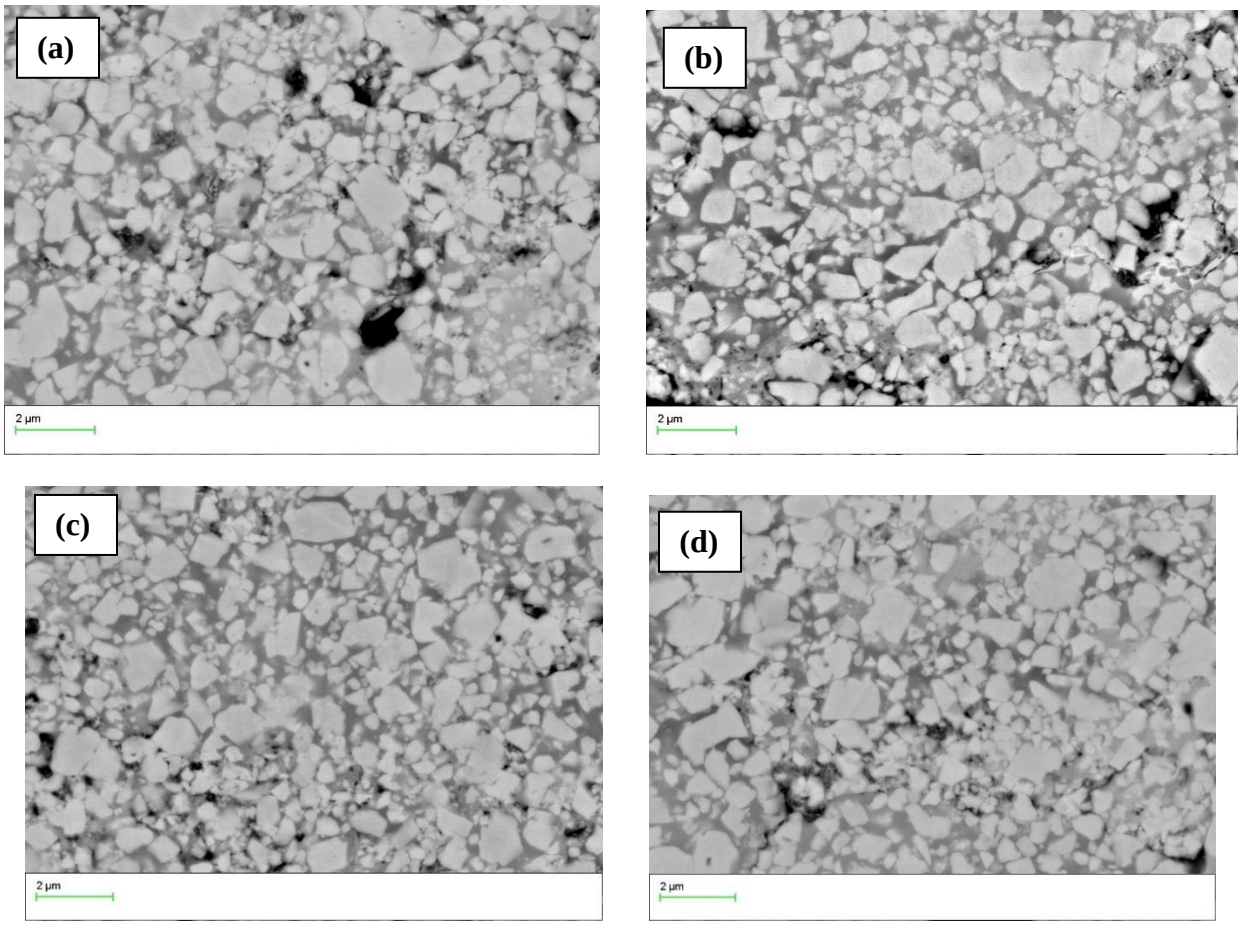

Figure 4.10. FESEM micrograph showing coating cross-sections. (a) WC-10wt%Co-4wt%Cr (b) WC-10wt%Co-4wt%Cr-0.5wt%Ru (c) WC-10wt%Co-4wt%Cr-1wt%Ru (d) WC-10wt%Co-4wt%Cr-2wt%Ru.

Figure 4.11 shows the FESEM EDS elemental maps of a cross section for sample with 1wt%Ru. From the elemental maps distribution of elements such as W, Cr, and Cr is quite good, but the distribution of Ru was not good enough. This was because of the size of Ru used. The distribution of W, Cr, and Co elements was good because the supplied powder shown in Figure 4.2 was milled and sintered.

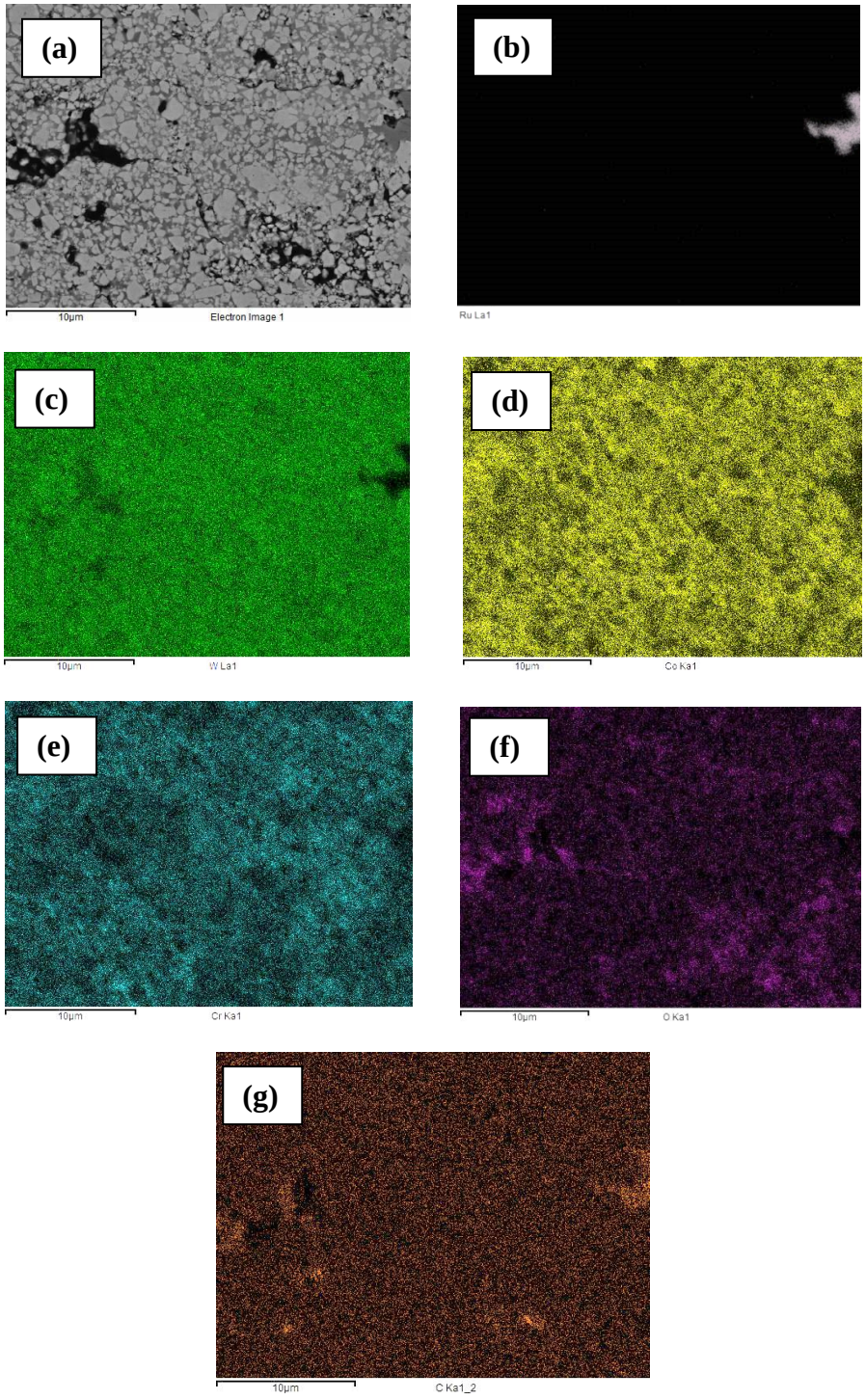

Figure 4.11. FESEM micrograph showing coating cross-section elemental maps at higher magnification. (a) Electron image (b) Ru elemental map (c) W elemental map (d) Co elemental map. (e) Cr elemental map. (f) O elemental map. (g) C elemental map.

4.4 Phase composition of coatings(XRD)

XRD analysis was done using Bruker D2 phaser with LynxEye detector and the XRD matching was done using EVA software. XRD results are shown in Figure 4.12. The XRD analyses results showed WC, W_2C, and Co. WC phase was the most dominant phase and W_2C formed because of decarburization of WC by high heat from HVOF process.

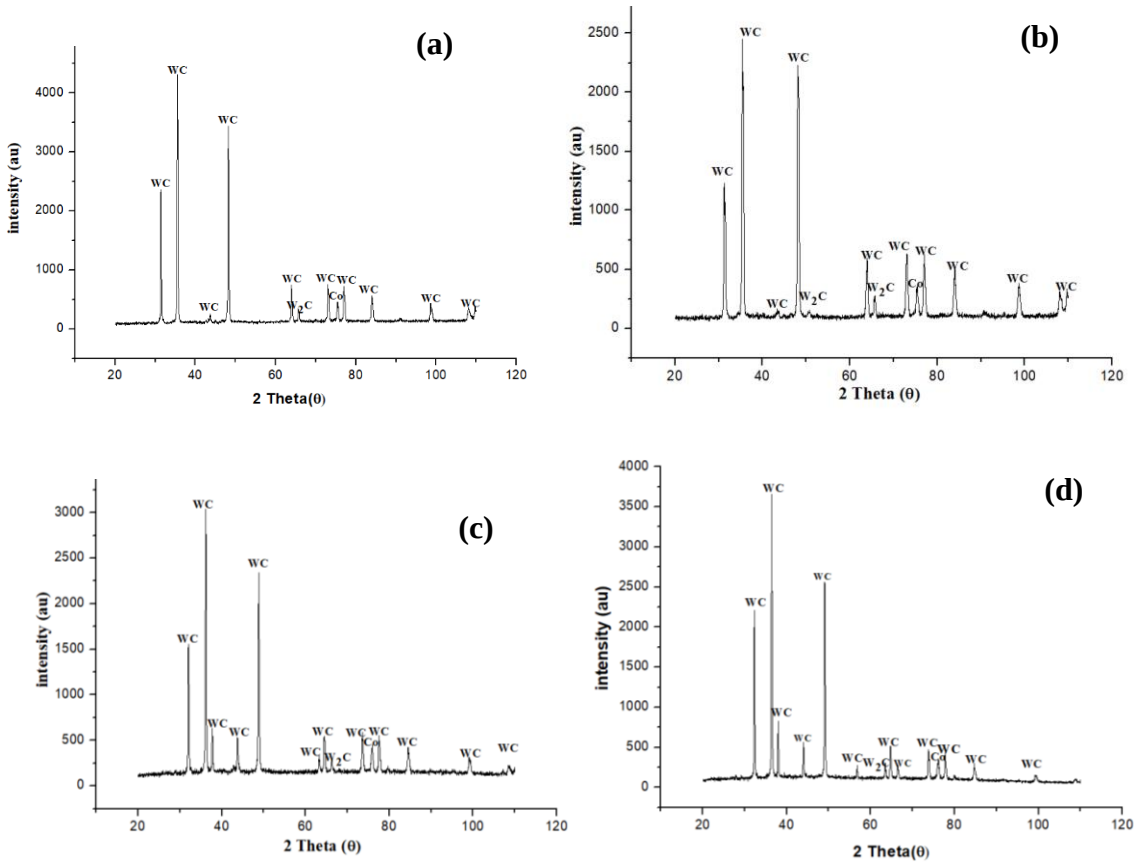

Figure 4.12. X-ray diffraction patterns for (a) WC-10wt%Co-4wt%Cr coating(b) WC-10wt%Co-4wt%Cr-0.5wt%Ru coating (c) WC-10wt%Co-4wt%Cr-1wt%Ru coating (d) WC-10wt%Co-4wt%Cr-2wt%Ru coating.

4.5 Grain size and contiguity

Table 4.3 shows the average WC grain size, contiguity, binder volume fraction and binder mean free path with their standard deviations and Figure 4.13 shows the comparison of WC grain size, contiguity, binder volume fraction and binder mean free path and the grain sizes were not too different and they ranged from 0.34µm to 0.62µm. Sample with 2wt%Ru had the smallest average grain size while sample that had no Ru added had the highest grain size of 0.62µm. Sample with no Ru added had the lowest contiguity of 0.44 and the sample with 1wt%Ru had the highest contiguity of 0.60. The binder volume fraction of the coatings were not too different either, sample that had 2wt%Ru added had the least binder volume fraction of 0.37 and the sample with 1wt%Ru addition having the most binder volume fraction of 0.44. Sample with no Ru had the highest binder mean path of 0.26 while sample with 2wt%Ru had the least binder mean free path of 0.08.

Table 4.3. Comparison of coating contiguity, WC grain size, binder volume fraction and binder mean free path.

Coating	Contiguity	Grain size (µm)	Binder vol fraction	Binder mean free path(λ)
0wt%Ru	0,44 ± 0.04	0,62 ± 0.03	0,43 ± 0.03	0,26 ± 0.03
0.5wt%Ru	0,48 ± 0.03	0,49 ± 0.06	0,38 ± 0.03	0,16 ± 0.03
1wt%Ru	0,60 ± 0.02	0,38 ± 0.07	0,44 ± 0.01	0,12 ± 0.01
2wt%Ru	0,59 ± 0.03	0,34 ± 0.04	0,37 ± 0.03	0,08 ± 0.01

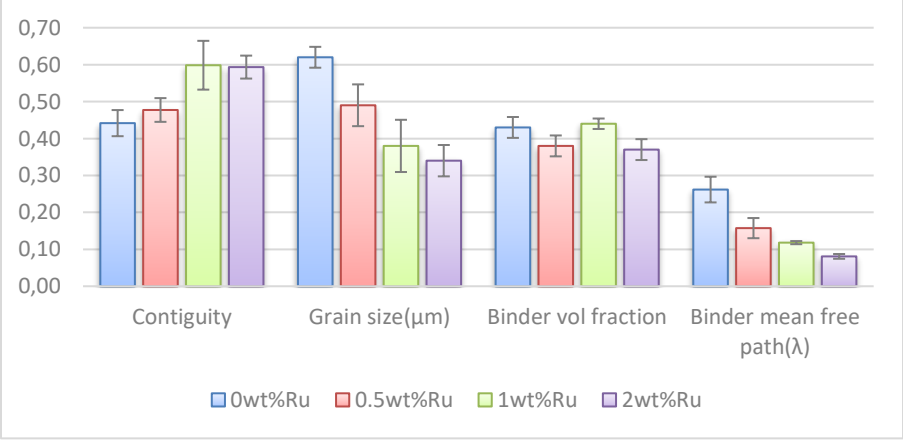

Figure 4.13. Comparison of contiguity, WC grain size, binder volume fraction, and binder mean free path for all the coatings.

4.6 Hardness and thickness of the coatings

The Macro-Vickers hardness machine was used to determine the hardness of the coatings. Ten micro-indentations were made per sample to get the average VHN. Table 4.4 and Figure 4.14 shows the graph and results of the average hardness number respectively. Sample with 2wt%Ru added had the lowest average hardness of 925 with standard deviation of 127 while sample with 1wt%Ru had the highest hardness average of 1026 with standard deviation of 45. The difference in hardness number between the sample with the highest hardness average of 1026 and lowest hardness average of 925 was 101 units, which is a very small number in terms of hardness variations. In general, the hardness variations between all four coatings were not that different.

Table 4.4. Comparison of coating hardness and thickness.

HVOF Coatings	Hardness, $HV_{0.5}$	Thickness(μm)
0wt%Ru	1009 ± 58	243 ± 3.86
0.5wt%Ru	964 ± 73	252 ± 12.90
1wt%Ru	1026 ± 45	250 ± 6.60
2wt%Ru	925 ± 127	265 ± 13.11

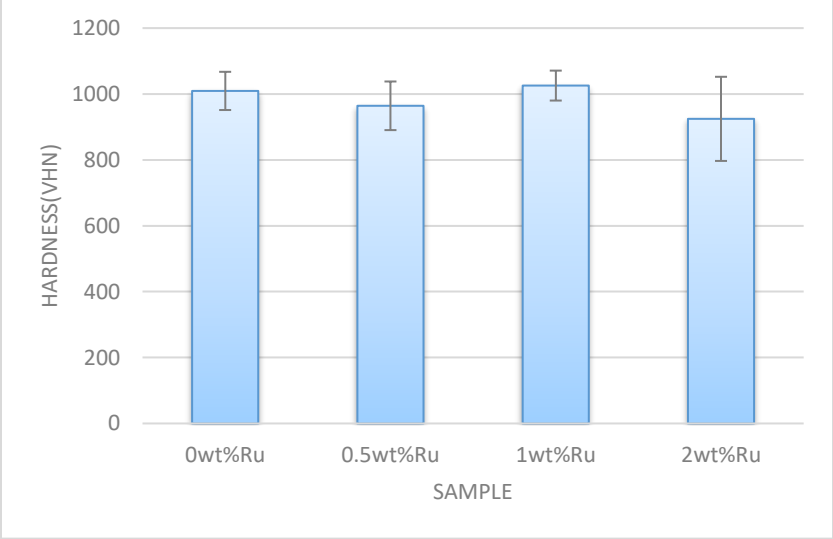

Figure 4.14. Graph comparing hardness of all coatings.

Figure 4.15 shows the comparison of coating thickness. Sample with 2wt%Ru had the highest thickness of 265 µm and sample with 0wt%Ru had the lowest thickness of 243 µm. Coating thickness is a property that is controlled by coating parameters and coating conditions. Ru addition should not affect the coating thickness.

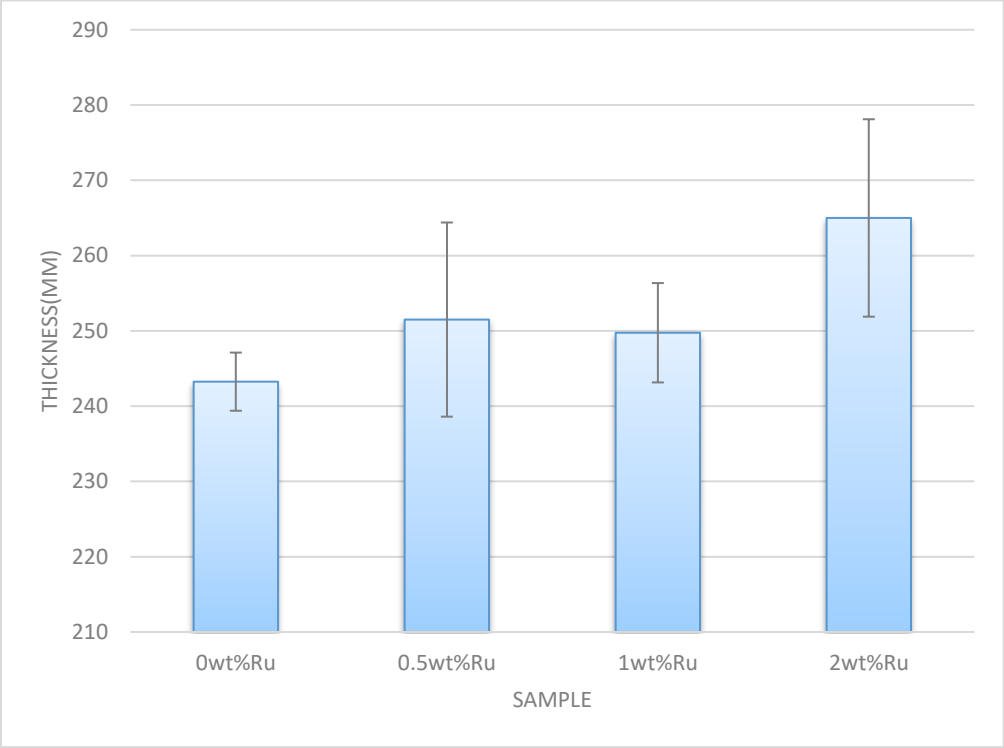

Figure 4.15. Comparison of coating thichness for all coatings.

Figure 4.16(a-d) shows the SEM micrographs of hardness indentations. The indentations are very similar is size hence the hardness numbers are not too different. The load of 500 g was used hence there was no evidence of crack propagations from the indentation corners. Fracture toughness could not be performed because there was no evidence of cracks observed.

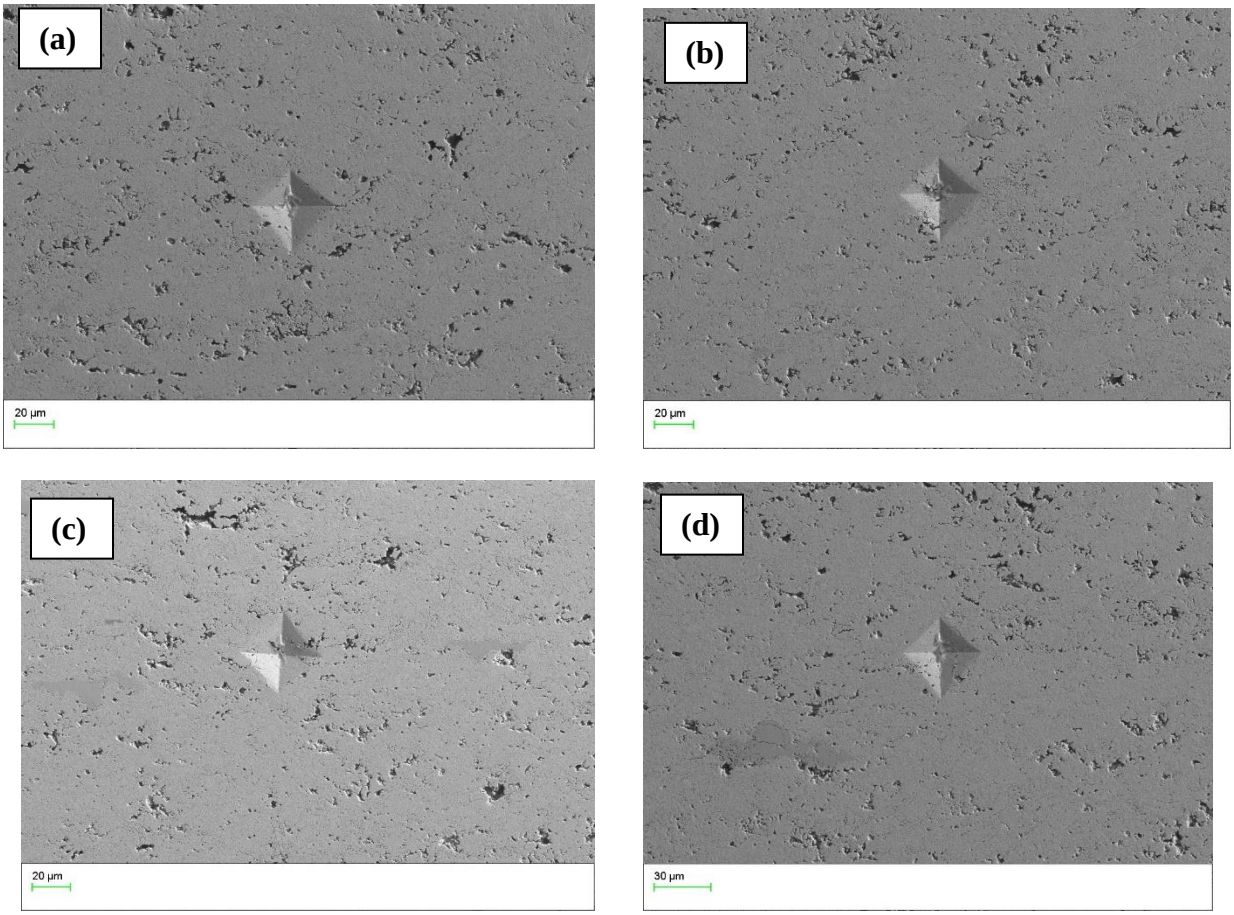

Figure 4.16. FESEM micrograph showing coating indentation for hardness testing. (a) WC-10wt%Co-4wt%Cr (b) WC-10wt%Co-4wt%Cr-0.5wt%Ru (c) WC-10wt%Co-4wt%Cr-1wt%Ru (d) WC-10wt%Co-4wt%Cr-2wt%Ru.

Chapter 5: Sliding wear, electrochemical corrosion and tribo-corrosion results

5.1 Introduction

This chapter shows the results for sliding wear testing, electrochemical corrosion results and tribo-corrosion results. Sliding wear tests, Electro-chemical corrosion tests, and Tribo-corrosion tests were performed on the as coated surfaces. Samples surfaces that were exposed to friction test, electrochemical corrosion test, and tribo-corrosion test were analyzed using FESEM to determine the wear mechanism, corrosion mechanism and tribo-corrosion mechanism.

5.2 Sliding wear results

The friction and sliding results of each coating against the 100Cr ball are shown in Figures 5.1. Figure 5.2 shows the comparison of coefficient of friction. All the coefficient of friction curves showed two regions, which were the run-in region and the static state region. The run-in phase occurred between 0m and 20m sliding distance for all the samples. The Static state regions occurred between 20m and 300m for all the samples. Sample with 2wt%Ru had the highest average coefficient of friction, while sample 0.5wt%Ru had the lowest average coefficient of friction at both the static state and dynamic state.

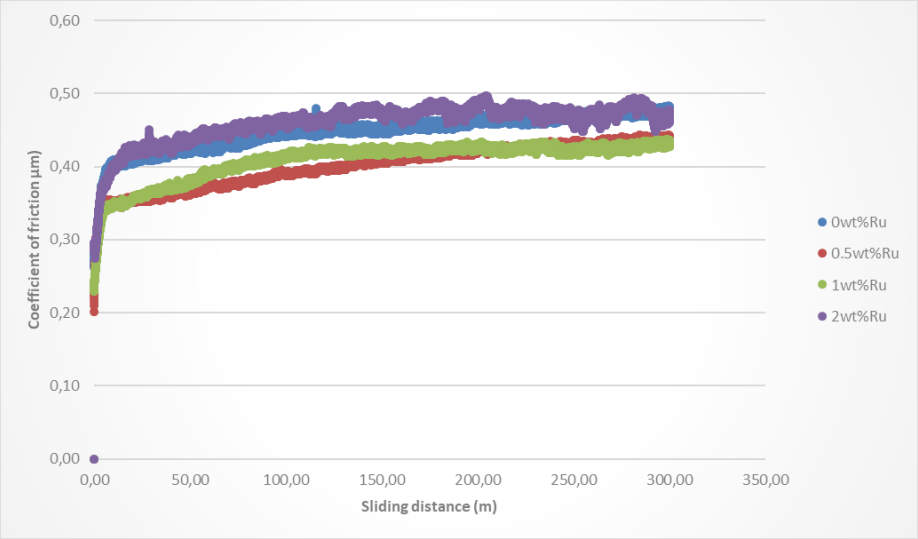

Figure 5.1. Coefficient of friction (µm) vs sliding distance (m).

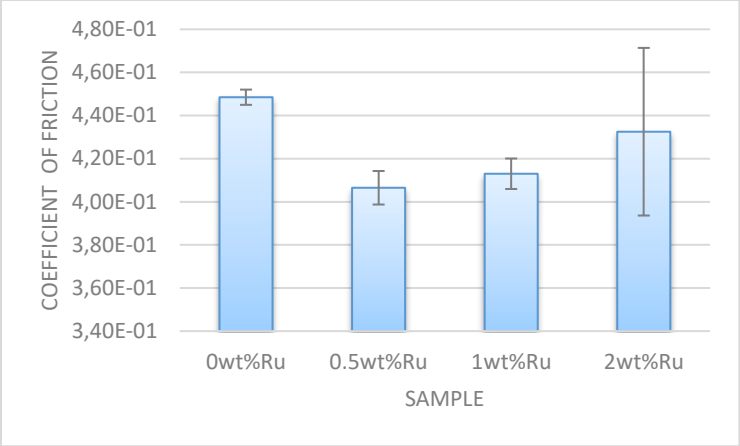

Figure 5.2. Comparison of average coefficient of friction for all the coatings.

Figure 5.3 shows the 100Cr ball wear rates that were used for different samples. The ball that was used for sample with no Ru had the highest wear rate while the ball that was used for sample with 2wt%Ru had the lowest wear rate. The ball used for sample with 0.5wt%Ru had the second lowest wear rate, while the ball used for 1wt%Ru had the second highest wear rate. Appendix A6 shows the graph with the comparison of wear rate and porosity.

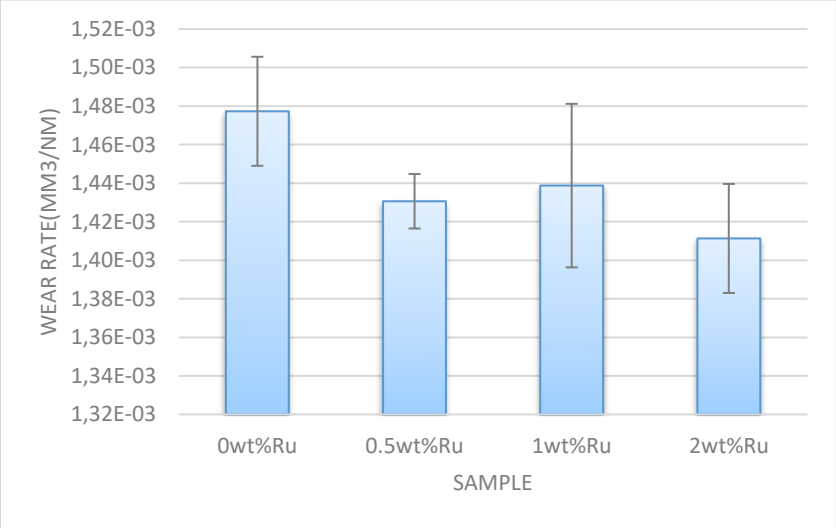

Figure 5.3. Comparison of 100Cr ball of wear rates.

Figure 5.4 shows the comparison of coating wear rates. Sample with 2wt%Ru had the highest wear rate while sample with 1wt%Ru had the lowest wear rate. The sample with no Ru had the second lowest wear rate, while sample with 0.5wt%Ru had the second highest wear rate.

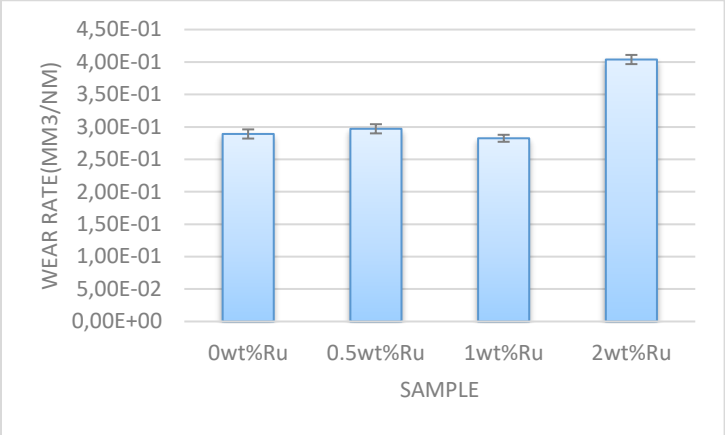

Figure 5.4. Comparison of coatings wear rates.

Figure 5.5 shows SEM micrographs of 100Cr ball after friction and sliding test. The diameters of the wear scars were very similar in size and shape. Smearing of the ball and wear debris were evident on all the ball wear scars.

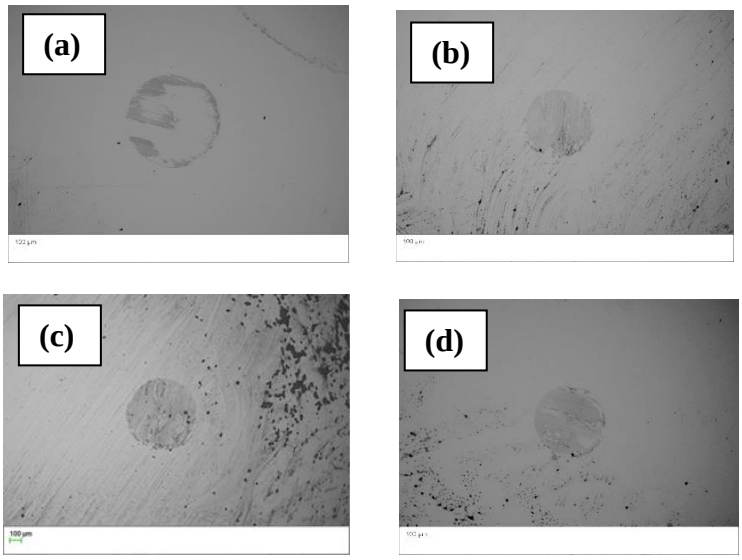

Figure 5.5. BSD FESEM micrographs of 100Cr balls showing wear scar diameters for all samples at lower magnifications (a) No Ru (b) 0.5wt%Ru (c) 1wt%Ru (d) 2wt%Ru.

Figure 5.6 shows higher magnification of ball wear scars for all coatings. The wear mechanism for all the balls were smearing of the particles and ploughing of the wear surface.

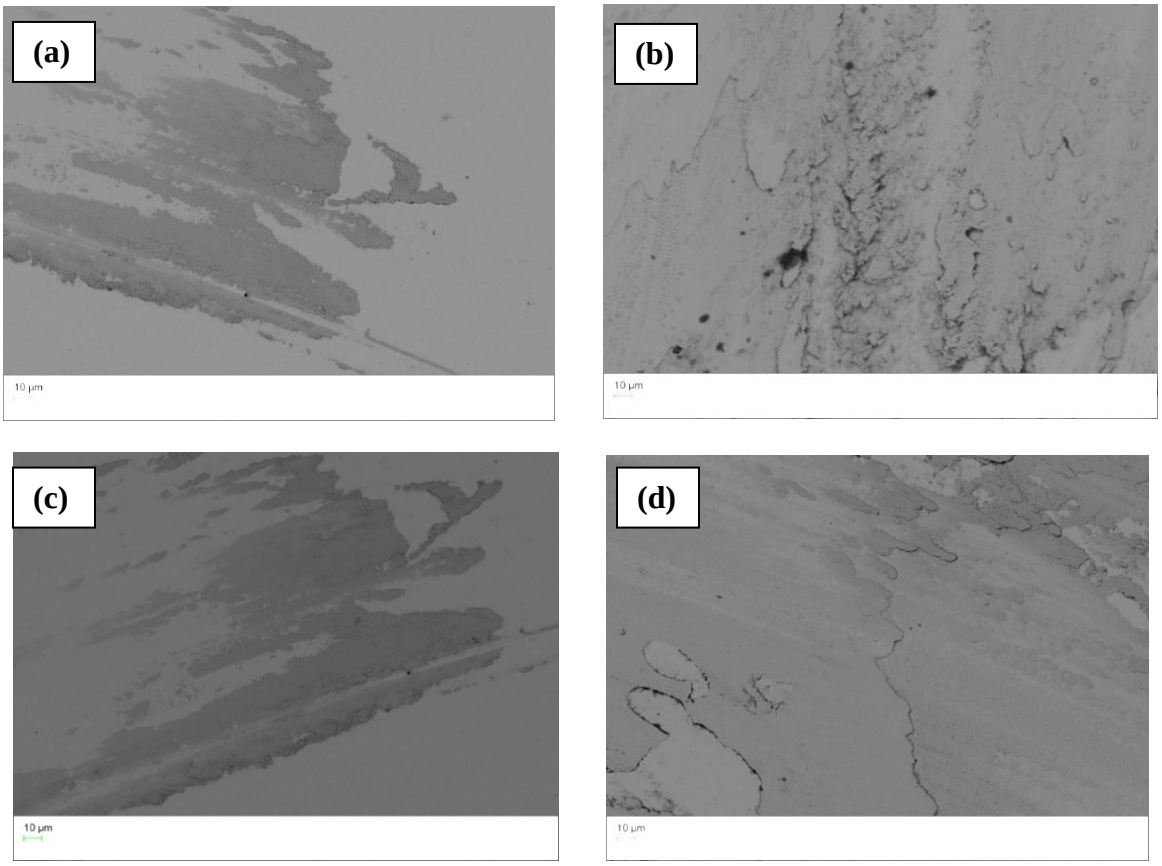

Figure 5.6. BSD FESEM micrographs of 100Cr balls showing wear scar diameters for all samples at higher magnifications (a) No Ru (b) 0.5wt%Ru (c) 1wt%Ru (d) 2wt%Ru.

Figure 5.7 shows wear mechanisms for all the coating at lower magnifications. It was evident that there was oxide formation on the surface due to friction between the ball and the surface. It seems like the 100Cr ball was worn out more than the coating because it is softer than the coating.

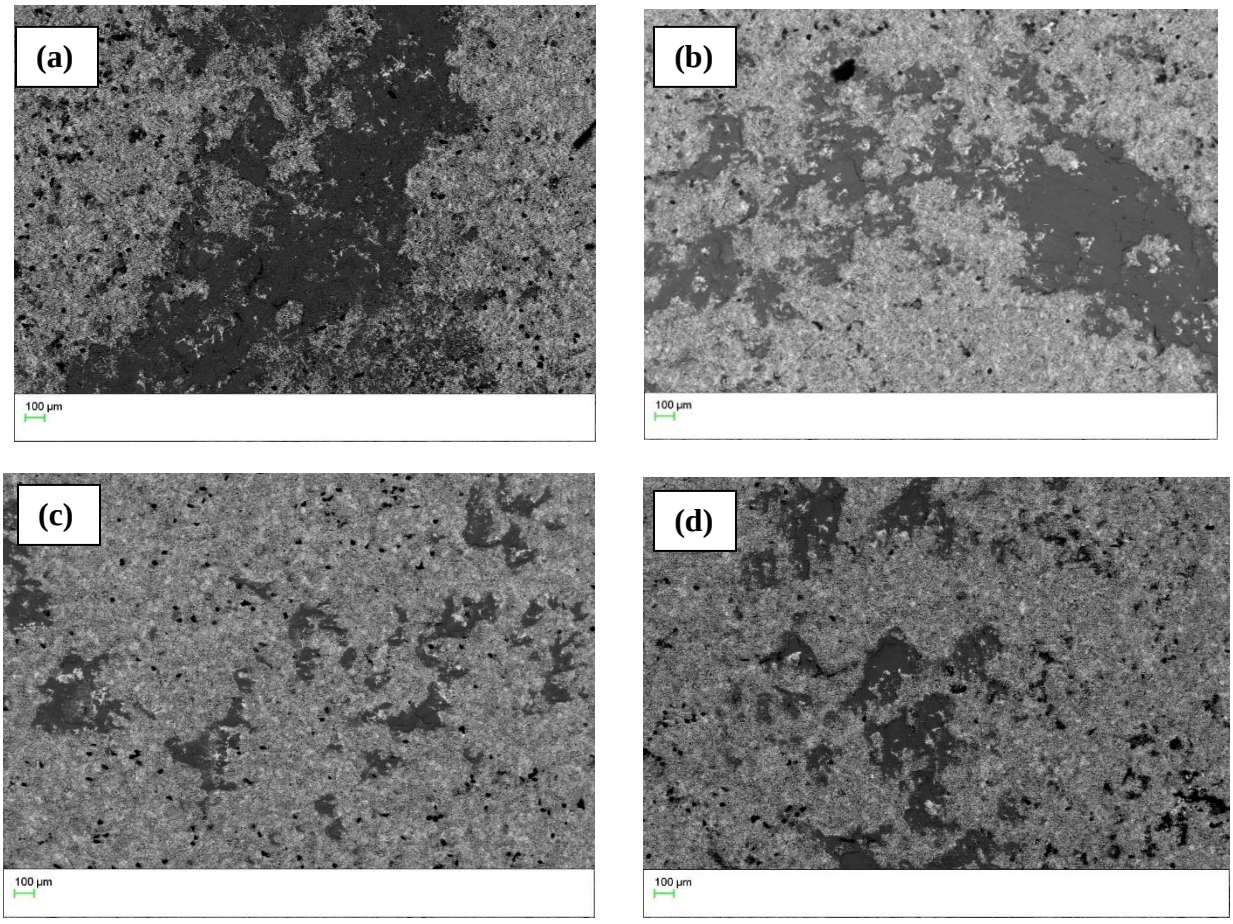

Figure 5.7. BSD FESEM micrographs of coatings showing wear scars for all samples at lower magnifications (a) No Ru (b) 0.5wt%Ru (c) 1wt%Ru (d) 2wt%Ru.

Figure 5.8(a-d) shows wear mechanisms for all the alloys. The wear mechanisms were found to be very similar. The wear mechanism observed were ploughing of wear particles, grooves formation which were parallel to the sliding direction, smearing on worn surface, and debris formation.

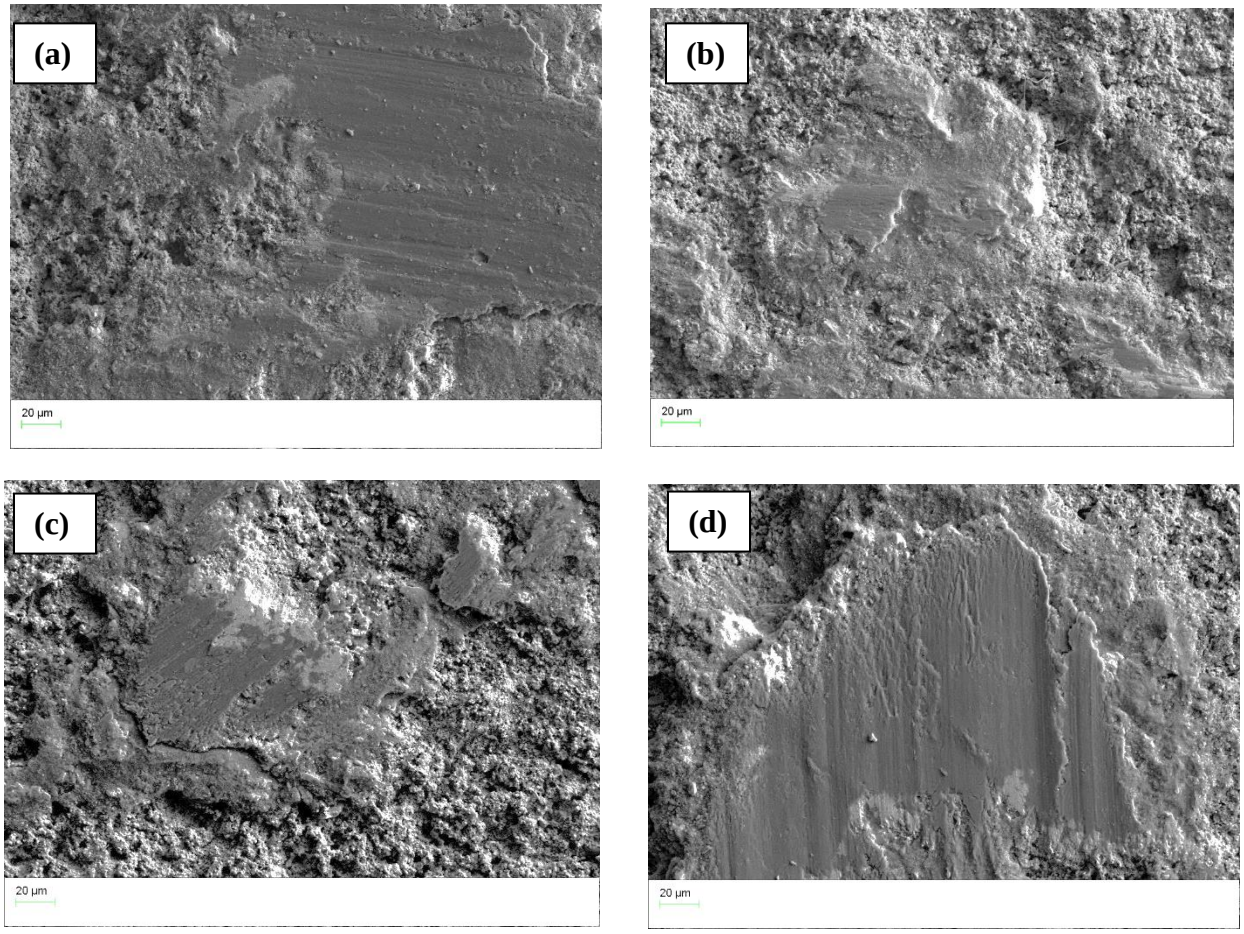

Figure 5.8. FESEM micrographs of coatings showing wear scars for all samples at higher magnifications (a) No Ru (b) 0.5wt%Ru (c) 1wt%Ru (d) 2wt%Ru.

Figure 5.9 shows the FESEM EDS elemental maps of worn area for sample with no Ru. It is evident that the 100Cr ball smeared on the coating surface and left some debris and there was some oxide formation due to friction action between the ball and the coating surface. Traces of Fe were observed on the wear track after wear testing as a results of 100Cr ball smearing on the coated surface.

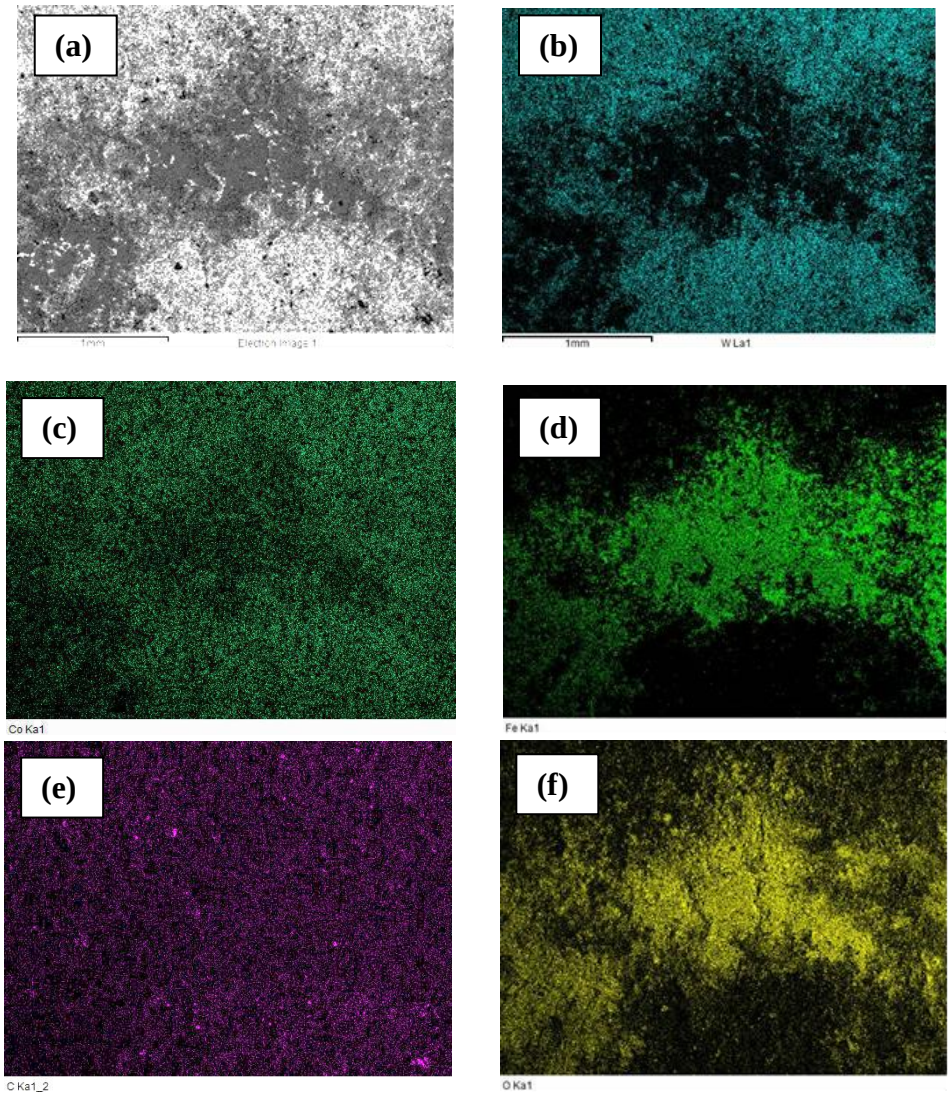

Figure 5.9. FESEM micrograph showing coating surface elemental maps at after sliding wear at lower magnification. (a) BSD electron image (b) W elemental map (c) Co elemental map (d) Fe elemental map. (e) C elemental map. (f) O elemental map.

5.3.1 Electrochemical corrosion results

Electrochemical corrosion tests were done in synthetic mine water at pH of 3 and pH 1. Potentiodynamic scans were done immediately after exposure and then again after 12 hours exposure to compare the results of delayed corrosion testing. Figure 5.10 shows the comparison of potentiostatic measurements over a period of 12 hours and Figure 5.11 shows the average OCP values obtained after 12 hours. The sample with no Ru addition had the lowest average OCP and also had the lowest corrosion potential, and the sample with 2wt%Ru had the highest average OCP and corrosion potential. Samples with 0.5wt%Ru and 1wt%Ru had almost the same OCP values.

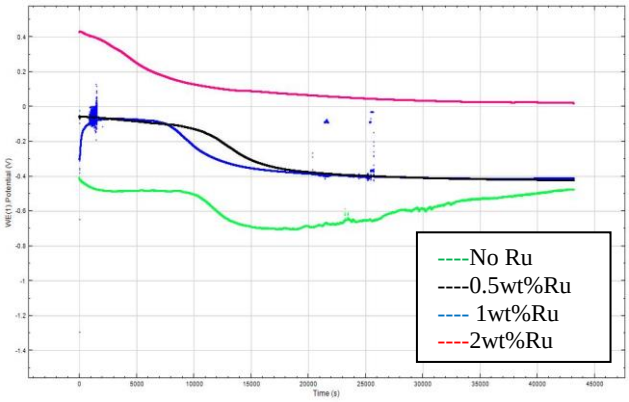

Figure 5.10. Potentiostatic scans for all coatings over a period of 12 hours in synthetic mine water at pH 3.

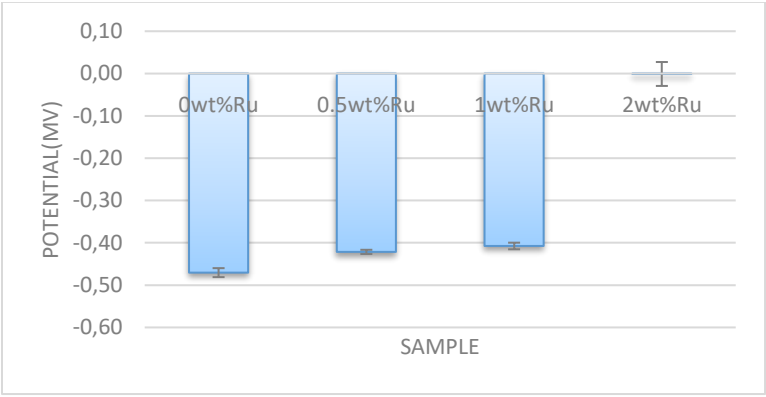

Figure 5.11. Comparison of average OCP values over a period of 12 hours in synthetic mine water at pH 3.

Figure 5.12 shows the corrosion polarization curves of all the coatings tested in synthetic mine water at pH 3, the samples were tested after 12 hours exposure to get the delayed corrosion characteristic behaviour. The sample with no Ru had the lowest current density in comparison to all other samples. The sample with 2wt%Ru had the highest free corrosion potential in comparison with other curves and the sample with no Ru had the lowest free corrosion potential. The sample with 0.5wt%Ru and 1wt%Ru had very similar electrochemical behaviours. Their anodic current densities and free corrosion potentials were very similar.

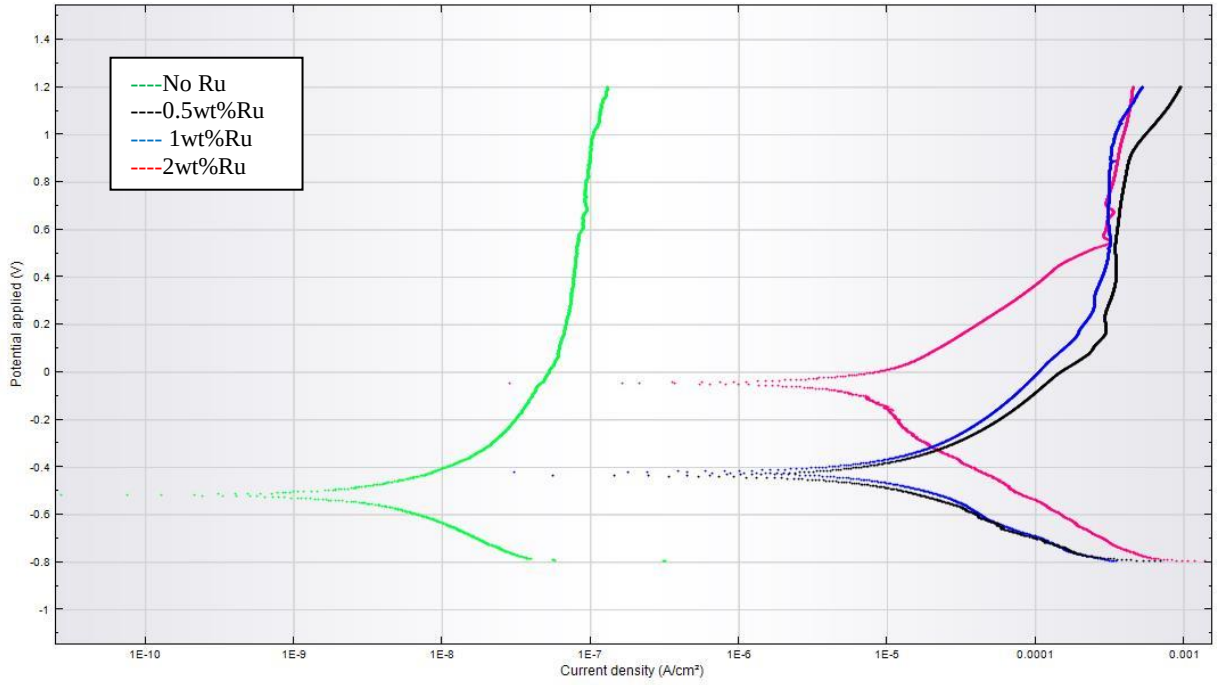

Figure 5.12. Comparison of polarization curves in synthetic mine water after 12 hours OCP at pH 3.

Figure 5.13 shows the corrosion polarization curves of all the coatings tested in synthetic mine water at pH 3, the samples were tested immediately after exposure to get the instant corrosion characteristic behaviour. The sample with no Ru had the lowest current density in comparison to all other samples, and the sample with 2wt%Ru had the highest free corrosion potential in comparison with other curves and the sample with no Ru had the lowest free corrosion potential. The anodic current densities and free corrosion potentials were very similar for sample with 0.5wt%Ru and 1wt%Ru sample. The passive potential range was not so clear for all the samples.

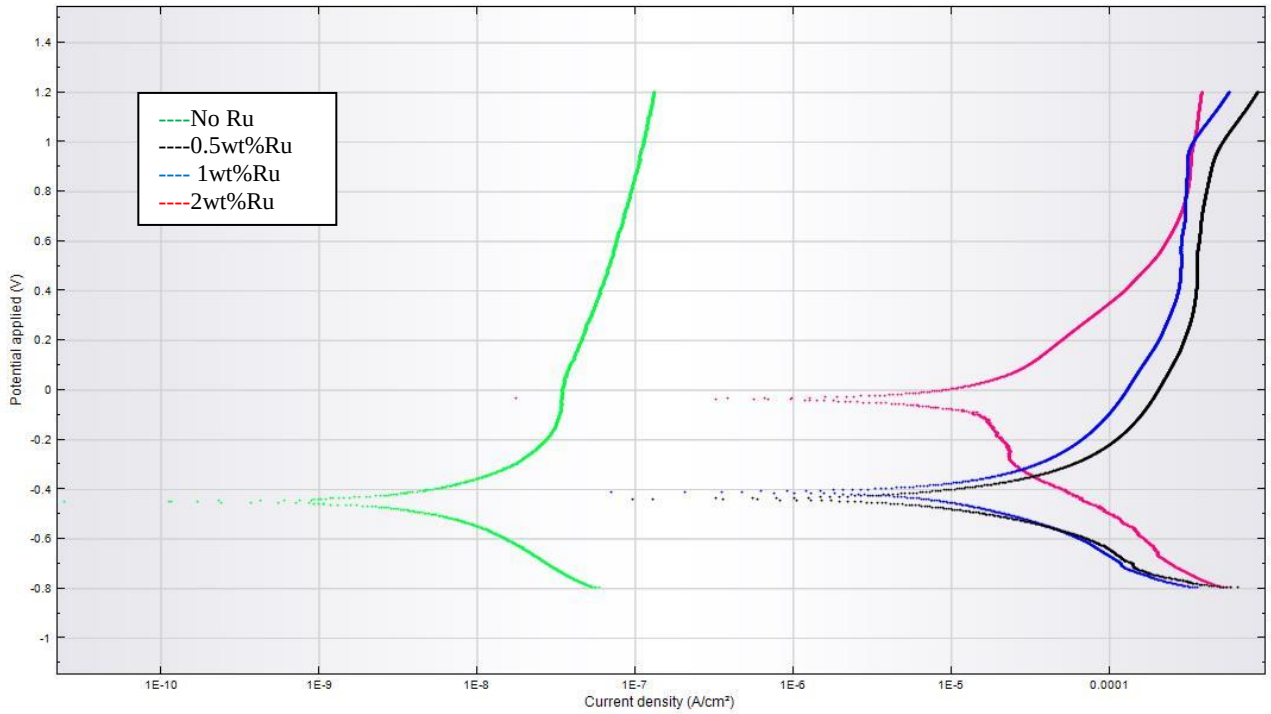

Figure 5.13. Comparison of polarization curves in synthetic mine water after immediate exposure at pH 3.

Figure 5.14 shows the corrosion polarization curves of all the coatings tested in synthetic mine water at pH 1, the samples were tested immediately after exposure to get the instant corrosion characteristic behaviour. All the curves shows at this pH of 1 were not stable, they were very in-continuous. The sample with 1wt%Ru had the lowest current density and the highest free potential, and sample with 2wt%Ru had the lowest free corrosion potential and highest anodic current density. The anodic current densities and free corrosion potentials were very similar for sample with 0.5wt%Ru and 1wt%Ru sample. The passive potential range for sample with 2wt%Ru was between 0.2 and 0.7 V.

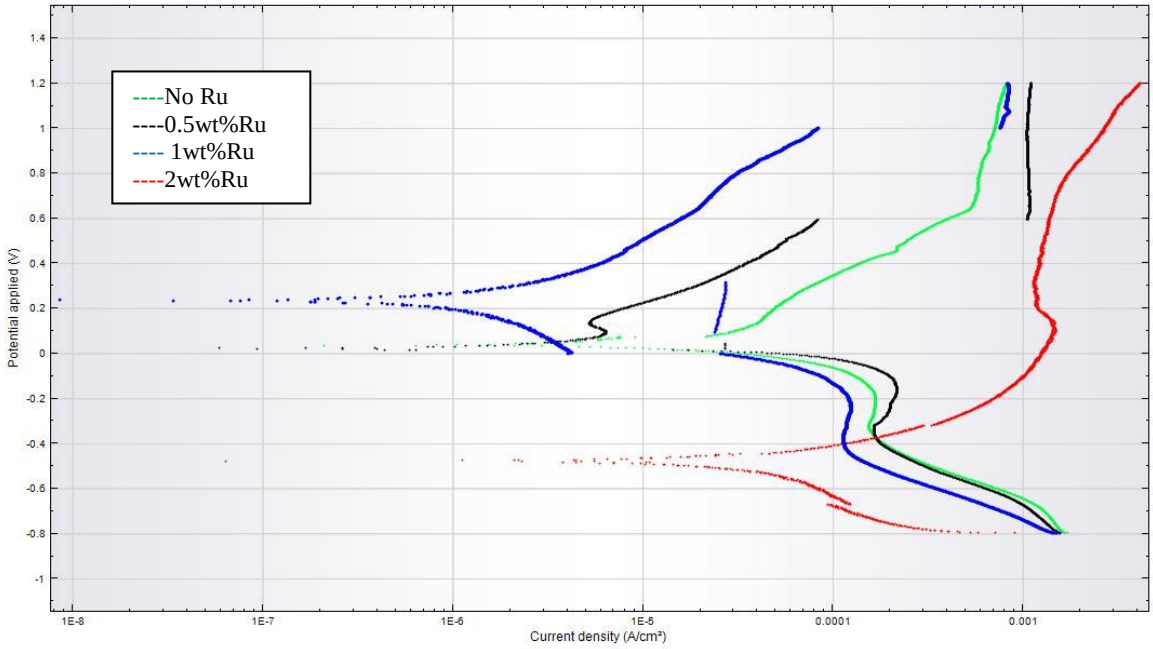

Figure 5.14. Comparison of polarization curves in synthetic mine water after immediate exposure at pH 1.

Figure 5.15 shows the comparison of corrosion rates for all coatings in synthetic mine water at pH 1 and pH 3. The corrosion rates for samples that were tested immediately after exposure at pH of 1 were the lowest even though the potentiodynamic curves were not that stable. Samples that were tested immediately at pH of 3 had the highest corrosion rates. The samples that were tested in synthetic mine water at pH 3 after 12 hours exposure had mild corrosion rates. From this results it is evident that sample with no Ru had much better corrosion resistance in synthetic mine water at pH of 1. At the pH of 3 their corrosion resistance is a bit higher than at lower pH of 1.

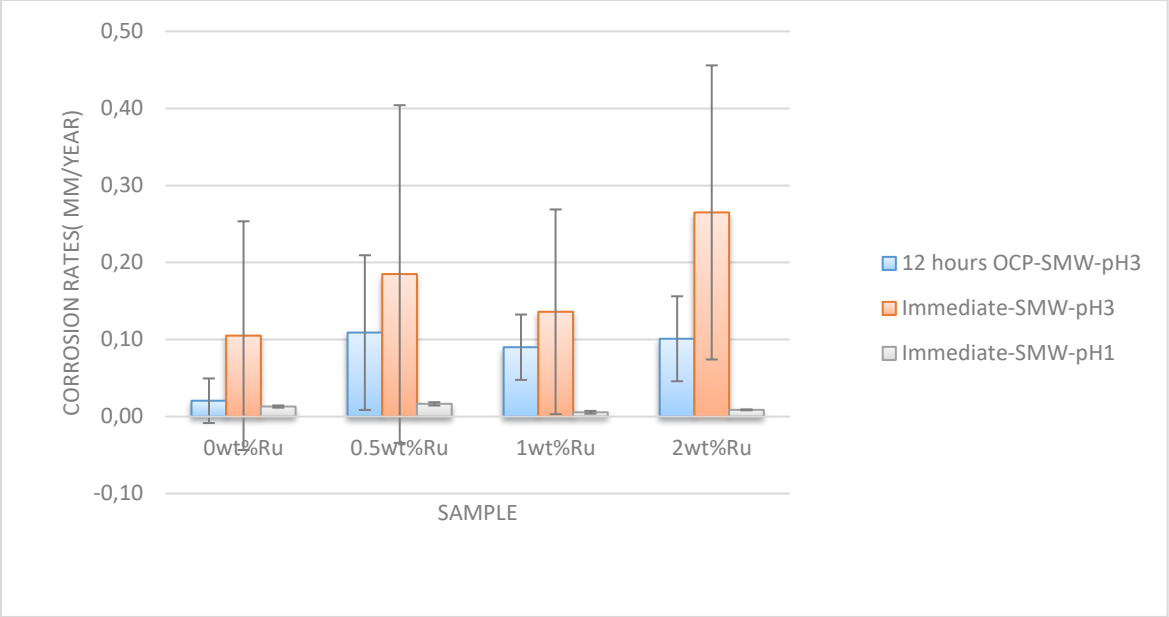

Figure 5.15. Comparison of corrosion rates for coatings in synthetic mine water at pH 1 and pH 3.

5.3.2 Micrographs of post electrochemical corrosion results

Figure 5.16 shows the FESEM micrographs of all the coatings surface after corrosion testing. For all the samples the corrosion attack was very similar with some formation of corrosion products. EDS analysis of the surface is shown in Table 5.1. Elements such as Na, Cl, and Ca were part of elements present in the synthetic mine water that was used for the corrosion test.

Table 5.1. EDS elemental results on corroded surface.

Elements	wt%
C	19.10
O	13.14
Na	1.11
Cl	0.36
Ca	0.88
Cr	3.87
Fe	2.12
Co	10.00
Cu	2.04
Ru	0.35

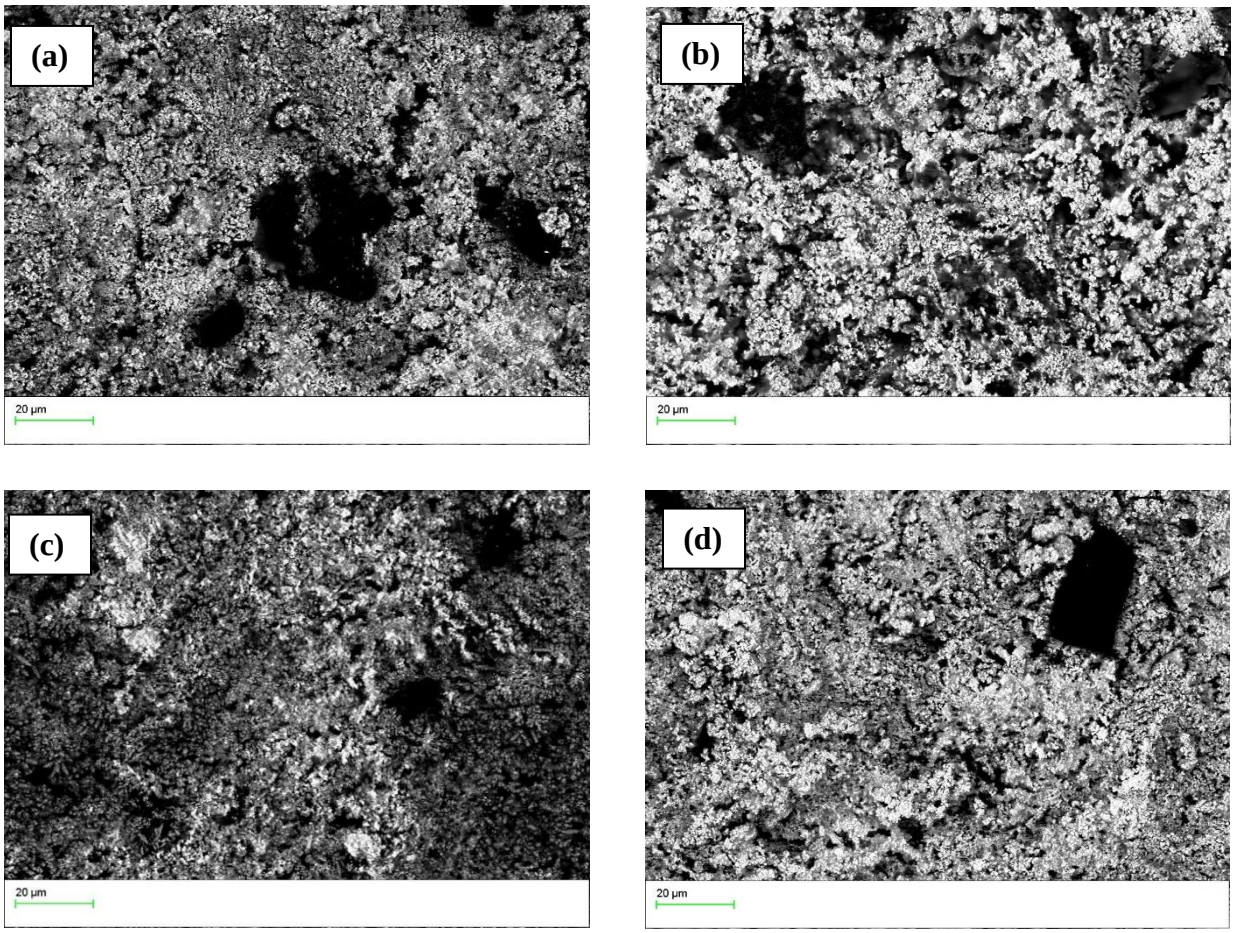

Figure 5.16. FESEM micrographs after electrochemical corrosion testing. (a) Sample with No Ru (b) Sample with 0.5wt%Ru (c) Sample with 1wt%Ru (d) Sample with 2wt%Ru.

Figure 5.17 shows the FESEM EDS elemental maps for coating sample surface after corrosion test. The maps are for a sample with no Ru. Elements such as W, Co, Cr, and O were evenly distributed as evident from the maps.

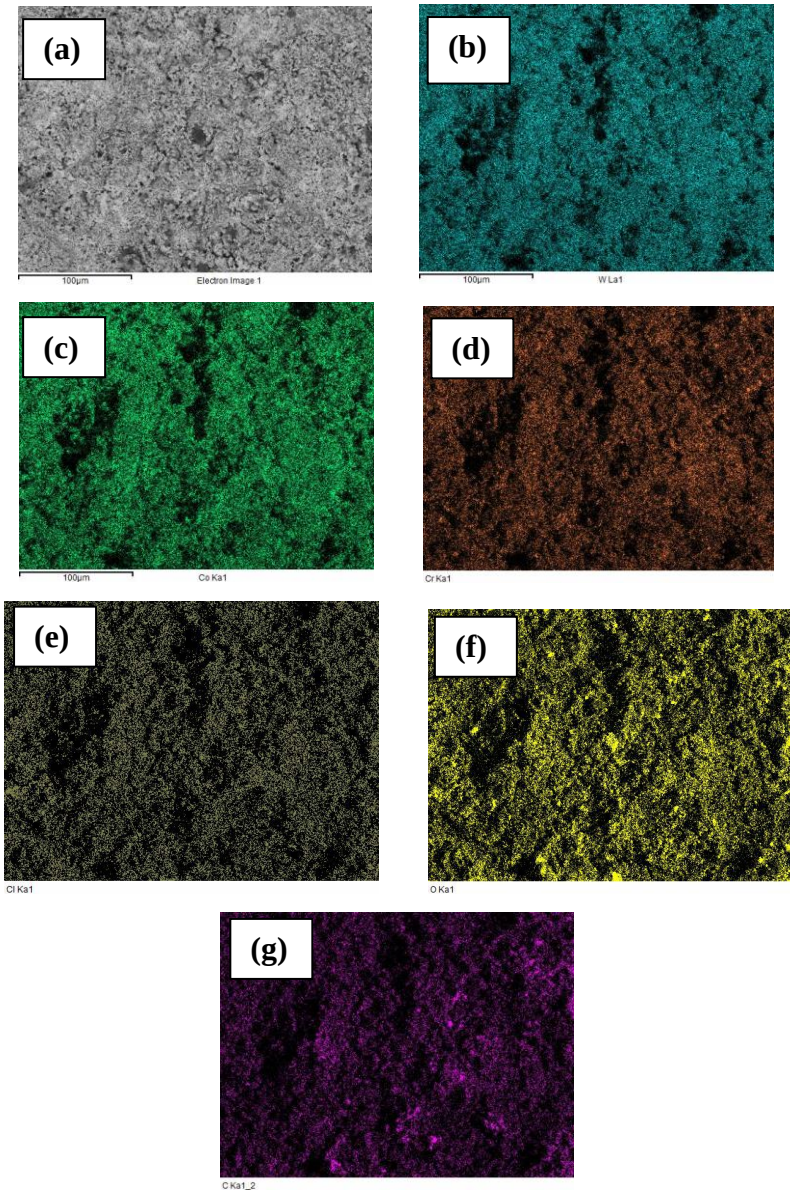

Figure 5.17. FESEM micrograph showing coating surface elemental maps at after electrochemical corrosion testing at lower magnification. (a) BSD electron image (b) W elemental map (c) Co elemental map (d) Cr elemental map (e) Cl elemental map (f) O elemental map (g) C elemental map.

5.4.1 Tribo-corrosion results

Figure 5.18 shows the comparison of potentiodynamic curves for all coatings in synthetic mine water at pH 1. The potentiodynamic curves were obtained during ball on disk sliding wear test to determine the effect of wear on corrosion characterization. Sample with 2wt%Ru had the lowest free corrosion potential while the anodic current density for all samples were very similar. The samples were stable in the solution compared to the results obtained while there was no ball on disk action at the same conditions of synthetic mine water at pH 1.

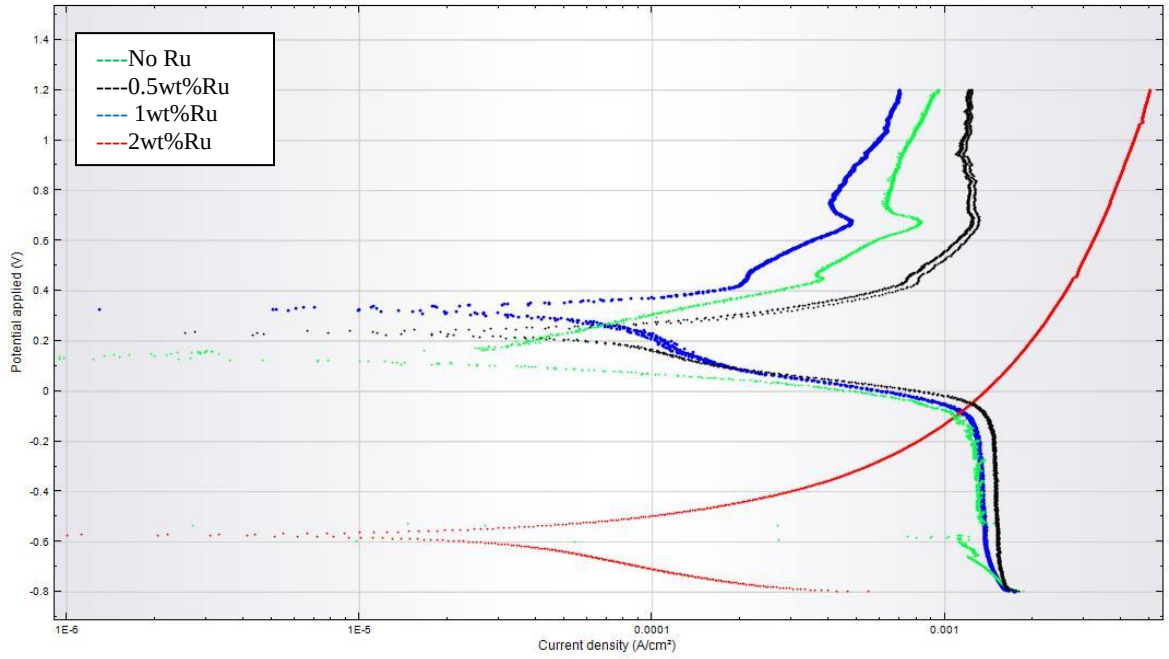

Figure 5.18. Comparison of polarization curves in synthetic mine water at pH 1 for tribo-corrosion test with friction test.

Figure 5.19 shows the comparison of corrosion rates for all coatings in synthetic mine water at pH 1. Corrosion rates were obtained while samples where undergoing pin on disk wear test. Sample with 2wt% Ru addition had the lowest corrosion rate followed by the sample with no Ru added. Sample with 0.5wt%Ru and sample with 1wt%Ru addition had a bit higher corrosion rates.

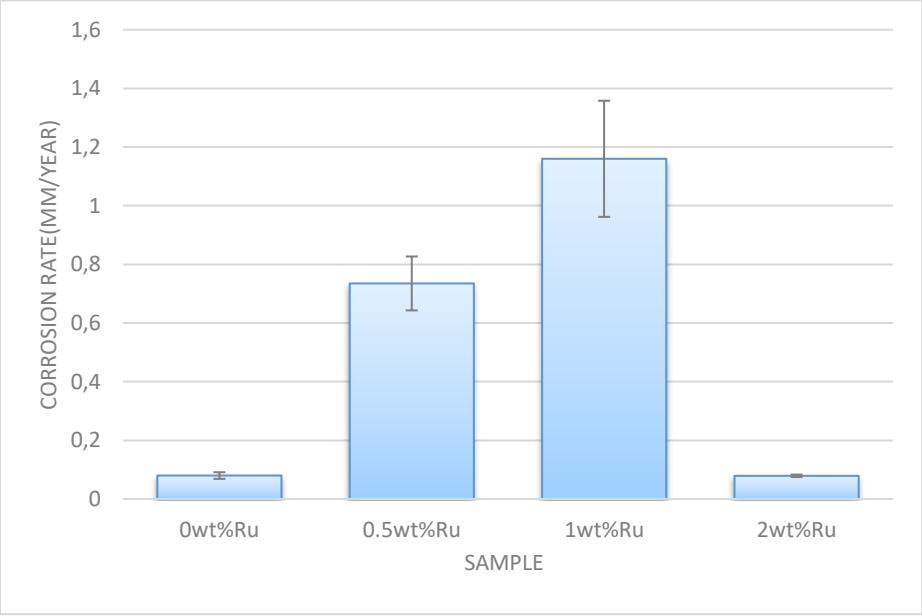

Figure 5.19. Comparison of Tribo-corrosion rates.

Figure 5.20 shows the comparison for potentiodynamic polarization curves for coatings with no Ru (with friction and without friction). Sample tested with no friction had a bit lower free corrosion potential and the anodic current density for both samples were very similar. The sample tested while there was friction action was more stable.

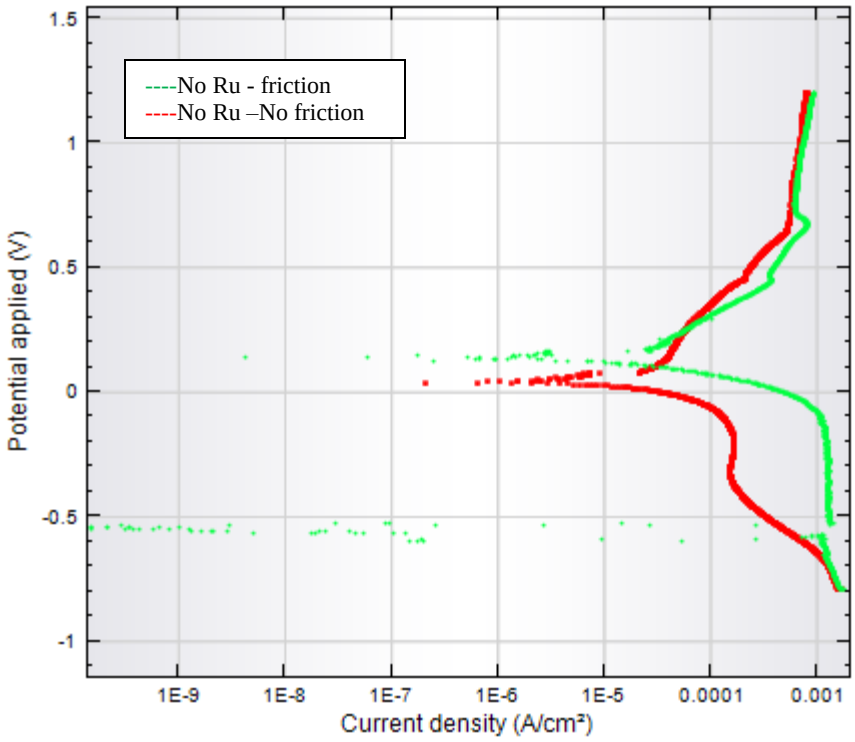

Figure 5.20. Potentiodynamic polarization curves for coatings with no Ru (with friction and without friction) in synthetic mine water at the pH of 1.

Figure 5.21 shows the comparison for potentiodynamic polarization curves for coatings with 0.5wt%Ru (with friction and without friction). Sample tested with no friction had a bit lower free corrosion potential and the anodic current density for sample with no friction was lower than for sample with friction. Sample tested while there was friction was more stable in the solution.

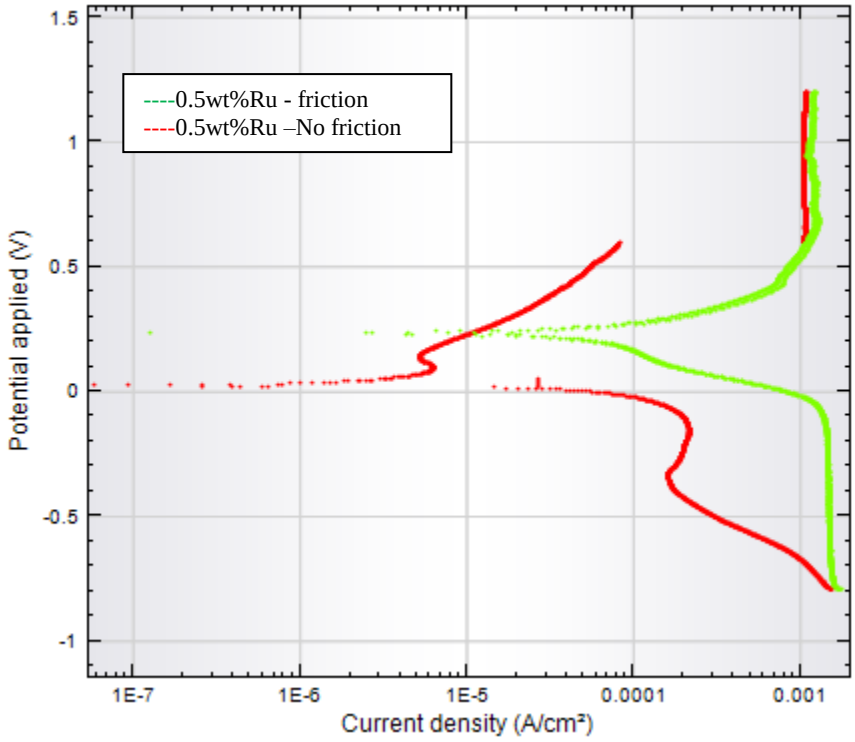

Figure 5.21. Potentiodynamic polarization curves for coatings with 0.5wt%Ru (with friction and without friction) in synthetic mine water at the pH of 1.

Figure 5.22 shows the comparison for potentiodynamic polarization curves for coatings with 1wt%Ru (with friction and without friction). The sample tested with no friction had a bit lower free corrosion potential and the anodic current density for sample with no friction was lower than the for sample with friction. The sample tested while there was no friction was not stable in the solution.

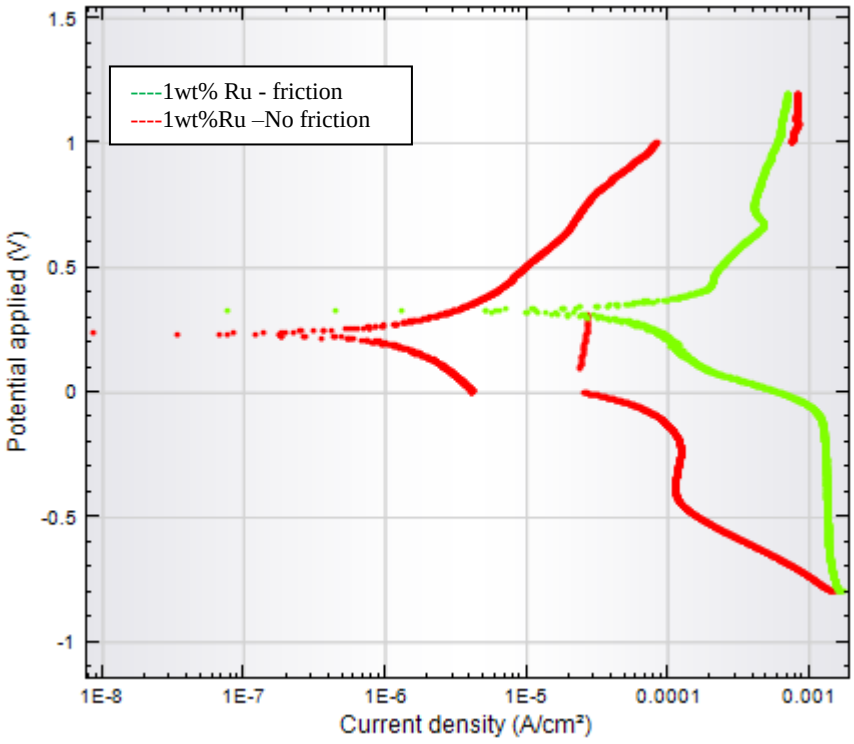

Figure 5.22. Potentiodynamic polarization curves for coatings with 1wt%Ru (with friction and without friction) in synthetic mine water at the pH of 1.

Figure 5.23 shows the comparison for potentiodynamic polarization curves for coatings with 2wt%Ru (with friction and without friction). The sample tested while there was no friction was not stable in the solution. The sample tested while there was friction had a lower free corrosion potential and the anodic current density for sample with no friction was a bit lower than the for sample with friction.

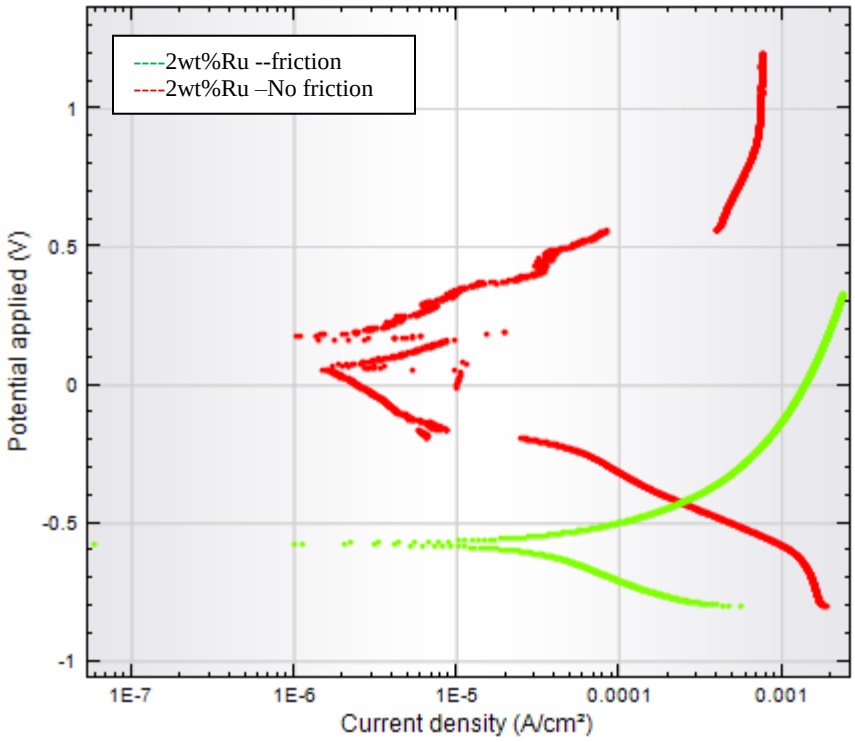

Figure 5.23. Potentiodynamic polarization curves for coatings with 2wt%Ru (with friction and without friction) in synthetic mine water at the pH of 1.

5.4.2 Micrographs of post tribo-corrosion results

Figure 5.24 shows FESEM micrographs for coatings after tribo-corrosion test. The tribo-corrosion mechanism for all the coatings were very similar. There was little contact areas between the ball and the coating because a very small load of 2 Newtons was used for tribo-corrosion tests.

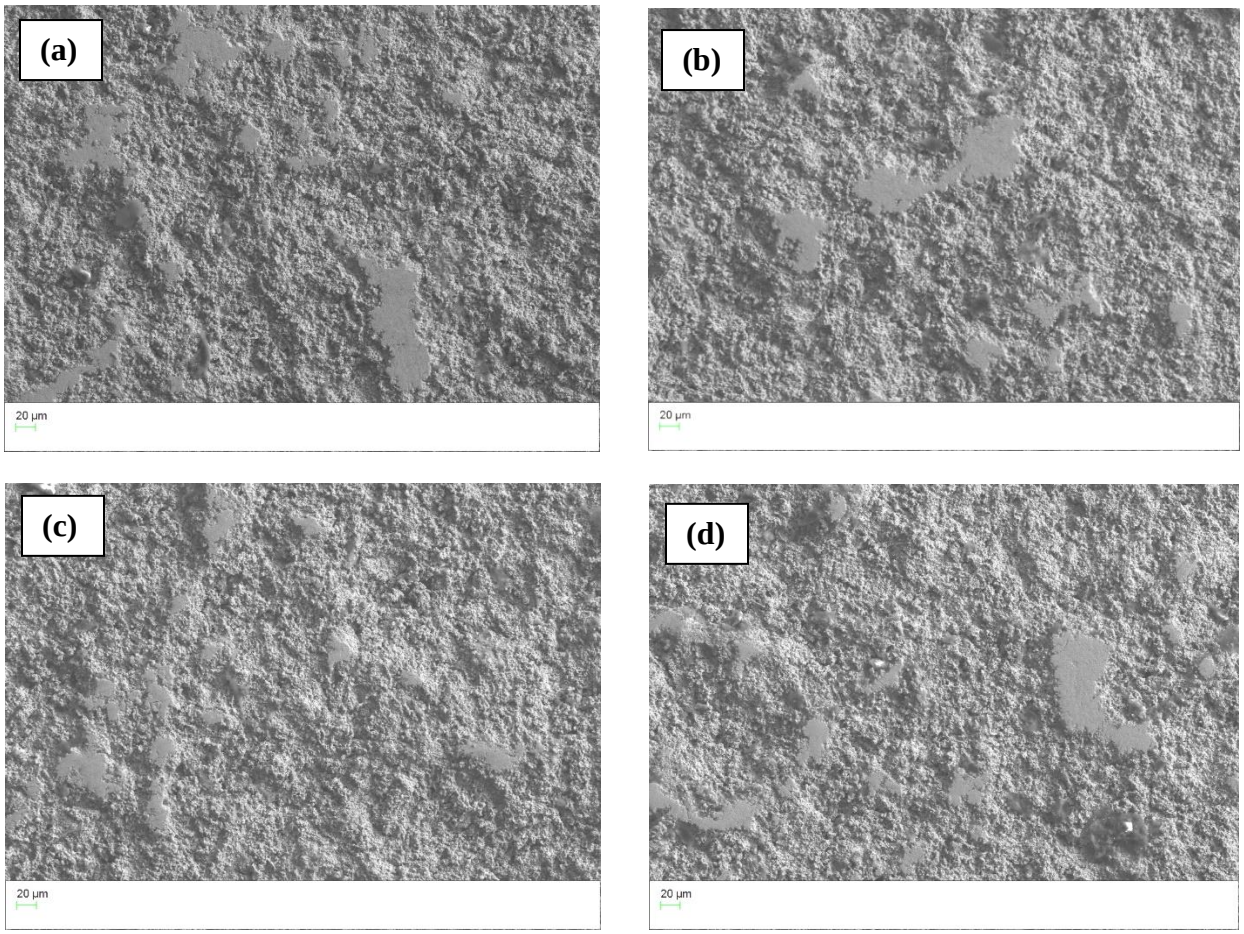

Figure 5.24. Surface FESEM micrographs of samples after tribo-corrosion test. (a) Sample with no Ru (b) Sample with 0.5wt%Ru (c) Sample with 1wt%Ru (d) Sample with 2wt%Ru.

Figure 5.25 shows FESEM micrographs maps for coatings after tribo-corrosion test. The distribution of elements in the maps was very even. Traces of aluminium and oxygen can be seen on maps as a result of using alumina balls for tribo-corrosion testing.

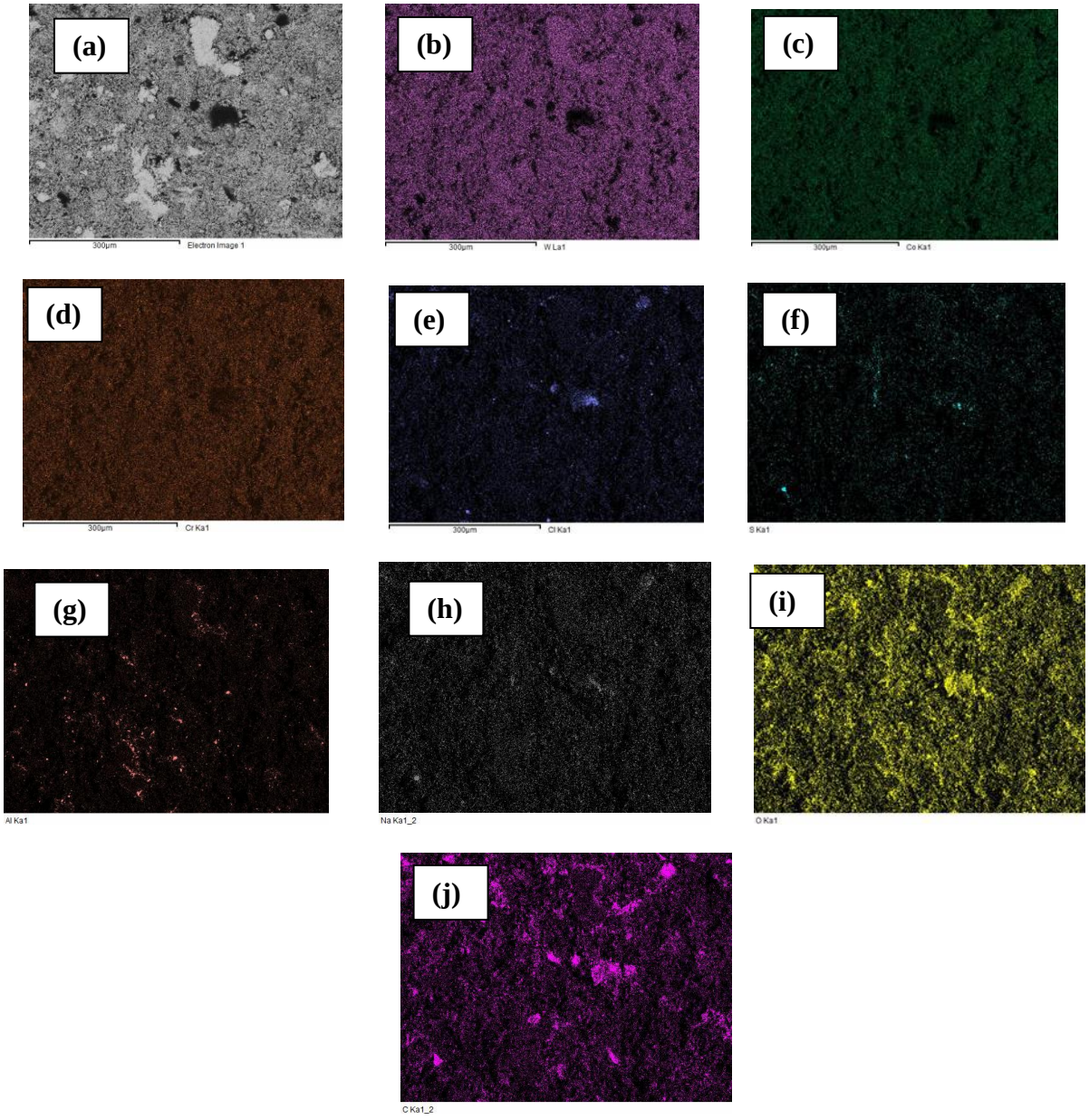

Figure 5.25. FESEM micrograph showing coating surface elemental maps at after tribo-corrosion testing at lower magnification for sample with no Ru. (a) BSD electron image (b) W elemental map (c) Co elemental map (d) Cr elemental map (e) Cl elemental map (f) S elemental map (g) Al elemental map (h) Na elemental map (i) O elemental map (j) C elemental map.

Figure 5.26 shows the comparison of corrosion rates for sample with friction and without friction in synthetic mine water at pH 1. Samples tested while there was no friction had the lowest corrosion rates. The sample with 1wt%Ru addition had the highest corrosion rate followed by the sample with 0.5wt%Ru. The sample with no Ru addition and sample with 2wt%Ru had very similar corrosion rates. The corrosion rates with no friction was almost zero.

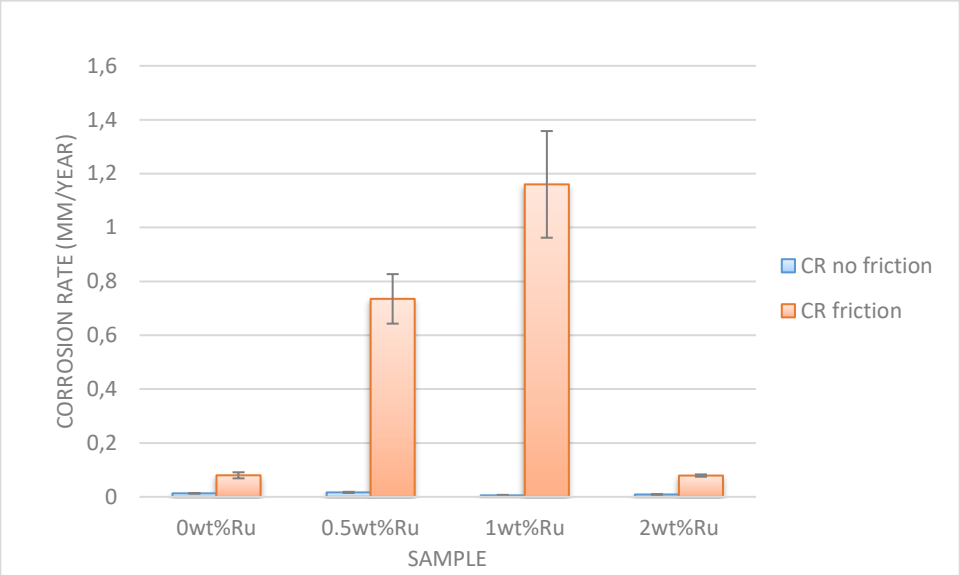

Figure 5.26. Comparison of corrosion rates for sample with friction and without friction in synthetic mine water at pH 1.

Chapter 6: Discussion of results

Characterization

The as received WC-10Co-4Cr powders were spherical in shape and had a wide size range distribution. The as received powders were very porous. As received Ru powder had a sponge-like structure and was irregular in shape. The size distribution for the Ru powder was very wide. The blending after mixing WC-10-4Cr powder and Ru powder was not very good as some of single WC-10Co-4Cr agglomerated particles were not close to the Ru particles from the micrographs observed. The size difference between Ru particles and WC-10Co-4Cr particle was huge. Surface micrographs of the coatings show that the coatings were very porous and were similar to the micrographs obtained by Machio [52]. Elemental maps from the cross section showed that the distribution of Cr, W, and Co was very good while the distribution of Ru was not good. The cross-sectional micrographs also showed that there was a good bonding between the coating and the substrate with no cracking. There was less interference (fewer inclusions) between the coating and the substrate. High magnification of the coatings showed a spat-like structure, which is similar to what Machio [52] reported. Phase analysis results showed that the dominant phase was WC and some traces of W_2C were also observed. W_2C phase was present as a result of decarburization of WC phase because of high heat associated with HVOF. In general, Ru distribution throughout the coating was poor.

Grain size and contiguity

The WC grain size were not very different for all the coatings. Sample with 2wt%Ru had the lowest grain size of 0.34μm followed by the sample with 1wt%Ru which had average WC grain size of 0.38μm. The sample with no Ru had an average WC grain size of 0.62μm which was the highest for the coatings. Ru addition to the hardmetal coatings caused a reduction in WC grain size. The sample with the highest Ru addition also had the highest contiguity of the coating. Therefore, it appeared that Ru addition increased the contiguity of the coating. The binder volume fraction for the coating were very similar. The sample with the highest Ru also had the lowest binder volume fraction of 0.37 and the sample with 1wt%Ru had the highest binder volume fraction of 0.44. The binder mean free path decreased with an increase in Ru content of the coating. The sample with 2wt%Ru had the lowest binder mean free path of 0.08 and the sample with no Ru

had a binder free path of 0.26. This is in agreement with results from Shing et al. [36] showed that Ru addition had an effect of decreasing WC grain size on sintered WC-Co samples.

Hardness and thickness

The sample with 2wt%Ru addition had the lowest hardness of 925VHN, while the sample with no Ru addition had the highest hardness of 1009VHN. Previous work done by Shing et al. [36] on the effect of Ru additions on the hardness, toughness and grain size of the WC-Co showed an opposite trend to what was observed in this work. Their [36] work was done on the sintered WC-Co samples while the current work was done on HVOF coated samples. HVOF and sintering are two different processes with different processing times, pressures and temperatures. During sintering samples are pressed under high pressures and sintered for long hours whereas for HVOF process powders are sprayed to the substrate at very high velocities forming a bond between the coating and substrate. During sintering, the sample goes through long diffusion times and for HVOF coatings the diffusion time is very short. Powders that are used for sintering are normally milled to finer particles and for the HVOF process, the powders are much bigger in size than for sintering process. Fine milled particles cannot be used for HVOF process as they can clog or block the gun. Samples with 2wt%Ru had the thickest coating thickness and sample with no Ru had thinnest coating thickness.

Sliding wear

All the coefficient of friction curves showed two regions, which are the run-in region and the static state region. Sample with 2wt%Ru had the highest average coefficient of friction, while sample 0.5wt%Ru had the lowest average coefficient of friction. The ball that was used for the sample with no Ru had the highest wear rate while the ball that was used for sample with 2wt%Ru had the lowest wear rate. This was expected because the sample with no Ru had a low wear rate. The ball used for sample with 0.5wt%Ru had the second lowest wear rate, while the ball used for 1wt%Ru had the second highest wear rate. The 2wt%Ru sample had the highest wear rate while the 1wt%Ru sample had the lowest wear rate. Wear rate of the coatings increases with increase in porosity of the samples (Appendix A6). The sample with no Ru had the second lowest wear rate, while the 0.5wt%Ru sample had the second highest wear rate. The wear mechanism for all the balls were smearing of the particles and ploughing of the wear surface. It was evident that there

was lot of oxide formation on the surface due to friction between the ball and the surface. The 100Cr ball smeared on the coating surface and left some debris and there was some oxide formation due to friction action between the 100Cr ball and the coating surface. Ru addition had an effect of increasing the wear rates, as the wear rates slightly increased with increase in wt%Ru. This was expected because the wear rate for a material increases as the hardness decreases, but not always as shown by the work of Reshetnyak and Kaybarsepp [59]. The hardness of the coatings decreased with an increase in wt%Ru. The sample with the highest hardness had the lowest wear rate.

Electrochemical corrosion

The sample with no Ru addition had the lowest average OCP and therefore, the lowest corrosion potential. The sample with 2wt%Ru had the highest average OCP and corrosion potential. Whereas the sample with 0.5wt%Ru and 1wt%Ru had almost the same OCP values. However, the sample with no Ru had the lowest current density in comparison to all the other samples. The samples with 0.5wt%Ru and 1wt%Ru showed very similar electrochemical behaviour.

For the samples tested immediately after exposure in synthetic mine water at pH 3, the sample with no Ru again showed the lowest current density. The 2wt%Ru sample showed the highest free corrosion potential and the sample with no Ru had the lowest, or most active, free corrosion potential. The anodic current densities and free corrosion potentials were very similar for the 0.5wt%Ru and 1wt%Ru samples. There was not a clear passive potential range for any of the samples.

After 12 hours exposure in synthetic mine water at pH 3, the sample with no Ru had the lowest current density compared to all the other samples. The 2wt%Ru sample showed the highest free corrosion potential in comparison with other curves and the sample with no Ru had the lowest free corrosion potential. Again the 0.5wt%Ru and 1wt%Ru samples showed very similar electrochemical behaviour. Their anodic current densities and free corrosion potentials were also very similar.

The samples tested immediately after exposure in synthetic mine water at pH 1, the 1wt%Ru sample had the lowest current density and the highest free potential. The 2wt%Ru had the lowest free corrosion potential and highest anodic current density. The anodic current densities and free

corrosion potentials were very similar for the 0.5wt%Ru and 1wt%Ru samples. All the curves at the pH of 1 were not very stable.

Comparing the corrosion rates for samples tested immediately after exposure at pH of 1 and 3 showed that at pH 1 the corrosion rates were the lowest even though the potentiodynamic curves were not that stable. The samples that were tested immediately at pH of 3 had the highest corrosion rates. The samples that were tested in synthetic mine water at pH 3 after 12 hours exposure had lower corrosion rates, showing a passivation effect with exposure. From these results it is evident that sample with no Ru had much better corrosion resistance in synthetic mine water at pH of 1. However, at pH of 3 the corrosion resistance of all the samples was slightly lower than at the lower pH of 1.

For all the samples the corrosion attack was very similar with some formation of corrosion products. The EDS analysis of these corrosion products on the surface showed the typical elements, such as Na, Cl, and Ca, which were present in the synthetic mine water.

Tribo-corrosion

The sample with no Ru showed the best results under tribo-corrosion conditions. The calculated corrosion rates for this sample were similar with and without the tribo-action, and the polarisation characteristics were also very similar. However, the samples with Ru additions showed a significant increase in corrosion rate when exposed to tribo conditions. The 0.5wt% and 1wt%Ru samples showed similar behaviour with a significant increase in corrosion rates, especially on the 1wt%Ru sample. In contrast the 2wt%Ru sample showed a significant decrease in the corrosion rate under tribo conditions and behaved similarly to the sample with no Ru addition. This was also evident in the polarisation characteristics, with only a significant shift in the corrosion potential of the alloy.

Chapter 7: Conclusions and recommendations

7.1 Conclusions

- WC-10Co-4Cr coatings were successfully coated on mild steel using the HVOF process. The grain size decreased with an increase in Ru content. The binder volume fraction for all the samples were very similar and was not really affected by the Ru addition. The hardness of the coatings decreased with the addition of Ru except for the 1wt%Ru sample.

- Ru additions to the coatings led to increased wear rates during sliding wear tests and the coefficient of friction curves increased with Ru addition. However, the sample with no Ru added had the highest average coefficient of friction.

- Ru additions increased the open circuit potential (OCP) for the coatings, as the sample with highest OCP value had the highest Ru additions thereby making the sample more noble and improving the stability. Ru additions only improved the corrosion resistance of the coatings in synthetic mine water at pH of 1. However, at pH of 3 the addition of Ru decreased the corrosion resistance.

- The tribo-corrosion rates were higher than electrochemical corrosion rates for synthetic mine water at pH 1. This was caused by the removal of the passive layer during the tribo-corrosion tests. Tribo-corrosion rates decreased with increasing Ru content in the coating.

What is the effect of Ru additions of up to 2wt% to WC-Co-Cr HVOF coating on corrosion properties, tribo-corrosion properties and friction wear properties?

Ru additions to WC-Co-Cr HVOF coatings had an effect of decreasing the corrosion rate in synthetic mine water at pH of 1. Ru additions increased the wear rates of the coatings since the hardness was decreased by Ru additions.

How does Ru additions to WC-Co-Cr affect the microstructure and hardness of the coatings?

The microstructure of the coatings were not affected as seen from the FESEM results. However, the addition of Ru to coatings had an effect of decreasing the hardness as the hardness of the coatings decreased with Ru addition.

7.2 Recommendations

- It can be recommended that coatings with better Ru distribution be produced and corrosion testing, tribo-corrosion testing, and wear testing be conducted on the samples with good Ru distribution.
- Heat treatment can be done on the current samples to have better Ru distribution and further testing can be done on the heat-treated samples.
- Further open circuit potential measurements can be done on tribo-corrosion samples to determine how stable they are in the solution.
- Further TEM work can be done to fully understand the phase change or transformation from WC to W_2C.
- It can also be recommended that a harder wear ball can be used to investigate the effect of using a more abrasive ball on the coatings.
- There is still big scope to do more research related to the possible applications of Ru, as in South Africa we are the primary source of Ru and finding new applications for the element will mean more mining opportunities and growing the economy of our country.

REFERENCES

[1] J.H. Potgieter, N. Thanjekwayo, P. Olubambi, N. Maledi and S.S. Potgieter-Vermaak, Influence of Ru additions on the corrosion behaviour of WC–Co cemented carbide alloys in sulphuric acid, International Journal of Refractory Metals and Hard Materials, 29 (2011) 478–487.

[2] J.H. Potgieter, Alloys cathodically modified with noble metals, Journal of Applied Electrochemistry, 21 (1991) 471-482.

[3] J.H. Potgieter, W.O. Barnard, G. Myburg, K. Varga, P. Baradlai and L. Tomcsanyi, Corrosion behaviour of duplex stainless steels containing minor ruthenium additions in reducing acid media, Journal of Applied Electrochemistry, 26 (1996) 1103-1110.

[4] A.M. Human & H.E. Exner, The Relationship Between Electrochemical Behaviour and In-service Corrosion of WC Based Cemented Carbides, International Journal of Refractory Metals and Hard Materials, 15 (1997) 65-71.

[5] N.B. Nelwalani, Evaluation of erosion-corrosion on ruthenium enriched hardmetal coatings, MTech Dissertation (2014), University of Johannesburg, Johannesburg.

[6] C.N. Machio, G. Akdogan, M.J. Witcomb and S. Luyckx, Performance of WC-VC-Co thermal spray coatings in abrasion and slurry erosion tests, Wear, 258 (2005) 434-442.

[7] C.N. Machio, D.S. Konadu, J.H. Potgieter, S. Potgieter-Vermaak and J. van der Merwe, Corrosion of WC-VC-Co hardmetal in neutral chloride containing media, Hindawi Publishing Corporation ISRN Corrosion Volume (2013), Article ID 506759.

[8] J. Berget, T. Rogne and E. Bardal, Erosion-corrosion properties of different WC-Co-Cr coatings deposited by the HVOF process- influence of metallic matrix composition and spray powder size distribution, Surface and Coatings technology, 201 (2007) 7619-7625.

[9] H. Engqvist, G.A. Botton, S. Ederyd, M. Phanuel, J. Fondelius and N. Axên, Wear phenomena on WC-based face seal rings, International Journal of Refractory Metals and Hard Materials, 18 (2000) 39 – 46.

[10] V.A.D. Souza and A. Neville, Corrosion and synergy in a WC-Co-Cr HVOF thermal spray coating—understanding their role in erosion–corrosion degradation, Wear, 259 (2005) 171–180.

[11] E.N. Ogunmuniwa, Processing, characterization and tribological assessment of novel WC-VC-Co coatings and alloys, PhD dissertation (2013), University of the Witwatersrand, Johannesburg.

[12] L. Fedrizzi, S. Rossi, R. Cristel and P.L. Bonora, Corrosion and wear behavior of HVOF cermet coatings used to replace hard chromium, Electrochimica Acta, 49 (2004) 2803-2814.

[13] A.J. Gant, M.G. Gee and A.T. May, The evaluation of tribo-corrosion synergy for WC-Co hardmetals in low stress abrasion, Wear, 256 (2004) 500-516.

[14] M. Magnania, P.H. Suegamaa, A.A.C. Reccob, J.M. Guilemanyc, C.S. Fugivaraa and A.V. Benedettia, WC-Co-Cr Coatings Sprayed by High Velocity Oxygen-Fuel (HVOF) Flame on AA7050 Aluminum Alloy: Electrochemical Behavior in 3.5% NaCl Solution. Materials Research, 10 (2007) 377-385.

[15] A.K. Maiti, A. Mukhopadhyay and R. Raman, Effect of adding WC powder to the feedstock of WC–Co–Cr based HVOF coating and its impact on erosion and abrasion resistance, Surface and Coatings Technology, 201 (2007) 7781–7788.

[16] C. Osborne, L. Cornish and S. Luyckx, On the preparation of fine V_8C_7–WC and V_4C_3–WC powders, International Journal of Refractory Metals and Hard Materials, 15 (1997) 163–8.

[17] B.W. Madsen, Measurement of erosion-corrosion synergism with a slurry wear test apparatus, Wear, 123 (1988) 127–142.

[18] W.J. Tomlinson and N.J. Ayerst. Anodic polarization and corrosion of WC-Co hardmetals containing small amounts of Cr_3C_2 and/or VC, Journal of Materials Science, 24 (1989) 2348–2352.

[19] G.S. Brady, H.R. Clauser and J.A. Vaccari, Materials Handbook, 15th Edition. MacGraw-Hill, New York, (2002).

[20] L.L. Sheir, R.A. Jarman and G.T. Burstein, Corrosion, Volume 2, Corrosion control, 3rd Edition. Butterworth-Heinemann, Oxford (2000).

[21] R.F. Bunshah, Handbook of hard coatings deposition technologies, properties and applications, Noyes, Norwich (2001).

[22] B. Vivian, Selecting process valves for in-service reliability, Process Engineering, 1 (1988) 33–36.

[23] M.H. Ghandehari, Anodic Behaviour of Cemented WC-6% Co Alloy in Phosphoric Acid Solutions, Journal of the Electrochemical Society, Volume 127, Issue 10 (1980) 2144-2147.

[24] M.A. Human, T.I. Northdrop, B.S. Luyckx and M.N. James. A comparison between cemented carbides containing cobalt and nickel-based binders, Journal of Hard Materials, 2 (1991) 247-257.

[25] B. Bozzini, G.P. De Gaudenzi, A. Fanigliulo and C. Mele, Anodic behaviour of WC-Co type hardmetal. Materials and Corrosion, 54 (2003) 295–303.

[26] J.E. Cho, S.Y. Hwang and K.Y. Kim, Corrosion behavior of thermal sprayed WC cermet coatings having various metallic binders in strong acidic environment, Surface and Coatings Technology, 200 (2006) 2653–2662.

[27] C. Joshi, Characterization and corrosion of bcc-tantalum coating deposited on aluminum and steel substrate by dc magnetron sputtering, MSc Dissertation (2003), New Jersey Institute of Technology, New Jersey.

[28] D.A. Jones, Principles and prevention of corrosion: second edition, Canada: Macmillan Publishing Company, (1992).

[29] C. Allen, Corrosion of galvanised steel in synthetic mine waters, British Corrosion Journal, 26 (1991) 93-100.

[30] S.P. Broccardo, An investigation into the corrosion resistance of WC-VC-Co hardmetals, MSc Dissertation (2003), University of the Witwatersrand, Johannesburg.

[31] Y.F. Qiao, T.E. Fischer & A.H. Dent. The effects of fuel chemistry and feedstock powder structure on the mechanical and tribological properties of HVOF thermal-sprayed WC–Co coatings with very fine structures, Surface Coatings Technology, 172 (2003) 24–41.

[32] R. Schwetzke and H. Kreye, Microstructure and properties of tungsten carbide coatings sprayed with various High Velocity Oxygen Fuel spray systems, Journal of Thermal Spray Technology, Vol. 8(3) (1999) 433-439.

[33] Y.Y. Ozbek, N. Canikoglu and M. Ipek, The surface properties of WC–Co–Cr based coatings deposited by High Velocity Oxygen Fuel Spraying, ACTA PHYSICA POLONICA A. Vol. 131 (2007) 186-189.

[34] D.A. Stewart, P.H. Shipway and D.G. McCartney, Influence of heat treatment on the abrasive wear behaviour of HVOF sprayed WC–Co coatings, Surface and Coatings Technology, 105 (1998)13–24.

[35] L.Makhele-Lekala, S.Luyckx and [36F.R.N.Nabarro, Semi-empirial relationship between the hardness, grain size and mean free path of WC-Co, International Journal of Refractory Metals & Hard Materials, 19 (2001) 245-249.

[36] T.L. Shing, S. Luyckx, I.T. Northrop, I. Wolff, The effect of ruthenium additions on the hardness, toughness and grain size of WC-Co, International journal of refractory metals and hard material, 19 (2001) 41-44.

[37] D.G.F. O'Quigley, S. Luyckx and M.N. James, An Empirical Ranking of a Wide Range of WC-Co Grades in Terms of their Abrasion Resistance Measured by the ASTM Standard B 611-85 Test, International journal of refractory metals and hard materials, 15 (1997) 73-79.

[38] S. Hong, Y. Wu, W. Gao, J. Zhang and Y. Zheng, Slurry erosion-corrosion resistance and microbial corrosion electrochemical characteristics of HVOF sprayed WC-10Co-4Cr coating for offshore hydraulic machinery, International journal of refractory metals and hard materials, 17 (2018) 7-13.

[39] W.J.Tomlinson and C.R. Linzell, Anodic polarization and corrosion of cemented carbides with cobalt and nickel binders, Journal of Materials Science, 23 (1988) 914-918.

[40] N.P. Thanjekwayo, The influence of Ru additions on the corrosion behaviour of WC-Co cemented carbide in corrosive media, MSc dissertation (2009), University of the Witwatersrand, Johannesburg.

[41] C. Bonjour and A.Actis-Data, Effects of Ruthenium Additions on the Properties of WC-Co Ultra Micrograins, Powder Metallurgy Tool Material, (2004) 543-549.

[42] Z. H. Masuku, P. A. Olubambi, J. H. Potgieter, and B. A. Obadele, Tribological and corrosion behavior of HVOF-sprayed WC-Co-based composite coatings in simulated mine water environments, Tribology Transactions, 58 (2015) 337–348.

[43] R.J.K. Wood, Tribo-corrosion of coatings: a review. J. Phys. D: Appl. Phys. 40 (2007) 5502–5521.

[44] D.S. Konadu, J. van der Merwe , J.H. Potgieter , S. Potgieter-Vermaak and C.N. Machio, The corrosion behaviour of WC-VC-Co hardmetals in acidic media, Corrosion Science, 52 (2010) 3118–3125.

[45] I.M. Hutchings, Tribology: Friction and Wear of Engineering Materials, Edward Arnold, (1992) London.

[46] B. Bhushan, Introduction to Tribology, John Wiley & Sons Inc. (2002), New York.

[47] C.M. Cotell, J.A. Sprague and F.A. Smidt, Jr. Surface Engineering Volume 5 of the ASM Handbook. (1994), ASM International Handbook Committee, United States of America.

[48] F. Moyo, Using ruthenium to modify surface properties of austenitic stainless steel for improved corrosion resistance, PhD dissertation (2017), University of the Witwatersrand, Johannesburg.

[49] L. Chipise, P.K. Jain and L.A. Cornish, Influence of Ru on the hardness and fracture toughness of WC-VC-Co alloys, International Journal of Refractory Metals & Hard Materials, 77 (2018) 54–60.

[50] P.J. Blau, Friction, Lubrication, and Wear Technology volume of ASM Handbook, (1992) ASM International Handbook Committee, United States of America.

[51] L. Chipise, P.K. Jain and L.A. Cornish, Magnetic and microstructural aspects of WC-VC-Co-Ru alloys, International Journal of Refractory Metals & Hard Materials, 76 (2018) 49-56.

[52] C.N. Machio, Preparation, characterization and testing of WC-VC-Co HP/HVOF thermal spray coatings, PhD dissertation (2005), University of the Witwatersrand, Johannesburg.

[53] R.M. Genga, Microstructure and properties of selected WC-cemented carbides manufactured by SPS method, PhD dissertation (2014), University of the Witwatersrand, Johannesburg.

[54] G.S. Upahyaya, Cemented Tungsten Carbide Production, Properties and Testing. Noyes Publications. (1998) New Jersey, USA.

[55] J.W. Van der Merwe and D. Tharandt, Corrosion resistance of laser-cladded 304L stainless steel enriched with ruthenium additions exposed to sulphuric acid and sodium chloride media, The Journal of the Southern African Institute of Mining and Metallurgy, 115 (2015) 499-505.

[56] D. Landolt, S. Mischler and M. Stemp, Electrochemical methods in tribocorrosion: a critical Appraisal, Electrochimica Acta. 46 (2001) 3913–3929.

[57] L. Fedrizzi, L. Valentinelli, S. Rossi and S. Segna, Tribocorrosion behaviour of HVOF cermet coatings, Corrosion Science, 49 (2007) 2781–2799.

[58] M.G. Fontana, Corrosion Engineering 3rd edition, McGraw-Hill Book Company, 1987, New York.

[59] Reshetnyak, H and Kaybarsepp, J, Mechanical properties of hard metals and their erosive wear resistance, Wear, 177 (1994) 185-193.

[60] Dănăilă, E and Benea, L, The Effect of Normal Force on Tribocorrosion Behaviour of Ti-10Zr Alloy and Porous TiO2–ZrO2 Thin Film Electrochemical Formed, Materials Science and Engineering, 209 (2017) 012015.

APPENDIX

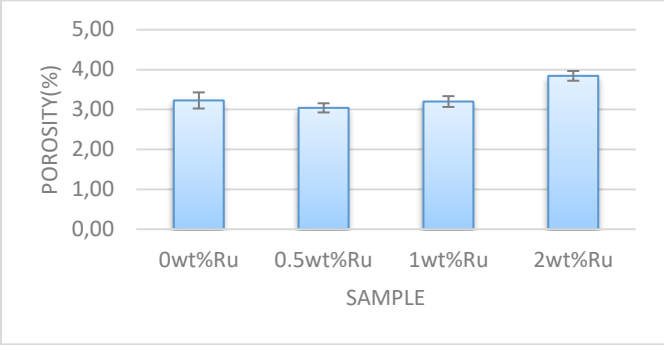

Appendix A1: Graph comparing percentage porosity of the coatings.

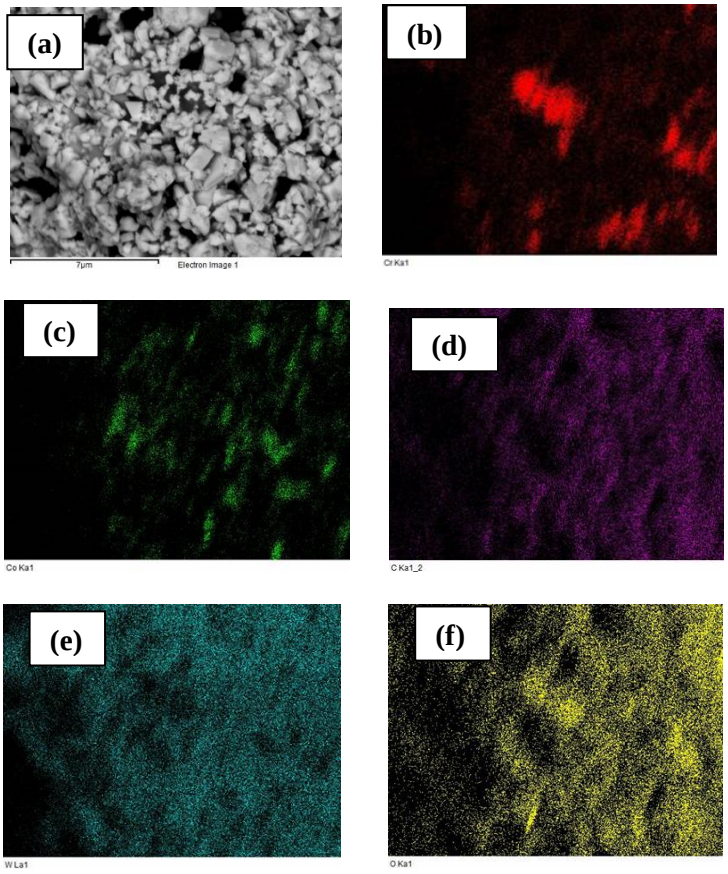

Appendix A2. WC-10Co-4Cr as received power elemental maps. (a) BSD electron micrograph (b) Cr elemental map (c) Co elemental map (d) C elemental map (e) W elemental map (f) O elemental map

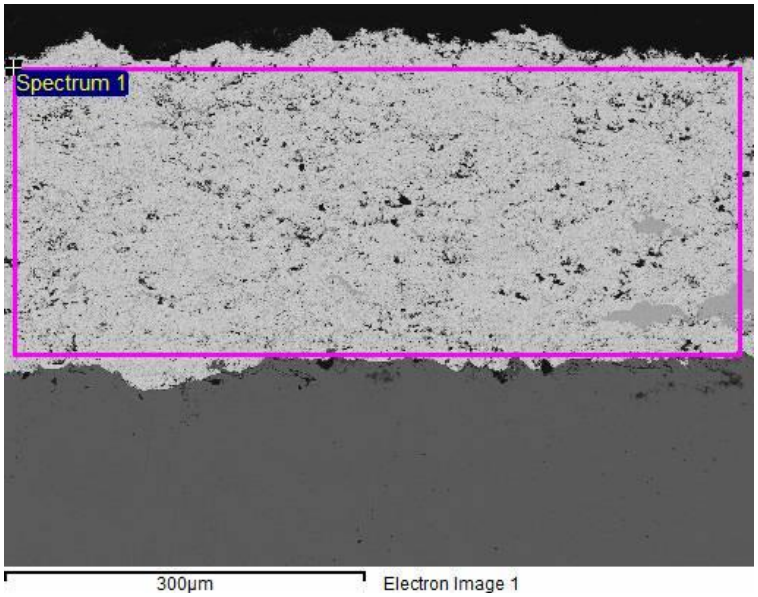

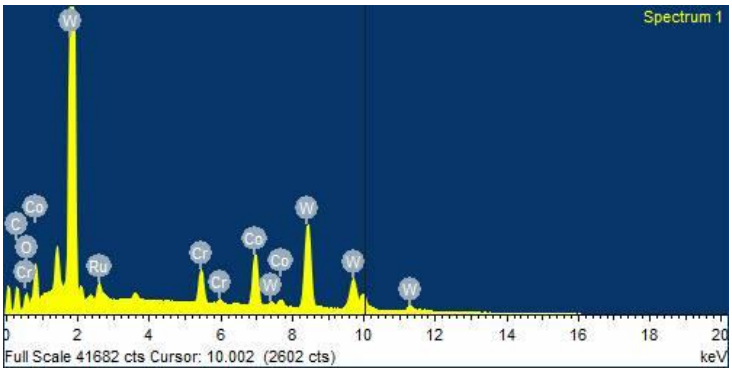

Appendix A3. WC-10Co-4Cr-2Ru coating EDS elemental composition.

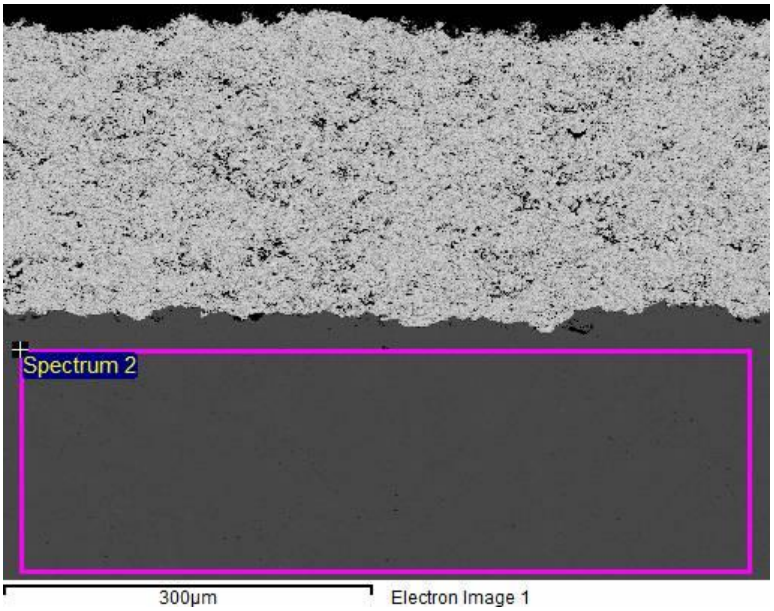

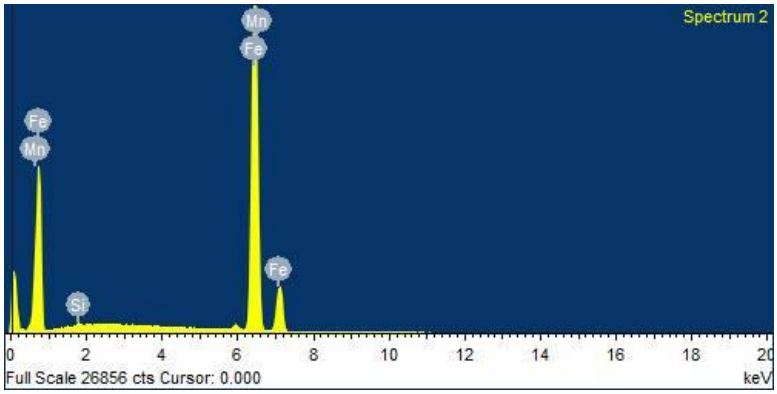

Appendix A4. WC-10Co-4Cr-2Ru substrate EDS elemental composition.

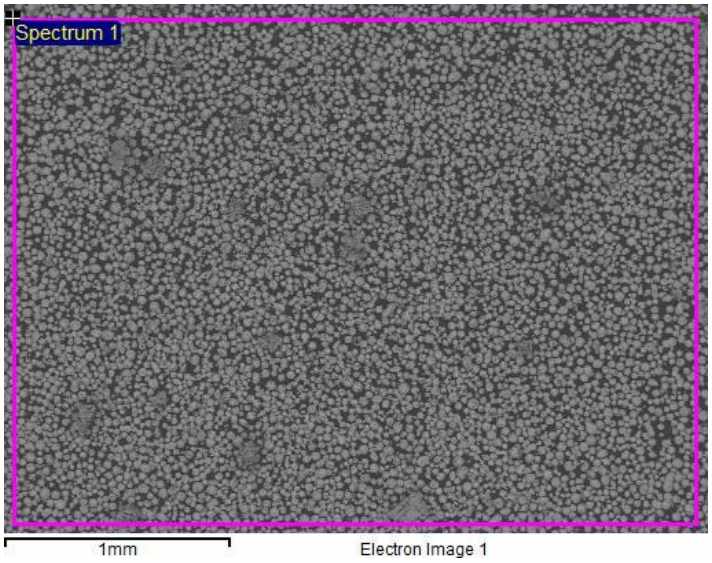

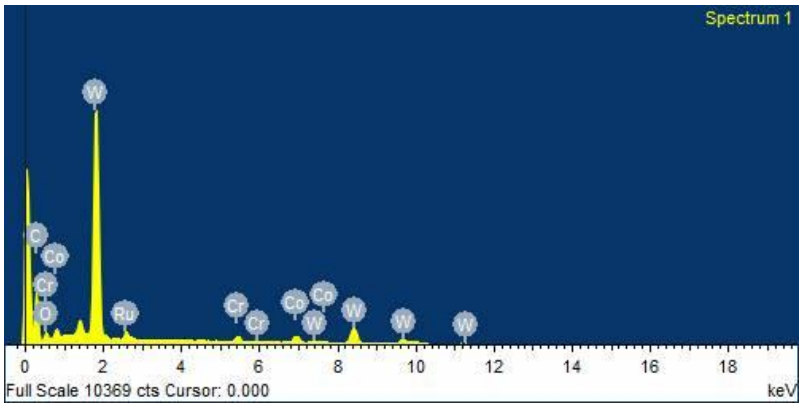

Appendix A5. WC-10Co-4Cr-2Ru powder after mixing EDS elemental composition.

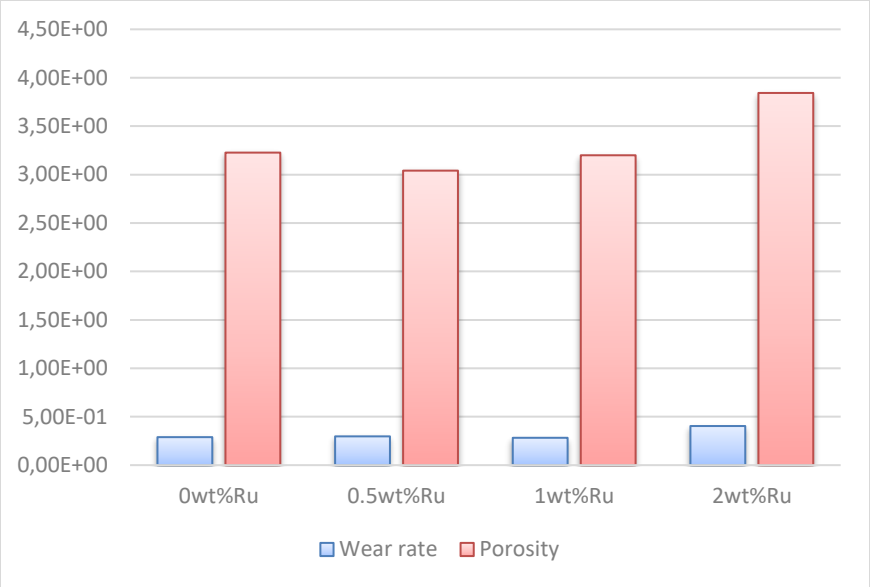

Appendix A6. Comparison of porosity and wear rate.